DISSERTATION

FROM BCG VACCINATION ROUTES TO LUNG AND GUT MICROBIOTA: AVENUES TO TACKLE *MYCOBACTERIUM TUBERCULOSIS* INFECTION

Submitted by

Fabiola Silva-Angulo

Department of Microbiology, Immunology, and Pathology

In partial fulfillment of the requirements

For the Degree of Doctor of Philosophy

Colorado State University

Fort Collins, Colorado

Summer 2021

Doctoral Committee:

Advisor: Marcela Henao-Tamayo

Tiffany Weir
Zaid Abdo
Angelo Izzo

ABSTRACT

FROM BCG VACCINATION ROUTES TO LUNG AND GUT MICROBIOTA: AVENUES TO TACKLE MYCOBACTERIUM TUBERCULOSIS INFECTION

Tuberculosis is an infectious lung disease responsible for approximately 1.4 million human deaths, world-wide every year. The causal agent of tuberculosis, *Mycobacterium tuberculosis* (*M. tuberculosis*), has been estimated to latently infect one-third of the human population. Currently, the BCG vaccine, a live attenuated strain of *Mycobacterium bovis*, is the only vaccine available to control the disease. Although the BCG vaccine has been the most widely administered worldwide and has been used for more than 100 years, tuberculosis dissemination remains uncontrolled and highly prevalent, especially in developing countries. Several questions about the effect that local microbiota and the administration route of BCG vaccination make on tuberculosis immunopathogenesis remain unanswered. These questions are critical for developing new approaches to control the disease. BCG vaccination is administered intradermally, however, some studies have suggested that BCG vaccination efficacy may dependent on the administration route. Vaccination through the natural route of *M. tuberculosis* infection and a combination of other routes have been studied in animal models with varying results. Currently, the analysis of vaccination through the natural infection site is an attractive approach to priming innate immunity.

The first study of this thesis examined the immune response induced after BCG vaccination using different routes (aerosol, subcutaneous, intravenous, and intranasal) in C57BL/6 mic and their response to pulmonary *M. tuberculosis* infection. The study was focused on specific markers of both CD4+ and CD8+ T cells. Our data suggested differences in the adaptive immune response based on the route of BCG vaccination and mainly elicited by CD4+ T cell immune response, with the intranasal delivery the most effective in decreasing the growth of *M. tuberculosis* in lungs.

Another crucial question is the effect of *M. tuberculosis* infection and BCG vaccination on the structure, diversity, and potential function of the host lung and gut microbiota. Thus, the objective for the second study of this thesis was to characterize the effect of BCG vaccination and *M. tuberculosis* infection on the lung and gut micro- and mycobiota of C57BL/6 mice. Results indicated that BCG vaccination and *M. tuberculosis* infection in mice altered the relative lung abundance of Firmicutes and Bacteroidetes phyla compared to the control non-vaccinated, non-infected group. Lung diversity was most affected after *M. tuberculosis* infection. A multivariate regression approach was used to compare the profile evolution of gut and lung microbiota. More genera had modified relative abundances associated with BCG vaccination status at the gut level compared with lung. Conversely, genera with modified relative abundances associated with *M. tuberculosis* infection were numerous at lung level, and indicated that the local host response against infection impacted the whole microbial flora while the immune response after vaccination modified mainly the gut microbiota. This study demonstrated that parenteral vaccination

with a live attenuated microorganism induced both lung and gut dysbiosis, which may play a crucial role in the immune response to *M. tuberculosis* infection.

ACKNOWLEDGMENTS

I would like to offer special thanks to Elizabeth Creissen who with her sense of humor brought light to cloudy days.

Thank you to dr. Angelo Izzo for believing in me and giving me the opportunity to embrace this long and rewarding journey.

Thank you, dr. Marcela Henao-Tamayo, and dr. Zaid Abdo, for all their support especially in moments of uncertainty and doubt. Their mentorship and advice made all the difference in helping me finish this dissertation.

Finally, I would like to thank my husband, Diego, for his tremendous and invaluable support during all these years.

DEDICATION

“Be the rainbow in someone else’s cloud.”
-Maya Angelou

I dedicate this dissertation to my loving grandfather Alvaro Angulo (1926-2019), who taught me humility, kindness to others, and that the life has sweetness and bitterness, but it is always worth living.

And to all laboratory animals that throughout the years have given their lives for the good of humanity.

TABLE OF CONTENTS

Chapter I

Literature Review

Structure of the Respiratory System

In-depth knowledge of the respiratory system is necessary to understand and detect pathological and functional changes derived from physical or biological injuries. For instance, in the 1960s, the discovery of the surfactant and its essential role in lung physiology led researchers to isolate and culture lung cells and elucidate their biochemistry characteristics and role in lung homeostasis (Gail and Lenfant, 1983).

From an anatomic viewpoint, the airway's conducting system includes nostrils, nasal cavity, paranasal sinuses, nasopharynx, larynx, trachea, and bronchi. A pseudostratified ciliated columnar epithelium lines all these structures with a variable proportion of goblet cells (Hanshew et al., 2017). The transitional system toward the lower respiratory tract is composed of bronchioles, where ciliated cells appear scarcer until they disappear entirely in distal bronchioles (Zachary and McGavin, 2012).

The human lung is divided into five lobes. The right lobes are subdivided into three lobes (the upper, middle, and lower lobes), and the left in two lobes (the upper and lower) (Joel et al., 2011). The volume of air reaching the human lung every day is around 9000 L (Zachary and McGavin, 2012). Airways are made up of smooth muscle, epithelium, and connective tissue. The trachea is about 12 cm in length and is composed of 16 to 20 rings of hyaline cartilage with a membranous wall composed of collagen and elastic fibers, which allows the esophagus to expand (Brand-Saberi and Schafer 2014). Once the trachea is proximal to the lung, the cartilage decreases in size and density and is modified by smooth muscle. The tracheal and bronchial mucosa is composed of a pseudostratified ciliated columnar epithelium with goblet cells. The respiratory tract's base membrane is a bilaminar structure made up of the basal lamina and the lamina reticularis. Composed of

type IV collagen, fibronectin, proteoglycans, laminin, and entactin-nidogen complexes. The lamina propria, which is beneath the basal membrane, contains elastic fibers, and the submucosa displays mucus and serous glands (Rock et al., 2009; Joel et al., 2011). The bronchial mucosa comprises four major cell types: ciliated cells, goblet cells, basal cells, and neuroendocrine cells (Gail and Lenfant, 1983; Ma et al., 2018). Ciliated cells are present in the trachea, bronchi, and bronchioles, and their role is to eliminate foreign particles and microorganisms toward the larynx via the mucociliary clearance mechanism (Ng et al., 2004; Rock et al., 2010). Bronchi are about 3 to 5 cm in length and composed of goblet cells. The goblet appearance gives the name that these cells have due to the mucus granules in the apical zone (Marchant, 2005). These granules are continuously released in the lumen by an apocrine-type secretion. The basal cells are pluripotent and the progenitor of all ciliated and non-ciliated cells of the bronchial mucosa. Finally, the neuroendocrine cells are more predominant in the fetal lung, and they are more abundant as individual cells near the airway bifurcations in bronchi and bronchioles (Joel et al., 2011; Ouadah et al., 2019).

The bronchioles are membranous, lacking cartilages, and conducting to the acinus, the lung's functional unit (Joel et al., 2011; Murray, 2010). The bronchioles lack goblet cells, and they are lined by ciliated columnar epithelial cells (Marchant, 2005, Murray, 2010) and nonciliated cuboidal Clara cells. The Clara cells are stem cells, essential for repair and remodeling (Zachary and McGavin, 2012). They are characterized by a prominent Golgi and numerous periodic-acid-Schiff (PAS)-diastase positive secretory granules in the apical cytoplasm. The ciliated cells decrease in number as they approach the Bronchoalveolar junction. These two anatomical separations are connected through Lambert's canals (Joel et al., 2011).

The alveolar ducts result from a bronchiole division and terminate in alveolar sacs, which are formed by four or more alveoli. A fine network of elastic fibers helps perform a uniform expansion and retraction of the lung during respiration. These fibers are plated by a layer of alveolar epithelial cells that forms a fragile membrane between the air and capillaries to allow gas exchange (Joel et al., 2011; Schittny 2017). It has been estimated that in

humans, the alveoli surface is approximately 200 m^2 (Zachary and McGavin, 2012). Two types of cells are part of the alveoli: The alveolar type I pneumocyte or alveolar epithelial type 1 cell (AEC-1) and the alveolar type II pneumocyte or Alveolar epithelial type 2 cells (AEC-2). AEC-1 have a flattened central nucleus and an expansive cytoplasm. In number, these cells are approximately 40% of the alveoli but cover up to 90% of the alveolar surface. AEC-2 are cuboidal cells that constitute the other 60% of the alveolar cells but cover only 5% of the alveolar surface. These cells have a large basal nucleus with a prominent nucleolus and osmophilic laminar inclusions, the precursors of surfactant, which help reduce tension and collapse (Shiraishi et al., 2019). The surfactant produced by AEC-2 is composed of phospholipids, especially dipalmitoyl lecithin, and glycoproteins (Murray, 2010; Guillot et al., 2013; Nabhan et al., 2018).

Additionally, AEC-2 cells also act as progenitor cells that may mature into an AEC-1. Other cells in the alveolar wells include fibroblasts, mesenchymal cells, pericytes of capillaries, and myofibroblasts responsible for the metabolism of elastic and collagen fibers in the alveolar walls. Lymphocytes, macrophages, plasma cells, neutrophils, eosinophils, and basophils may be present in the alveoli, but in small numbers (Joel et al., 2011; Barkauskas et al., 2017). Finally, the uptake of oxygen and carbon dioxide release occurs by the difference in pressure of these two gases via passive diffusion across the alveolar-capillary membrane (Murray, 2010; Guillot et al., 2013; Barkauskas et al., 2017).

Lung Vascular, Lymphatic Supply and Innervation

The pulmonary capillary system is the largest in the body. In adults, the capillary may reach a surface area of 70 m^2 and contain approximately 9% of the total blood volume (Zachary and McGavin, 2012). The lung's dual blood supply is adapted to receive a high volume of blood flow with a minimal change in pressure. Thus, the arterial bronchial system delivers oxygen at high pressure (Mack et al., 2020). The arteries' diameter varies in the lung, and these can be classified histologically as elastic, muscular, and non-muscular. The lung is rich in lymphatic supply; however, under normal conditions,

lymphatics ducts are collapsed, challenging to see microscopically. The superficial or pleural plexus drains the lung via pleura visceralis, and the parenchymal plexus drain the bronchoalveolar bundles via the hilar lymph nodes (Aung et al., 2019). Even though there is a communication between pleural and parenchymal plexus, there is an independent lymphatic draining work (Joel et al., 2011).

Lung innervation includes parasympathetic and sympathetic fibers. Parasympathetic or cholinergic fibers predominate in humans and dominate activities such as bronchoconstriction and mucus secretion, and adrenergic receptors respond to chemical stimulation and blockade (Aung et al., 2019). Peptidergic fibers and neuroepithelial bodies have also been identified; however, their physiological function is not yet defined (Murray, 2010; Murray 2011).

Lung Immune Cells and Lung Associated Immune System

Predominant lung innate immune cells include macrophages and dendritic cells (DCs) equipped with a wide variety of pathogen-associated molecular pattern (PAMPs) receptors and damage-associated molecular pattern (DAMPs) receptors (Guilliams et al., 2013). Lung macrophages are divided into two populations: alveolar macrophages (AMs) and interstitial macrophages (IMs). AMs usually are in close contact with the type I and type II alveoli epithelial cell, and they integrate the first line of defense against pollutants and pathogenic microorganisms. In a steady lung state, AMs cells form 90-95% of the cellular content of the lung (Kopf et al., 2015). The peroxisome proliferator-activated receptor γ (PPARγ) is the typical transcription factor in AMs and is induced by the cytokine granulocyte-macrophage colony-stimulating factor (GM-CSF). The lack of GM-CSF or PPARγ induces alveolar proteinosis due to the unavailability of catabolizing surfactant. The role of AMs is also essential as they oversee cleaning the airways of microorganisms, dead cells, and airborne particles, thus avoiding oxygen uptake issues. These cells are technically easy to obtain from bronchoalveolar lavage as they can travel from one adjacent alveolus to others through the pores of Kohn (Evren et al., 2019).

Two AM phenotypes (M1 or classically activated and M2 or alternatively activated) may be identified according to their cytokines and transcription factors profile (Yuan et al., 2015; Orecchioni et al., 2019; Snyder and Farber, 2019). M1 type macrophages are induced by microbes and proinflammatory cytokines from Th1 cells. This process enhances the M1 killing ability and makes them release proinflammatory cytokines allowing the recruitment of immune cells into the lung. In contrast, M2 macrophages are induced by Th2 cells cytokines and release anti-inflammatory cytokines that allow the physiological lung restoration by collagen restoration and phagocytosis of damaged cells. Therefore, these two macrophages' populations are critical for lung immune defenses, infection resolution, and lung tissue recovery (Hu and Christman, 2019; Yunna et al., 2020).

IMs are founded between the alveoli and the blood vessels, and due to technical reasons, they have been studied far less than AMs. As AMs, IMs are phagocytic cells that exhibit antigen-presenting cell characteristics through the Major Histocompatibility Complex class II (MHC-II) (Schyns et al., 2018). While AMs are easily obtained from Bronchoalveolar lavage (BAL), the isolation of IMs requires obtaining tissue samples and performing a series of procedures for cell tissue disaggregation and cell purification (Liegeois et al., 2018). To date, it is known that IMs secrete growth factors and cytokines critical for cell regeneration. This process modulates immune responses and angiogenesis in the bronchi and alveoli (Reddy and Mehta, 2017). By the secretion of immunosuppressive interleukin (IL) IL-10, IMs regulate lung homeostasis (Branchett and Lloyd, 2019).

Lung DCs are sentinel cells that are crucial to maintaining lung homeostasis. According to their developmental lineage, they can be classified as conventional DCs (cDCs), plasmacytoid DCs (pDCs) and monocyte-derived DCs (moDCs). cDCs are specially adapted to regulate T cell proliferation, survival, and effector function (Upham and Yang, 2017; Fekete et al., 2018). Depending on their localization within the lung, DCs may be continuously or rarely exposed to materials or pathogens inhaled. As an example, DCs located in the conducting airways rarely contact foreign particles. However, DCs located

in the alveolar septa are exposed continuously (Kopf et al., 2015). After an immunogenic stimulus, DCs migrate to the T-cell area within the mediastinal lymph node in a C-C chemokine receptor type 7 (CCR7) dependent manner (Lambrecht et al., 2001; Sichien et al., 2017). In the mediastinal lymph node T-cell area, DCs activate naïve T cells, and their signals may favor the nature of the immune response (T helper (Th)1, Th2, Th17, B cell help) or immune tolerance (Condon et al., 2011; Upham and Yang, 2017).

Natural killer (NK) cells are innate lymphocytes that secrete pro and anti-inflammatory cytokines. In lung homeostasis, NK cells account for 10-20% of lymphocytes in humans and mice. They are in the lung parenchyma and have lytic activity. NK cells possess both Toll-like receptor (TLR) 3 and TLR9; therefore, they can directly be activated by bacteria and viruses-infected cells. NK cells carry NKp46 activating receptors that bind to influenza haemagglutinins, allowing them to recognize and lyse infected cells. NK cells can be activated by contact-dependent mechanisms or cytokines such as IL-2, IL-12, and Interferon gamma (IFN-γ) (Cong and Wei, 2019). High levels of L-selectin permit their entry to lymph nodes, and the expression of Cluster of differentiation (CD)11b/CD18 facilitates the recruitment to inflammation sites. Besides viral and bacterial infections, NK cells have also played roles in lung cancer, chronic obstructive pulmonary disease (COPD), and asthma (Cong and Wei, 2019; Hervier et al., 2019). After the rise of IFN-γ generated by a viral lung infection, the number of NK cells increases in the peripheral blood. Likewise, depletion of lung or systemic NK cells during early influenza infection increases morbidity and mortality. Nonetheless, an over-increase of these cells induced by high-dose influenza affects mice survival due to an exacerbated inflammation that induces lung damage (Nogusa et al., 2008; Abdul-Careem et al., 2012; Zhou et al., 2013). NKT cells express features of both NK and T cells (for example, they express αβ T cell receptor (TCR)). These cells do not require a previous antigen presentation to execute the lytic activity. They can stimulate or suppress immune responses in part due to modulation of the Th1/Th2 balance (Sokhatska et al., 2019). Unlike conventional T cells (e.g., CD8+ and CD4+ T cells), after thymic egress, NKT cells are prepared to induce cytolysis and secrete cytokines and chemokines. Additionally, they can recognize conserved antigens like lipids, small metabolites, and peptides presented by CD1d (a

non-classical MHC). In mice, NKT cells account for about 2-5% of the cells present in the lung, and they may be present in both the lung vasculature and the parenchyma (Trottein and Paget, 2019).

As NKT cells, Mucosal associated invariant T (MAIT) cells are another subset of unconventional T cell. In the lung, they are present in about 2% in C57BL/6 and around 0.3% in BALB/c mice. These cells express chemokine receptors that mediate tissue homing such as C-C chemokine receptor (CCR) 9, C-X-C chemokine receptor (CXCR) 6, and α4β7, giving them the ability to travel to the lung, intestine, skin, and liver. MAIT cells can recognize riboflavin, and folic acid metabolites under the context of MHC-I related (MR1) restricted antigens (Rahimpour et al., 2015; Wen et al., 2021). They also may be activated by many cytokines such as interleukin (IL)-2, IL-7, IL-23, IL-1β, and IFN-γ, and recruit CD4+ and CD8+ T cells through the production of IFN-γ, tumor necrosis factor-(TNF)-α, IL-17A, and GM-CSF (Meierovics et al., 2013; Trottein and Paget, 2019). In some lung diseases, MAIT cells have been associated with severity and protective impacts. For example, in COPD, MAIT cells have been associated with negative outcomes; however, in cystic fibrosis (CF), lung MAIT cell deficiency has been correlated with an increase of *Pseudomonas aeruginosa* been related to adverse prognosis (Wen et al., 2021).

CD4+ T cells are a critical component of the cellular adaptive immune response. After stimulation of a naïve CD4+ T cell in the lung draining lymph node, this cell has the potential to differentiate into different T helper (Th) subsets, including T helper effector cells (Th1, Th2, Th17, T regulatory (Treg) cells, and T follicular helper (Tfh) cells. The importance of the CD4+ T cells falls on their abilities to enhance functions of innate immune cells and B and CD8+ T cells (Hirahara and Nakayama, 2016; Nguyen et al., 2019; Zhu and Zhu, 2020). Once the infection is controlled and cleared, a small portion of T cells remains as memory T cells. These cells have been categorized as effector memory, central memory, and tissue-resident memory T cells whose function is to mediate immune defense against reinfection. The first two subsets of memory T cells can circulate in non-lymphoid organs and secondary lymphoid organs, respectively. However,

the tissue-resident memory T cell resides in tissues as a defense line to augment innate immunity and recruit CD4+ and CD8+ T cells during potential reinfection (Shin and Iwasaki, 2013). The clinical ongoing of most infectious and non-infectious lung diseases are critical under the balance of CD4+ Th1 and Th2 cells. For example, patients with pulmonary sarcoidosis with a less pronounced Th1 immune response (characterized by proinflammatory cytokines) have been associated with a better prognosis (Prasse et al., 2000; Wahlstrom et al., 2001).

Naïve CD8+ T cells are stimulated by DCs in the lung draining lymph node. After respiratory viral infection, antigen-specific CD8+ T cells increase in frequency in the lung and airways. The mechanisms used by these cells include cell-cell contact through surface molecules such as CD95 and CD95L. CD8+ T cells can also express TNF-related apoptosis-inducing ligand (TRAIL) that interacts with its receptors DR4 or DR5 to destroy infected cells. Furthermore, these cells secrete proinflammatory cytokines such as IFN-γ and TNF-α and secrete perforin and granzymes to cause membrane destruction and induce apoptosis. Following infection clearance, and as similar as CD4+ T cells, CD8+ T cells form a long-lasting memory population whose purpose is to protect against reinfection. Based on the expression of the activation marker CD45RA in humans and the lymphoid homing receptor CCR7, the human memory CD8+ T cells can be categorized in Naïve (CD45RA+CCR7+), central memory (CD45RA-CCR7+), effector memory (CD45RA-CCR7-), and late effector memory (CD45RA+CCR7-) cells. Besides, the respiratory syncytial virus induces primary effector memory phenotype, and these cells also express high levels of CD27, CD28, and CCR5 and low levels of CD62L (Schmidt and Varga, 2018).

Pathology of Tuberculosis in the Human Lung

Primary Tuberculosis (TB)

Primary TB is the infection of an individual without a previous history of infection with *M. tuberculosis*. A single lesion characterizes this infection in the upper lobes in the lung (Murray, 2010), which is the part of the lung that receives the most significant air volume.

Pathologically, this single lesion, rarely multifocal or bilateral, is typically rounded, circumscribed, solid, 10-15 mm of diameter, and gray or white with an inflammatory focus. At this stage, the histological lesion is composed of histiocytes mixed with inflammatory cells that typically evolve to a soft granuloma with a necrotic center (Garaeva et al., 2017). *M. tuberculosis*, may be found free or within phagocytes in the granuloma. Typically, after one week of primary infection, *M. tuberculosis* drains along the peribronchial lymphatic channels to the ipsilateral tracheobronchial lymph nodes (Joel et al., 2011).

Disease progression is not usual in primary TB, and in this case, the lesion undergoes involution, shrinkage, fibrosis, and calcification (Garaeva et al., 2017). In this stage, *M. tuberculosis* may persist for years in a dormant phase until the immune system is suppressed. When the primary TB does not heal, the lesion may enlarge and develop multiple lesions in Hilar lymph nodes with caseous masses that compress the bronchi and may conduce to vascular dissemination (Joel et al., 2011).

Secondary Tuberculosis

Secondary TB arises in individuals that have previously been exposed to *M. tuberculosis*. Usually, these cases result from the reactivation of asymptomatic primary tuberculosis (WHO, 2003). Secondary TB by reinfection may also occur. Therefore, we have two possible scenarios: secondary TB due to *M. tuberculosis* reactivation of a previously infected individual or *M. tuberculosis* reinfection (also called exogenous reinfection). Reinfection mainly occurs in areas where TB is present in high incidence. However, in low-incidence countries, *M. tuberculosis* reinfection may increase due to the spread of multidrug resistance and HIV infection (Bandera et al., 2001). The monitoring of these two scenarios has epidemiological, and disease control importance as epidemiologists may assess the effectiveness of anti-TB treatment (Shen et al., 2017). Secondary TB commonly begins in the apical segment of one or both upper lobes. The granulomas' central necrosis, previously observed in the primary TB, becomes more prominent, leading to cavitation if the granuloma is in contact with bronchus, or fibrous encapsulation if there is no connection with an airway (Garaeva et al., 2017). The destruction of the lung by cavitation may produce bleeding as the first clinical sign of TB. New cavities contain

very few bacilli, but the microorganism grows massively in number when fibrosis and necrotic layers are formed (Neumuller et al., 1994). The cavity wall is then composed of a thin layer with caseous necrotic tissue surrounded by fibrosis (Joel et al., 2011). Different types of granulomas have been found in humans and non-human primates (NHP). Interestingly, some different granulomas have been observed within the same individual, supplying unique microenvironments that may promote killing, replication, or *M. tuberculosis* persistence (Neumuller et al., 1994).

The caseous granuloma is the most common lesion and is mainly found in latent TB and active disease (Figure 1.1). It is surrounded by peripheral fibrosis and composed of epithelial-like macrophages, neutrophils, B cells, CD4+, and CD8+ T cells (Lyashchenko et al., 2020). The granuloma center is caseous, a hypoxic and necrotic stage formed by dead macrophages. In this type of granuloma, *M. tuberculosis* might be found in macrophages, in the hypoxic center, or near the fibrotic area. The non-necrotizing granuloma is mainly found in active disease in humans, mice, and guinea pigs and formed mainly by macrophages and lymphocytes. In this type of lesion, *M. tuberculosis* is present in macrophages. The fibrotic granuloma is usually observed in latent and active TB and is predominantly composed of fibroblasts with minimal macrophages (Barry et al., 2009).

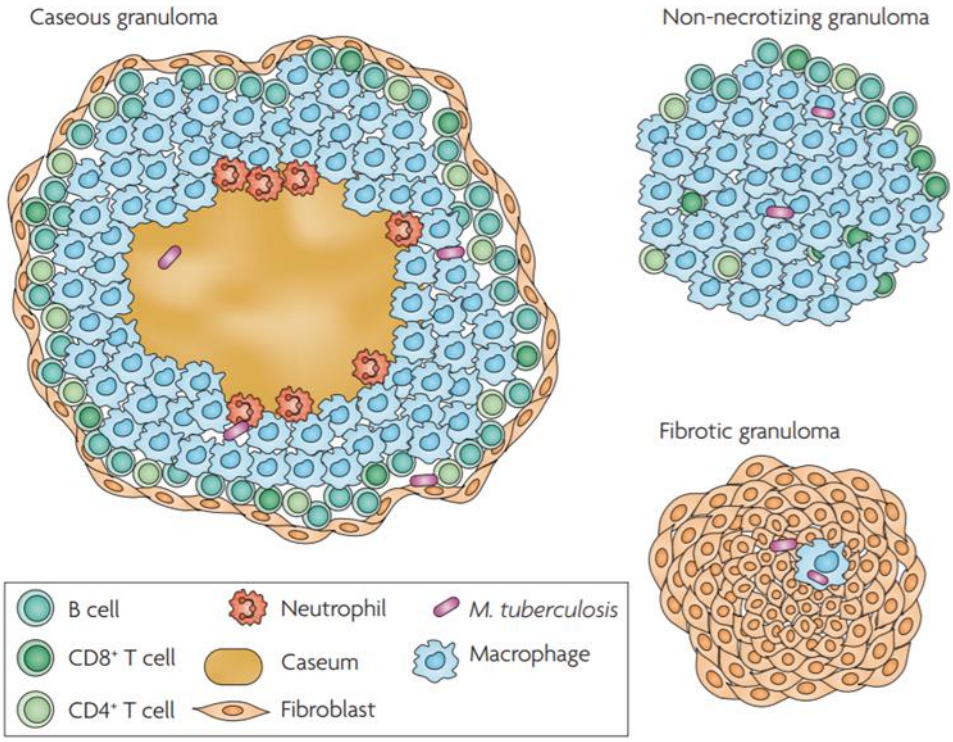

Figure 1.1 Types of tuberculous granulomas found in humans and non-human primates (From Barry et al., 2009).

Microscopic characteristics of TB lesions

There are no pathognomonic characteristics related to TB; however, the presence of acid-fast bacilli in granulomas suggests diagnosis (Russell et al., 2009). A neutrophil response is characteristic of early TB. In this stage, many bacilli can survive due to their thick cell wall. Some bacilli will be ingested by macrophages that will stimulate lymphocytes to produce chemoattractant to enhance the arrival of more macrophages, and at the same time, will improve their ability to kill the ingested bacilli. Next, the macrophages will then develop a granular eosinophilic cytoplasm with a high cytoplasmic-nuclear ratio forming the basis of the early granuloma (Russell et al., 2009, Ramakrishnan, 2012). Chronic lesions are characterized by Langhans multinucleate giant cells, composed of fused macrophages with a lymphocyte collection in the periphery. Central necrosis results from the tubercle's enlargement, and fibroblasts appear in the peripheral lymphocyte zone. At this time, if the immune system is strong enough, the infection is contained within the macrophages in a barrier formed by lymphocytes and fibroblasts.

Nonetheless, if the individual has comorbidities, the tubercle will be enlarged, resulting in tuberculous pneumonia. The different components of a developed granuloma are easily observed at lower power objective in the microscope. Lesions are characterized by central necrosis, histiocytes, lymphocytes, eosinophils, and collagenous fibrosis. On the other hand, it is easy to identify necrotizing and non-necrotizing granulomas and macrophages with anthracitic pigmentation with medium power objective. Finally, using high power objective, Langhans multinucleated giant cells and other individual cells are well defined. Acid-fast bacilli are typically found in the central necrotic zone and the interface between necrotic and viable cells (Joel et al., 2011; Ramakrishnan, 2012; Cadena et al., 2017).

Microbiome

The term, human microbiome refers to the genetic pool of bacteria, archaea, fungi, protists, and viruses that inhabit the human body (Marchesi and Ravel, 2015; Jagodzinski et al., 2019). This genetic pool may be different in composition among people, and such differences may be attributed to diet, environment, host genetics, early microbial exposure, age, culture, and location (Human Microbiome Project Consortium, 2017; Thomas et al., 2017). However, distinct body areas tend to contain similar microbe species (Human Microbiome Project Consortium, 2017). Today, the microbiome is considered a critical component in human development, health, and disease that may influence vaccination response (Silbergeld, 2017; Zimmermann and Curtis, 2018). It has been estimated that the human body is composed of $3x10^{13}$ eukaryotic cells and $3.9x10^{13}$ microorganisms, and the gut, the skin, and the oral cavity are the areas with the highest biomass. Interestingly, the gut microbiota's complete genome contains over 100 times the number of genes in the human genome, constituting a complex network within eukaryotic cells (Thomas et al., 2017).

The available technology to characterize the human microbiome uses targeted sequencing of the 16S rRNA gene, whole-genome shotgun sequencing, or meta-omic

technologies to characterize the microbiome's activity and dynamic (Barko et al., 2018) The 16S rRNA sequencing techniques have some advantages, including amplifying several hypervariable regions to obtain a broad range of a complex mixed population (Schmidt et al., 2018). This technology provides the opportunity to obtain necessary information at an accessible price. On the other hand, disadvantages include limitations to determine genus-level taxonomic identification of bacteria that may not discriminate rare and low-abundance taxonomic groups from noise (Noecker et al., 2017; Sankaran and Holmes, 2019).

In the future, it will be essential to consider such disadvantages and develop novel computational methods for providing a more in-depth characterization of the microbiome. For example, it will be crucial to determine the strain-level variation to check disease progression.

To better understand how the microbiome may influence the health and disease in humans, the National Institute of Health (NIH) supported the Human Microbiome Project (HMP), which used the 16S rRNA and whole-genome shotgun of five different sites in 300 healthy western male and female individuals with samples from nasal cavity, skin, oral cavity, gastrointestinal tract, and urogenital tract. However, in this project, the lung microbiome was not included (Human Microbiome Project Consortium, 2017; Lloyd-Price et al., 2017).

The gut is one of the human body sites that has been most characterized through microbiome techniques. According to culture-based and sequencing studies, the large and the small intestine have the highest microbiome biomass, with approximately 150 to 400 species. Species predominant in the gut belong to the Firmicutes, Bacteroidetes, Actinobacteria, and Proteobacteria phyla (Cresci, 2015; Davenport et al., 2017). All these microorganisms create a complex ecosystem. Many of them have beneficial functions as they produce Short-chain fatty acid (SCFA), activate the formation of mucus barrier, metabolize xenobiotics, prevent pathogens colonization competitive exclusion, and

promote intestinal vascularization (Jacobs and Braun, 2014; Morrison and Preston, 2016; Dalile et al., 2019).

The diversity of a given body habitat is due to the number and abundance distribution of distinct organisms. This concept has been linked to human disease, where a low diversity in the gut has been associated with inflammatory bowel disease (IBD) and obesity, and high diversity in the vagina to bacterial vaginosis (Human Microbiome Project Consortium, 2017; Maruvada et al., 2017; Glassner et al., 2019). Furthermore, the HMP found that saliva has among the highest median alpha diversity (within samples) of Operational Taxonomic Units (OTUs) and lower beta diversity (among samples). The skin had a high beta diversity and an intermediate alpha diversity, and the vagina had a low beta and alpha diversity, but with high OTUs due to the presence of different *Lactobacillus* spp. (Human Microbiome Project Consortium, 2017).
The different pathways and microbiome interactions in the gut have been one of the most studied for elucidating the mechanism of homeostasis and immune self-tolerance. It has been established that the innate immune system and microbiota affect one another through complex interactions and pathways, where this crosstalk has been determined to be crucial for human health (Thaiss et al., 2016; Takiishi et al., 2017; Berni Canani et al., 2019; Das and Nair 2019).

Compared with bacterial metagenomics, the human gut and lung mycobiome have been poorly studied. Fungi represent approximately 0.01% to 0.1% of genes in stool samples, and most of them are uncultivable or difficult to culture. To analyze the mycobiome is critical to take into consideration unique differences in the microorganisms' structure. Unlike bacteria, the fungal cell wall is more difficult to lyse, and there is no consensus adopted in DNA extraction for mycobiome analysis (Enaud et al., 2018). In humans, the gut mycobiome is characterized by a low mass and low diversity (Nash et al., 2017). Ascomycota is the most predominant fungus phylum in the gut, followed by Zygomycota and Basidiomycota. Human symbionts such as *Candida*, *Cryptococcus*, *Malassezia*, and *Trichosporon* are usually present. Interestingly, the environmental fungi *Cladosporium*

sp., the food-associated fungi *Debaryomyces hansenii*, and *Penicillium roqueforti* have also been identified in the gut (Enaud et al., 2018; Hager and Ghannoum, 2018).

The role of mycobiome in host defense, homeostasis, and immunomodulation has been studied in the last years. The oral administration of *Saccharomyces boulardii* ($3x10^8$ CFU/mL) in BALB/c mice increases the secretion of Immunoglobulin A (IgA) anti-toxin A in mice exposed to *Clostridium difficile* toxin A (Qamar et al., 2001). *S. boulardii* administration has shown efficacy in patients with IBD and may help promote epithelial restitution by increasing IL-8, which promotes angiogenesis and mucosal healing (Thomas et al., 2011; Curro et al., 2016; Rodriguez-Nogales et al., 2018).

Saccharomyces cerevisiae is commonly present in the skin and intestinal tract (Nash et al., 2017). Their potential homeostatic and immunomodulatory effect can be elicited via chitin content. *In vitro and in vivo* studies with C57BL/6 mice have demonstrated that chitin from *S. cerevisiae* can induce immune response via IL-6 and TNF-α. Remarkably, the *in vivo* study determined that human monocytes previously stimulated with *S. cerevisiae* chitin enhanced the killing ability against *Staphylococcus aureus* and *Escherichia coli* (Rizzetto et al., 2016).

A type of trained innate immunity has also been observed in mice using the previous infection with nonlethal *Candida albicans*. A pre-injection with a sublethal dose of *C. albicans* ($2x10^4$ CFU/mouse) seven days before a lethal intravenous dose ($2x10^6$ CFU/mL) increased the survival of wild type mice. Interestingly, the protection against a lethal dose of *C. albicans* was also observed in T and B cell defective Rag1 deficient mice. Thus, after the depletion of NK cells and monocytes, the authors concluded that trained immunity against *C. albicans* was performed mainly by monocytes (Quintin et al., 2012; Cheng et al., 2014).

IgA is the most abundant antibody isotype in mucosal surfaces and is a central first line of defense in airways and intestines (Ladjemi et al., 2015; Solans and Locht, 2019; Chen et al., 2020). IgA production is induced as a dimer (dIgA) after microbial colonization in a

T-dependent and T-independent manner. The T-dependent IgA class production occurs in Peyer's patches' germinal centers and is antigen-specific (Bunker and Bendelac 2018). On the other hand, T-independent IgA production occurs in isolated lymphoid follicles and the lamina propria, generating polyreactive IgA with low microbiota affinity. Thus, IgA is secreted to the intestinal lumen to maintain intestinal homeostasis by protecting the mucosa from pathogens and preventing direct commensal association with the intestinal epithelium (Bunker and Bendelac, 2018; McCoy et al., 2019). Studies with germ-free (GF) and specific pathogen-free (SPF) mice have shown that GF mice have a significant reduction in IgA, a low number of intraepithelial lymphocytes (αβ+ and γδ+ T cells populations), and fewer regulatory T (Tregs) cells compared with SPF mice (Shi et al., 2017).

Another example of the interaction between immune pathways and the microbiome is *Bacteroides fragilis*, a common commensal bacterium that plays an essential role in mucosal homeostasis by promoting Foxp3+ T cells and inducing anti-inflammatory cytokines in the gut. Also, SCFAs produced by commensal bacteria regulate inflammatory responses by inducing Treg homeostasis (Shi et al., 2017). Thus, an intestinal microbiota disbalance may follow an intestinal dysfunction with a consequence of clinical intestinal disease. Inflammatory Bowel Disease (IBD) such as Crohn's disease and ulcerative colitis are characterized by intestinal inflammation through triggering abnormal immune responses (Adams and Bornemann, 2013; Harb, 2015; Torres et al., 2017; Veauthier and Hornecker, 2018).

Lung Ecosystem and Microbiome

Contrary to previous knowledge, the advances in high-throughput molecular sequencing technologies have demonstrated that the human lower respiratory tract's epithelial surfaces are colonized by a complex and dynamic microbiota, termed lung microbiome. Sequencing studies have demonstrated differences in the lung microbiome of healthy and diseased individuals, which poses a potential use as a prognostic marker, a therapeutic target of infectious diseases, and vaccine efficacy.

In a healthy state, the lung microbiota has low biomass but a high diversity (Invernizzi et al., 2020). It has been estimated that the mouse lung has between 10^3-10^5 CFU/g of microbial density and humans approximately $2.2x10^3$ bacterial genomes per cm^2 (Mathieu et al., 2018). In general terms, the respiratory tract is dominated by four phyla: Bacteroidetes, Firmicutes, Proteobacteria, and Actinobacteria. The Bacteroidetes and Firmicutes predominate in humans, whereas Proteobacteria and Firmicutes predominate in mice. In the healthy lung, prominent genera include *Prevotella*, *Veillonella*, *Streptococcus*, *Neisseria*, *Haemophilus*, and *Fusobacterium*. The density of microbes is determined by microbial immigration, microbial elimination, and its relative rate of division. The main route of microbial immigration to the lung is through inhalation, dispersion along mucosal surfaces, and microaspiration (Mathieu et al., 2018, Invernizzi et al., 2020). Microaspiration is the predominant route of microbial immigration due to the similarities of the lung and the oral microbiota. A delicate balance in the lower respiratory tract is obtained through microbial immigration and microbial elimination through mucociliary clearance, cough, and immune defenses (Zemanick et al., 2010; Scialo et al., 2021).
During lung disease, the balance is perturbed, inducing overgrowth of certain bacterial species, viruses, and fungi, leading to a decrease in richness. Common lung diseases that are associated with an overall decrease of richness are asthma, chronic obstructive pulmonary disease (COPD), cystic fibrosis (CF), and idiopathic pulmonary fibrosis (IPF) (Invernizzi et al., 2020). BAL sequencing studies have demonstrated a high density of oral commensals such as *Prevotella*, *Streptococcus*, *Fusobacterium*, *Rothia*, *Veilonella* is associated with inflammation characterized by an increase in neutrophils and Th17 phenotype lymphocyte (Wu and Senegal, 2018).

Numerous studies have recently supported crosstalk between the lung and the gut microbiome, termed "the gut-lung axis" (Figure 1.2) (Anand and Mande, 2018; Frati et al., 2019; Vaughan et al., 2019). The lung microbiome has, in fact, some similarities with the gut microbiome; for example, the healthy lung is dominated by Bacteroidetes, Firmicutes, and Proteobacteria, which are SCFA producing bacteria. In the gut, these types of bacteria produce SCFA via the bacterial fermentation of non-digestible carbohydrates: acetate, propionate, and butyrate. It is currently widely known that the gut may influence

the lung microbiome by directly seeding bacteria into the airways or distributing SCFAs. Interestingly, SCFAs may interact and modulate the recruitment, differentiation, activation, and survival of immune cells. Studies in mice have demonstrated that depleted gut microbiota increases the risk of asthma (Dang and Marsland, 2019; Invernizzi et al., 2020) and that intestinal dysbiosis induced by antibiotic treatment may cause an unbalanced immune response in the lung (Hong et al., 2016).

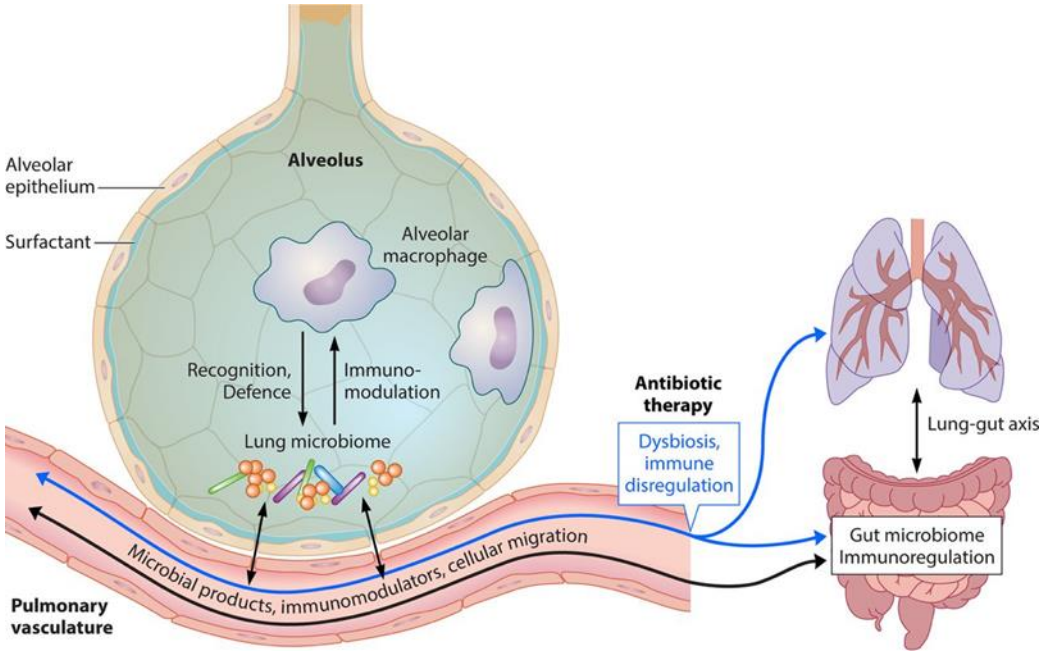

Figure 1.2. The gut-lung axis. Intestinal and pulmonary microbiota can interact directly and regulate lung immunity through cellular migration, microbial products, and immunomodulators (From Hong et al., 2016).

Lung Microbiome and Tuberculosis

M. tuberculosis is an extremely successful microorganism that undoubtedly has co-evolved with the human. For instance, Egyptian mummies dated from 2050 BC to 500 BC have been positive for *M. tuberculosis* (Zink et al., 2003). Besides, to date, it has been estimated that virtually one-third of the world population is infected with *M. tuberculosis* causing 1.4 million deaths per year (Koeken et al., 2019). Therefore, a thorough understanding of how the lung microbiome interacts with immune cells and influences the innate and adaptive immune response to *M. tuberculosis* is essential for developing new prevention and treatment strategies. Few studies had focused on changes in the lung and gut microbiome during *M. tuberculosis* infection or after BCG vaccination. Understanding

how the gastrointestinal microbiome may influence the lung microbiome and *M. tuberculosis* immune response will require a deep comprehension of microbial metabolites and pathways.

Some interesting studies are worthy of mention due to the relationship that certain bacteria have on *M. tuberculosis* immune response and vaccination. Reports show that individuals with latent TB infection (LTBI) and seropositive for *Helicobacter pylori* tend to have a high Th1 immune response and are less likely to develop active TB disease. Additionally, gut microbiome depleted mice through broad-spectrum antibiotics show higher susceptibility to *M. tuberculosis* and are more likely to disseminate *M. tuberculosis* to the liver and spleen. After gut microbiome depletion, *M. tuberculosis* dissemination may be explained due to an increased number of Treg cells and a reduced Th1 immune response (Namasivayam et al., 2018; Gupta et al., 2018). Bacterial diversity, obtained from sputum samples, tends to increase in TB patients compared with healthy controls, showing a unique set of bacteria including *Stenotrophomonas*, *Cupriavidus*, *Pseudomonas*, *Thermus*, *Sphingomonas*, *Methylobacterium*, *Diaphorobacter*, *Comamonas*, and *Mobilicoccus*. Overall, Firmicutes and Actinobacteria tend to dominate the sputum of TB patients, and Bacteroides and Proteobacteria tend to be higher in healthy individuals (Gupta et al., 2018).

Metabolic products of certain bacteria are present in the lung as SCFAs affecting TB outcomes. It has been observed that HIV positive individuals with increased production of butyric acid and propionic acid by *Prevotella* have a higher incidence of active TB. Butyrate inhibits Th17/Th1 immune responses to *M. tuberculosis* and increase the *M. tuberculosis* antigen-specific Treg cells in the lung (Gupta et al., 2018).

How TB drugs and vaccines may affect the lung microbiome is another question that has to be considered in developing new strategies to prevent TB.

Cellular Components in the Immune response to *M. tuberculosis*

Cellular Innate Immune Response to *M. tuberculosis*

The airway epithelial cells are the first barrier of airborne microorganisms, and therefore, they are the first cells encountering *M. tuberculosis*. Epithelial cells play a role in binding, recognizing, and internalizing *M. tuberculosis*, followed by the initiation of immune responses (Khader et al., 2019). After the first encounter with *M. tuberculosis*, airway epithelial cells express a variety of Pathogen recognition receptors (PRRs) such as TLRs, Retinoic acid-inducible gene I (RIG-1)-like receptors, Nucleotide-binding oligomerization domain-containing protein (NOD)-like receptors, and C-type lectins (Kaufmann et al., 2018, Bekale et al., 2019, Khade et al., 2019). The recognition of *M. tuberculosis* through these receptors induces cytokine production through the activation of different intracellular pathways. Some of the first cytokines and chemokines produced are TNF-α, IFN-γ, IL-6, IL-10, GM-CSF, IL-8, CXCL10, IL-27, Monocyte chemoattractant protein-1 (MCP-1), CXCL9. All these immune mediators induce the recruitment and activation of monocytes, lymphocytes, and polymorphonuclear cells to the lungs. Airway epithelial cells also express MHC-I, and therefore, may present intracellular antigens to resident CD8+ T cells. *M. tuberculosis*-immune cells early interactions include macrophages, DCs, neutrophils, NK cells as well as some non-conventional T cells such MAIT cells, γδ T cells, and NKT cells (Kaufmann et al., 2018, Gupta et al., 2018; Jiang et al., 2019; Pandey et al., 2019; Pean et al., 2019).

Macrophages play an essential role in *M. tuberculosis* pathogenesis, as they are the primary niche of *M. tuberculosis* in acute and chronic infections (Wang et al., 2015; Gupta et al., 2018; Shim et al., 2020). These cells can eliminate *M. tuberculosis* via nitrogen and oxygen-derived components, cytokines, phagosome acidification, and autophagy. Microenvironment signals drive macrophage differentiation to M1, M2, and myeloid suppressor cells (MSCs) populations (Weiss and Schaible, 2015). The M1 or classically activated macrophages produce immune-stimulatory cytokines such as IFN-γ, TNF-α, and GM-CSF. In contrast, M2 or alternatively activated macrophages are induced by IL-4, IL-13, IL-10, and TGF-β, which play a critical role in keeping the balance against an

exacerbated *M. tuberculosis* immune reaction (Kaufmann et al., 2018). MSCs have a similar function by secreting IL-10 and TGF-β, inducing T cells immunosuppression and regulating exacerbated inflammation. Macrophages are also a primary cellular type found in lung granulomas (Barry et al., 2009) (Figure 1.1). These exist in large numbers and various granulomas such as multinucleated giant cells, foamy cells, and epithelioid cells (Gupta et al., 2018). Foamy macrophages have a deficient ability to perform phagocytosis and antigen processing; *M. tuberculosis* mainly induces this through mycolic acids, lipopeptides, and early secretory antigen-6 (ESAT-6) (Russell et al., 2009, Liu et al., 2017, Huang et al., 2019).

DCs are key cell components in *M. tuberculosis* antigen presentation as they are the bridge between innate and adaptive immune response. DCs express mannose receptors (MRs) and DC-specific ICAM-grabbing nonintegrin (DC-SIGN) that can recognize the *M. tuberculosis* lipoprotein lprG and hexamannosylated phosphatidylinositol mannosides (PIMs) (Liu et al., 2017).

Neutrophils are the most abundant cell found in BAL of patients with active TB (Liu et al., 2017). Due to the presence of *M. tuberculosis*, neutrophils release elastase, collagenase, and myeloperoxidase, affecting both the surrounding host cells (lung parenchyma) and inducing *M. tuberculosis* damage.

NK cells have the cytolytic capacity and activity in the early phase of *M. tuberculosis* infection. Cell wall components of *M. tuberculosis*, such as mycolic acids, are ligands for the NKp44 receptor. In early infection, these cells are vital components that control mycobacterial growth through macrophage activation and produce cytoplasmic granules containing perforin, granulysin, and granzyme. The NK cells cytokine profile (IFN-γ, TNF-α, GM-CSF, IL-12, IL-22) can inhibit *M. tuberculosis* intracellular growth by enhancing phagolysosomal fusion and promoting γδ T cell proliferation (Liu et al., 2017). In mice, the depletion of NK cells at the time of BCG vaccination induces expansion of Treg cells and decreases the vaccine-induced protective immunity after challenge with *M. tuberculosis* (Gupta et al., 2018). Interestingly, in patients with active TB, NK cells have reduced

cytotoxicity and IFN-γ production and lower expression of NKp30 and NKp46, activating NK cell receptors (Liu et al., 2017).

MAIT cells are unique, innate cytotoxic T cells commonly present in blood and mucosal sites. These cells act in a non-classical MR1-restricted manner; they are stimulated by vitamin B metabolites from bacteria and yeast and respond with cytotoxicity and cytokine production (Wong et al., 2019). In response to *M. tuberculosis* infection, MAIT cells migrate from peripheral blood to the lung and induce the production of IFN-γ and TNF-α and secrete cytotoxic granules (Downey et al., 2019, Suliman et al., 2019).

The γδ T cells are a subset of CD3+ T cells that carry a T cell receptor encoding the Vγ and Vδ gene segments. These cells elicit immune responses through the interaction with DCs, CD8+ T cells, and NK cells and recognize non-peptide phosphate and unprocessed antigens. During early *M. tuberculosis* infection, γδ T cells are recruited to the lungs and express IFN-γ and IL-17, and they have also been found in high frequency in patients with active TB.

NKT cells express both NK and T cell markers and have regulatory and effector functions. It has been found that these cells have essential roles in *M. tuberculosis* pathogenesis in both humans and mice, producing IFN-γ, TNF-α, IL-17, IL-2, and IL-21. In mice, the administration of α-GalCer, an NKT cell agonist, improves the outcome of *M. tuberculosis* infection, and it has been found that patients with active TB usually have dysfunctional NKT cells (Gupta et al., 2018).

Cellular Adaptive Immune Response to *M. tuberculosis*

Indeed, the control of *M. tuberculosis* replication and protective immunity requires an adaptive immune response. The importance of CD4+ T cells has been shown in several studies. In the mouse model, infection with *M. tuberculosis*, for instance, mice rapidly die when they are CD4+ T cells depleted (Caruso et al., 1999), showing not only the importance of this cell but also that CD8+ T cells cannot control the infection by

themselves (Da Silva et al., 2015). Also, in the NHP model, CD4+ T cell depletion is enough to induce active TB disease (Sia and Rengarajan, 2019).

CD4+ T cells interact with infected macrophages to restrict *M. tuberculosis* intracellular replication. In mice, CD4+ T cells expressing the chemokine receptor CXCR3 are localized in the lung parenchyma and show more efficiency than those CD4+ T cells that are vasculature-restricted expressing CX3CR1, although these cells secrete higher IFN-γ after infection (Sakai et al., 2014, Sallin et al., 2017, Hoft et al., 2019). Overall, the production of IFN-γ by Th1 cells and CD8+ T cells is considered essential for *M. tuberculosis* control (Pasquinelli et al., 2009). Deficiencies in autosomal genes IFNGR1 and IFNGR2 and mutations affecting the IL-12 expression are fatal in patients with mycobacterial infections due to the inability to perform IFN-γ and IL-12 signaling. In general terms, IL-10 deficient mice tend to be less susceptible to *M. tuberculosis* infection in part due to an enhanced Th1 response. Some studies have also demonstrated that Th17, contributes to the immune response against *M. tuberculosis* (Lyadova and Panteleev 2015, Jean Bosco et al., 2018). Infections with the W-Beijing strain of *M. tuberculosis* induce Th17 immune responses, and mice deficient in IL-17 have an increased bacterial burden. Also, IL-17 receptor A subunit (IL-17RA) knockout mice show impaired control of *M. tuberculosis*. Besides, it has been found that healthy patients vaccinated with BCG have a high frequency of Th17 cell subset in their peripheral blood mononuclear cell (PBMC) and BAL compared with patients with active disease (Sia and Rengarajan, 2019).

Treg cells are another subset of CD4+ T cells that express Foxp3 and play a role in *M. tuberculosis* immunopathogenesis. These cells are a subset of T cells with immunosuppressing mechanisms through the production of IL-10, TGF- β, and IL-35 (Cardona and Cardona, 2019). These cells represent about 10% of the CD4+ T cells in lymphoid organs (Ito et al., 2019) and play a crucial role in preventing autoimmune diseases by their immunosuppressive action (Baecher-Allan et al., 2001; Sakagushi et al., 2008). The mechanisms of immune suppression and anti-inflammatory properties include consumption of IL-2, expression of CTLA4 (that inhibits CD28, which promotes T cell activation), and expression of IL-10 and TGF-β (Ito et al., 2019). Besides CD3 and

CD4, common phenotyping markers include Foxp3, CD25, CD39, and low levels of CD127. Recent studies have observed that thymic Tregs arise from two different progenitors: The CD25+Treg progenitor and the Foxp3^{lo} Treg progenitor. Unlike Foxp3^{lo} Treg progenitor, CD25+Treg progenitor shows a higher thymic self-antigens affinity (Owen et al., 2019). In the lung, Tregs control tissue damage, prevent fibrosis by controlling the expression of CXCL12, promote remodeling of extracellular matrix and the proliferation of alveolar cells (Ito et al., 2019). Treg cells have also been studied as a TB treatment marker. They increase their frequency in the blood during pulmonary and extrapulmonary TB and decrease with anti-TB drug therapy (Guyot-Revol et al., 2006; Burl et al., 2007). Treg cells increase in active TB (Kim et al., 2013; Lim et al., 2013), and inhibit the expansion of Th1 and CD8+ T cells and limit pulmonary inflammation and chronic disease (Sia and Rengarajan, 2019).

CD8+ T cells can kill infected cells and facilitate immunological memory. After the first encounter with an antigen, the naïve CD8+ T cell differentiates into antigen-specific central memory (TCM) and effector T cell (TEM). Later in life, in a second antigen encounter, TCM will expand and generate CD8+ T effector cells (Bohme et al., 2020). In general terms, these two T cell subsets differ in the presence or absence of lymph node homing markers. TCM are self-renewing, IL-2 producers, and CD62L+CCR7+; these markers allow them to recirculate through lymph nodes. TEMs lack these markers as they are usually found in non-lymphoid tissues (Gerritsen and Pandit 2016; Bohme et al., 2020). During chronic *M. tuberculosis* infection, CD8+ T cells develop mitochondrial deficiencies that result in increased glycolysis need. These changes sustain a suboptimal CD8+ T cell activity through the expression of terminal differentiation markers, a process called T cell exhaustion (Kurachi 2019). T cell activation, differentiation, and effector, and memory shifts require a suitable surrounding environment that may be altered by the T cell expression of immune checkpoint regulators such as PD-1 or CTLA-4. Recent studies have indicated that CD8+ T cells derived from *M. tuberculosis* infection are highly activated at the early stage of infection and continues until week 12 post-infection, showing upregulation of genes associated with T cell exhaustion (Russel et al., 2019). However, some studies have shown that metformin enhances CD8+ T survival and

increases oxidative phosphorylation and fatty acid oxidation. Regulation of T cell functions has also been observed in anticancer studies (Eikawa et al., 2015; Zhang, et al 2020). Similarly, in BCG-vaccinated guinea pigs, metformin enhances immunogenicity and protects against *M. tuberculosis* infection, as observed in a reduced *M. tuberculosis* load (Bohme et al., 2020). Mice depleted of CD8+ T cells live longer in *M. tuberculosis* infection studies than CD4+ T cells knockout mice. However, CD8+ T cells cytokines profiles, perforin, and granulysin play essential roles in limiting bacterial replication by activating macrophages or lysing *M. tuberculosis* infected macrophages (Zhang et al., 2011).

B cells are not only limited to antibody production; in fact, they can present antigens, produce cytokines (such as IL-4, IL-6, IL-12, and IFN-γ), modulate T cell immunity, and regulatory activities (known as regulatory B cells) through the production of IL-10, IL-35, and TGF-β). IL-35 producing B cells are present in a higher number in active TB patients (Dai et al., 2019; Lyashchenko et al., 2020). After immunization or *M. tuberculosis* infection, IgM receptors of naïve B cells can recognize T cell-dependent antigens, activate clones, and stimulate the development of plasma or B memory cells. Critical cells in this process also include Tfh and Antigen-presenting follicular dendritic cells (FDCs). The affinity of the B cell receptor with its antigen will stimulate the type of differentiation that they will develop: a higher affinity will select plasma cells, whereas a lower and intermediate affinity will select memory B cells and activated B cells, respectively (Linge et al., 2017; Lyashchenko et al., 2020). Humoral immunity may be essential to control initial (extracellular) *M. tuberculosis* infection. Moreover, it may avoid *M. tuberculosis* reactivation mechanisms within the granuloma through the FcR-mediated phagocytosis (Achkar et al., 2015). In addition, B cells, together with CD4+ and CD8+ T cells, are part of the lymphocytic cuff in the tuberculous granuloma suggesting a role in disease immunopathogenesis (Lyashchenko et at., 2020). Interestingly, B cell-depleted mice have an exacerbated neutrophilic recruitment and inflammation in the lung after *M. tuberculosis* challenge (Achkar et al., 2015; Sia and Rengarajan, 2019).

M. tuberculosis exposure does not confer immune memory by itself and instead follows complex pathogenesis. As discussed above, the CD4+ and CD8+ T cells play a significant

role during infection, and cytokines TNF-α and IFN-γ are critical components of immunity to infection. All these cells and cytokines will contain the infection and generate the granuloma, limiting tissue damage.

The BCG Vaccine

An effective vaccine is the one that is given to a young population without adverse side effects and confers long-lasting immunity thanks to immunological memory. The immunological memory is established after the first encounter with a pathogen, resulting in memory cell development. These cells may reside in tissue and lymph nodes and become activated after a second encounter with that pathogen to eliminate it and prevent disease. A vaccine may be developed with pathogen-derived components, live attenuated, killed, or inactivated bacterial toxins. Thus, the vaccine will have the key components to induce immune response and memory but lacking the capacity to induce disease. Therefore, if a vaccinated individual is exposed to the pathogen, the immune system will eliminate the pathogen and will prevent the disease.

The *M. bovis* Bacillus Calmette-Guérin (BCG) vaccine has been the most widely administered vaccine against an infectious agent and is the only one to control TB. BCG has been delivered to more than 3.5 billion people around the world (Ernst, 2012). However, this vaccine confers limited protection and how this protection occurs is not fully understood (Tran et al., 2014; MacDonald and Izzo, 2015).

The vaccine was developed by Albert Calmette and Camille Guérin in the early 1900s. It was developed from a virulent strain of *M. bovis* and attenuated by serial passing on potato slices supplemented with glycerol over 13 years (Netea and Crevel, 2014; Tran et al., 2014; Fatima et al., 2020). The attenuated strain was then tested in cows, monkeys, and apes. Finally, the vaccine was administered orally in humans in 1921. The strain was then sent out to laboratories worldwide and propagated in different ways with varying passage numbers, leading to the development of different variants of the vaccine (Tran et al., 2014; MacDonald and Izzo, 2015).

The cost-effectiveness of the vaccine and its partial protection makes BCG one of the best options to control TB. Thus, Denmark, Japan, and Russia are the primary BCG vaccine produces (Tran et al., 2014). Several countries worldwide, except for the US, Canada, and Italy, require children to be BCG vaccinated during childhood due to the WHO's expanded vaccination program (MacDonald and Izzo, 2015).

The variability in the efficacy of BCG vaccination is from 80% to no protection at all. This variability may have different reasons; one of them can be the BCG strain variation (Luo et al., 2009; Pai et al., 2016), at least 11 different types of BCG vaccine administered around the world. A sequence of independent mutations of the BCG vaccine occurred after Calmette and Guérin sent out the vaccine to other laboratories, due to differences in growth and storage methods. The genetic variation of the BCG strains could affect protection against infection due to changes in the cells' surface proteins (Sorensen et al., 2015; MacDonald and Izzo, 2015).

The vaccinated population's genetic diversity can be another reason for the variability in BCG vaccine efficacy (Pai et al., 2016). In general terms, any vaccine testing trial must consider the genetic diversity in the population. Single nucleotide polymorphisms within the genome can affect how an individual responds to infection or vaccination. For instance, mutations in the IFN-γ receptors increase the risk of disseminated disease following BCG vaccination. In addition, the impact other vaccines may have on the efficacy of BCG is another point to consider (MacDonald and Izzo, 2015; Butkeviciute et al., 2018).

Preexposure to the pathogen can also affect vaccine efficacy. The immune response of an individual previously exposed to *M. tuberculosis* or environmental nontuberculous mycobacteria (NTM) may be different from a person not previously exposed. Studies suggest that preexposure to NTM in children may confer some protection that the BCG vaccine cannot improve (Demangel et al., 2005; Poyntz et al., 2014). Finally, inaccurate diagnostic methods to determine previous exposure and non-exposure in individuals in a

population included in the vaccine efficacy may be conducive to bias (MacDonald and Izzo, 2015; Verma et al., 2020).

Animal Models used for Vaccine Efficacy Studies

There are advantages and disadvantages to the use of animal models. In general, a TB vaccine is considered to be effective in the animal model if it can reduce the colony forming units (CFU) in the lung by more than one Log_{10} CFU (MacDonald and Izzo, 2015). One Log_{10} CFU reduction represents approximately 90% reduction in the mycobacterial burden.

Mouse model

Advantages in using the mouse model for vaccine development are the cost-effectiveness, the access to inbred strains and genetically modified models, the availability of immunological reagents, and the mouse susceptibility to various *M. tuberculosis* strains (Bharath and Balasubramanian, 2011, MacDonald and Izzo, 2015). The Jackson and Charles Rivers Laboratories are two of the leading producers of inbred and genetically modified mice. The vast availability of knockout and knock-in models allows questions that would be unavailable by other methods. The availability of immunological reagents is another tremendous advantage to the use of the mouse model. Molecular assays are available from different resources after completion of the *in vivo* study. Antibodies are widely used for western blot, enzyme-linked immunosorbent assays (ELISA), and flow cytometry in the mouse model. The availability of mouse strains is also an important issue to consider in tuberculosis studies (Orme, 2016). There are different mouse strains with different susceptibility to *M. tuberculosis* infection, depending on factors as the route of infection, the dosage, and the *M. tuberculosis* strain. In general terms, C57BL/6 and BALB/c mice are resistant, and CBA, DBA/2, 129SvJ and C3HeB/FeJ are susceptible mice strains (Cooper 2015). Also, the mouse model itself differs in many ways in the human immune response and respiratory anatomy. For instance, mouse bronchial tree and lymphatics are less complex, and the vascular supply lacks a second circulatory supply with bronchial-associated lymphoid tissue (Orme,

2003). In terms of infection, immune cells use the same chemokines, integrins, and selectins, but the pathology is different. In some mouse strains, granulomas typically have a central accumulation of lymphocytes instead of the classical central necrosis observed in humans and guinea pig models. C3HeH/FeJ, and humanized mice are the mice that more closely resemble the human lung pathology after *M. tuberculosis* infection (Orme, 2003; Singh and Gupta, 2018).

Pulmonary TB in the mouse model

The *M. tuberculosis* H37Rv strain grows logarithmically in the lungs of BALB/c mice within the first three weeks following an aerosol exposure route of 100 CFU per animal. By week four, the bacterial load reaches approximately $5x10^5$ to $1x10^6$ CFU, and beyond four weeks, the bacterial growth slows down, and remains relatively constant (Barath and Balasubramanian, 2011). Early immune responses in the lung are characterized by the recruitment of neutrophils, IMs, and DCs. These cells become infected and form an early granuloma (Ernst, 2012). Visible lung lesions appear on the lung surface by week four, growing from pinpoint to 2 mm of diameter at this time. By eight weeks (early chronic phase), multiple pale and granulomatous lesions appear with diameters of 2-3 mm. At this time, the typical parenchyma architecture, the airway, and the alveolar spaces are affected by the infiltration of inflammatory cells (Orme and Ordway, 2016). By 20 weeks post-infection, lesions arise in the lung surface with around 5 mm of diameter, and in some cases, spread to half of the lung lobe. Foam cells, histocytes, and lymphocytes fill the perivascular and peribronchiolar regions and granulomatous bronchopneumonia is observed. The central necrotic granuloma, calcified lesions, and cavitary lesions are not observed in most mouse models but are present in human tuberculosis (Barath and Balasubramanian, 2011).

Guinea pig model

The guinea pig model is considered a gold standard to test *M. tuberculosis* vaccines and is the typical animal model to test before scaling to a larger animal model and humans (Orme and Ordway, 2016). This is because the guinea pig immune response resembles that of susceptible humans, showing similar pathogenesis. However, there is a lack of

inbred models that limit the experiment repeatability (Clark et al., 2015). Also, housing cost increases compared with the mouse model, needing larger cages and more space, thus reducing the number of animals included in a study. Moreover, adequate facilities for housing and veterinary expertise are needed (Basaraba and Orme, 2011).

Pulmonary TB in the guinea pig model

It is essential to consider some unique anatomic characteristics of the guinea pig respiratory system. The guinea pig pleura, in contrast with humans, has a thin layer of fibrous connective tissue. In humans, the terminal bronchioles end in respiratory bronchioles, but in guinea pigs, they end in alveolar ducts or a very low developed respiratory bronchiole (Clark et al., 2015). The clinical and pathologic characteristics of infected guinea pigs depend on the host and pathogen characteristics. The guinea pig immune status, dose, virulence, and strain influence disease progression. In general terms, with a low-dose aerosol, at day 15, histiocytes, lymphocytes, and granulocytes start forming infiltrates to form the granuloma (Basaraba and Orme, 2011).

In this animal model, four-stage pulmonary lesions after *M. tuberculosis* infection (strain Erdman TMCC 107) have been observed. All these stages are in a dynamic process controlled by the production and interaction of cytokines and chemokines, whose objective is to control bacterial dissemination (Ly et al., 2008). In the first stage (11 days after infection), the number of lymphocytes is minimal, and they do not show cellular organization. Epithelioid macrophages and granulocytes are prominent and scattered. In the second stage (21 days post-infection), the extent of lesions becomes multifocal, with epithelioid macrophages. Lymphocytes continue being in a few numbers; however, granulocytes are prominent and scattered around and in the core. At this point, it is observed fibrin deposition, fibroplasia, and granulomatous lymphadenitis. The third stage (day 31 post-infection) the classical granuloma with necrosis and fibroplasia is observed, and macrophages look epithelioid and foamy. In stage four, is observed scattered granulocytes throughout macrophage focus, and necrosis, mineralization, multinucleated giant cells, and purulent airway exudate is observable (Gonzalez-Juarrero et al., 2001; Turner et al., 2003; Orme and Basaraba, 2014).

Macaques

The pathogenesis of pulmonary TB in macaques and NHP closely resembles the human, including the latency stage of the disease. Most of the extrapulmonary manifestations reported in humans, such as skeletal, milliary, meningitis, cerebral, cardiac, and ocular TB, have been observed in the macaque model (Sharpe et al., 2016). However, due to the size of animals, the limited availability, the high cost and care, and the ethical considerations, the use of NHP is minimal and done after several vaccine studies have been tested in smaller animals (Flynn and Klein, 2011).

Pulmonary TB in the macaque model

The macaque infection model can mimic all pathological and clinical manifestations of human TB, including latent and active infection and reactivation. Intratracheal instillation or aerosol delivery is the usual way of infection in the model, and the inoculum varies depending on the study (Maiello et al., 2018). In vaccination studies, a high dose is commonly used (1000-3000 CFU). A low dose of 25 CFU is enough to induce active disease or latent infection within 6 to 8 months after infection in equal proportions. It is also possible to increase the incidence of active disease with a higher dose. Most of the macaques' infection studies have been done with the Erdman or H37Rv strains (Flynn and Klein, 2011; Hansen et al., 2018; Darrah et al., 2020).

The acute phase of the disease occurs within eight weeks post-inoculation. The first granulomatous lesions may develop in a non-necrotizing form. These lesions may be found in both lung and lymph nodes when associated with disseminated disease. Lesions then become necrotizing with central eosinophilic debris and epithelioid histiocytes surrounding the central necrosis (Maiello et al., 2018). Chronic lesions vary depending on the immunological balance. The granulomas at 3-5 months post infections are characterized by fibrous central organization in necrotizing granulomas with collagen fibers and some mineralization. Latent TB is usually observed in monkeys infected with a low dose. In this case, lesions are more difficult to observe and commonly limited to very small subpleural or interstitial granuloma (Flynn and Klein, 2011).

Cavitated granulomas and suppurative granulomas are also observed in macaques and occur in active TB (Zhang et al., 2018). The common characteristics observed in humans during TB reactivation is also reproducible in the NHP model and may occur at any point, including three years after infection. TB reactivation is characterized by chronic and acute histological lesions such as mineralization, necrotizing and non-necrotizing granulomas, and tuberculous pneumonia (Flynn and Klein, 2011).

The TB epidemiologic, economic, and social impact in the community makes the disease necessary to research. For decades, efforts have been made to develop and improve vaccines, drugs, and diagnosis. Many aspects of the immune response to *M. tuberculosis* and the role that the lung microbiome plays during *M. tuberculosis* infection is unknown. Thus, new research approaches are essential to control and eradicate this disease. A better understanding of the immunopathogenesis of *M. tuberculosis* needs to incorporate physiological knowledge and lung and gut microbiome studies. Therefore, future work studying BCG vaccination strategies and the importance of lung and gut microbiome play during *M. tuberculosis* infection are essential.
Thus, this research is primarily focused on two approaches:

1. To compare the immunity of BCG vaccination through the study of different routes of vaccination.
2. To assess the role of lung and gut microbiome interaction during *M. tuberculosis* infection and the effect of potential microbiome changes in protection after BCG vaccination.

References

Aung, H.H., A. Sivakumar, S.K. Gholami, S.P. Venkateswaran, B. Gorain, S. Md. An Overview of the Anatomy and Physiology of the lung. Chapter 1.

Bekale, R.B., Du Plessis, S.M., Hsu, N.J., Sharma, J.R., Sampson, S.L., Jacobs, M., Meyer, M., Morse, G.D., and Dube, A. (2019). Mycobacterium Tuberculosis and Interactions with the Host Immune System: Opportunities for Nanoparticle Based Immunotherapeutics and Vaccines. Pharm Res-Dordr 36.

Bosco, M.J., Wei, M., Hou, H.Y., Yu, J., Lin, Q., Luo, Y., Sun, Z.Y., and Wang, F. (2018). 1The exhausted CD4(+)CXCR5(+) T cells involve the pathogenesis of human tuberculosis disease. Int J Infect Dis 74, 1-9.

Brand-Saberi, B.E.M., and Schafer, T. (2014). Trachea: Anatomy and Physiology. Thorac Surg Clin 24, 1-+.

Bunker, J.J., and Bendelac, A. (2018). IgA Responses to Microbiota. Immunity 49, 211-224.

Burl, S., Hill, P.C., Jeffries, D.J., Holland, M.J., Fox, A., Lugos, M.D., Adegbola, R.A., Rook, G.A., Zumla, A., McAdam, K.P.W.J., and Brookes, R.H. (2007). FOXP3 gene expression in a tuberculosis case contact study. Clin Exp Immunol 149, 117-122.

Caruso, A.M., Serbina, N., Klein, E., Triebold, K., Bloom, B.R., and Flynn, J.L. (1999). Mice deficient in CD4 T cells have only transiently diminished levels of IFN-gamma, yet succumb to tuberculosis. Journal of Immunology 162, 5407-5416.

Clark, S., Hall, Y., and Williams, A. (2015). Animal Models of Tuberculosis: Guinea Pigs. Csh Perspect Med 5.

da Silva, M.V., Tiburcio, M.G.S., Machado, J.R., Silva, D.A.A., Rodrigues, D.B.R., Rodrigues, V., and Oliveira, C.J.F. (2015). Complexity and Controversies over the Cytokine Profiles of T Helper Cell Subpopulations in Tuberculosis. J Immunol Res 2015.

Davenport, E.R., Sanders, J.G., Song, S.J., Amato, K.R., Clark, A.G., and Knight, R. (2017). The human microbiome in evolution. BMC Biol 15, 127.

Downey, A.M., Kaptonek, P., and Seeberger, P.H. (2019). MAIT cells as attractive vaccine targets. Febs Letters 593, 1627-1640.

Enaud, R., Vandenborght, L.E., Coron, N., Bazin, T., Prevel, R., Schaeverbeke, T., Berger, P., Fayon, M., Lamireau, T., and Delhaes, L. (2018). The Mycobiome: A Neglected Component in the Microbiota-Gut-Brain Axis. Microorganisms 6.

Ernst, J.D. (2012). The immunological life cycle of tuberculosis. Nat Rev Immunol 12, 581-591.

Garaeva, A.F., Babushkina, N.P., Rudko, A.A., Goncharova, I.A., Bragina, E.Y., and Freidin, M.B. (2017). Differential genetic background of primary and secondary tuberculosis in Russians. Meta Gene 11, 178-180.

Gupta, N., Kumar, R., and Agrawal, B. (2018). New Players in Immunity to Tuberculosis: The Host Microbiome, Lung Epithelium, and Innate Immune Cells. Front Immunol 9, 709.

Hanshew, A.S., Jette, M.E., Rosen, S.P., and Thibeault, S.L. (2017). Integrating the microbiota of the respiratory tract with the unified airway model. Resp Med 126, 68-74.

Hoft, S.G., Sallin, M.A., Kauffman, K.D., Sakai, S., Ganusov, V.V., and Barber, D.L. (2019). The Rate of CD4 T Cell Entry into the Lungs during Mycobacterium tuberculosis Infection Is Determined by Partial and Opposing Effects of Multiple Chemokine Receptors (vol 87, e00841-18, 2019). Infection and Immunity 87.

Huang, L., Nazarova, E.V., and Russell, D.G. (2019). Mycobacterium tuberculosis: Bacterial Fitness within the Host Macrophage. Microbiol Spectr 7.

Invernizzi, R., Lloyd, C.M., and Molyneaux, P.L. (2020). Respiratory microbiome and epithelial interactions shape immunity in the lungs. Immunology 160, 171-182.

Jacobs, J.P., and Braun, J. (2014). Immune and genetic gardening of the intestinal microbiome. FEBS Lett 588, 4102-4111.

Jagodzinski, A., Zielinska, E., Laczmanski, L., and Hirnle, L. (2019). The early years of life. Are they influenced by our microbiome? Ginekol Pol 90, 228-232.

Kaufmann, E., Sanz, J., Dunn, J.L., Khan, N., Mendonca, L.E., Pacis, A., Tzelepis, F., Pernet, E., Dumaine, A., Grenier, J.C., et al. (2018). BCG Educates Hematopoietic Stem Cells to Generate Protective Innate Immunity against Tuberculosis. Cell 172, 176-+.

Khader, S.A., Divangahi, M., Hanekom, W., Hill, P.C., Maeurer, M., Makar, K.W., Mayer-Barber, K.D., Mhlanga, M.M., Nemes, E., Schlesinger, L.S., et al. (2019). Targeting innate immunity for tuberculosis vaccination. Journal of Clinical Investigation 129, 3482-3491.

Koeken, V., Verrall, A.J., Netea, M.G., Hill, P.C., and van Crevel, R. (2019). Trained innate immunity and resistance to Mycobacterium tuberculosis infection. Clin Microbiol Infect 25, 1468-1472.

Ladjemi, M.Z., Lecocq, M., Weynand, B., Bowen, H., Gould, H.J., Van Snick, J., Detry, B., and Pilette, C. (2015). Increased IgA production by B-cells in COPD via lung epithelial interleukin-6 and TACI pathways. Eur Respir J 45, 980-993.

Liu, C.H., Liu, H., and Ge, B. (2017). Innate immunity in tuberculosis: host defense vs pathogen evasion. Cell Mol Immunol 14, 963-975.

Lyadova, I.V., and Panteleev, A.V. (2015). Th1 and Th17 Cells in Tuberculosis: Protection, Pathology, and Biomarkers. Mediat Inflamm 2015.

Lyashchenko, K.P., Vordermeier, H.M., and Waters, W.R. (2020). Memory B cells and tuberculosis. Vet Immunol Immunop 221.

Maiello, P., DiFazio, R.M., Cadena, A.M., Rodgers, M.A., Lin, P.L., Scanga, C.A., and Flynn, J.L. (2018). Rhesus Macaques Are More Susceptible to Progressive Tuberculosis than Cynomolgus Macaques: a Quantitative Comparison. Infection and Immunity 86.

Marchant, W. (2005). Anatomy of the Larynx, Trachea and Bronchi. Anesthesia and Intensive care medicine 6:8.

Mack, S.M., Wu, C-W., Zhang, C., Harding, R., Pinkerton, K.E. (2020). Lung Anatomy and Aging.

Mathieu, E., Escribano-Vazquez, U., Descamps, D., Cherbuy, C., Langella, P., Riffault, S., Remot, A., and Thomas, M. (2018). Paradigms of Lung Microbiota Functions in Health and Disease, Particularly, in Asthma. Front Physiol 9, 1168.

McCoy, K.D., Burkhard, R., and Geuking, M.B. (2019). The microbiome and immune memory formation. Immunol Cell Biol 97, 625-635.

Murray, J.F. (2010). The structure and function of the lung. Int J Tuberc Lung Dis 14, 391-396.

Nash, A.K., Auchtung, T.A., Wong, M.C., Smith, D.P., Gesell, J.R., Ross, M.C., Stewart, C.J., Metcalf, G.A., Muzny, D.M., Gibbs, R.A., et al. (2017). The gut mycobiome of the Human Microbiome Project healthy cohort. Microbiome 5, 153.

Neumuller, G., Kiprov, S., and Szendey, B. (1994). [Radiology in tuberculosis]. Wien Med Wochenschr 144, 168-173.

Noecker, C., McNally, C.P., Eng, A., and Borenstein, E. (2017). High-resolution characterization of the human microbiome. Transl Res 179, 7-23.

Orme, I.M., and Ordway, D.J. (2016). Mouse and Guinea Pig Models of Tuberculosis. Microbiology Spectrum 4.

Pai, M., Behr, M.A., Dowdy, D., Dheda, K., Divangahi, M., Boehme, C.C., Ginsberg, A., Swaminathan, S., Spigelman, M., Getahun, H., et al. (2016). Tuberculosis. Nature Reviews Disease Primers 2.

Pasquinelli, V., Townsend, J.C., Jurado, J.O., Alvarez, I.B., Quiroga, M.F., Barnes, P.F., Samten, B., and Garcia, V.E. (2009). IFN-gamma Production during Active Tuberculosis Is Regulated by Mechanisms That Involve IL-17, SLAM, and CREB. Journal of Infectious Diseases 199, 661-665.

Qamar, A., Aboudola, S., Warny, M., Michetti, P., Pothoulakis, C., LaMont, J.T., and Kelly, C.P. (2001). Saccharomyces boulardii stimulates intestinal immunoglobulin A immune response to Clostridium difficile toxin A in mice. Infect Immun 69, 2762-2765.

Quintin, J., Saeed, S., Martens, J.H.A., Giamarellos-Bourboulis, E.J., Ifrim, D.C., Logie, C., Jacobs, L., Jansen, T., Kullberg, B.J., Wijmenga, C., et al. (2012). Candida albicans infection affords protection against reinfection via functional reprogramming of monocytes. Cell Host Microbe 12, 223-232.

Ramakrishnan, L. (2012). Revisiting the role of the granuloma in tuberculosis. Nature Reviews Immunology 12, 352-366.

Rizzetto, L., Ifrim, D.C., Moretti, S., Tocci, N., Cheng, S.C., Quintin, J., Renga, G., Oikonomou, V., De Filippo, C., Weil, T., et al. (2016). Fungal Chitin Induces Trained Immunity in Human Monocytes during Cross-talk of the Host with Saccharomyces cerevisiae. J Biol Chem 291, 7961-7972.

Russell, D.G., Cardona, P.J., Kim, M.J., Allain, S., and Altare, F. (2009). Foamy macrophages and the progression of the human tuberculosis granuloma. Nature Immunology 10, 943-948.

Sakai, S., Kauffman, K.D., Schenkel, J.M., McBerry, C.C., Mayer-Barber, K.D., Masopust, D., and Barber, D.L. (2014). Cutting Edge: Control of Mycobacterium

tuberculosis Infection by a Subset of Lung Parenchyma-Homing CD4 T Cells. Journal of Immunology 192, 2965-2969.
Sallin, M.A., Sakai, S., Kauffman, K.D., Young, H.A., Zhu, J.F., and Barber, D.L. (2017). Th1 Differentiation Drives the Accumulation of Intravascular, Non-protective CD4 T Cells during Tuberculosis. Cell Reports 18, 3091-3104.
Sharpe, S.A., White, A.D., Sibley, L., Gleeson, F., Hall, G.A., Basaraba, R.J., McIntyre, A., Clark, S.O., Gooch, K., Marsh, P.D., et al. (2017). An aerosol challenge model of tuberculosis in Mauritian cynomolgus macaques. Plos One 12.
Shi, N., Li, N., Duan, X., and Niu, H. (2017). Interaction between the gut microbiome and mucosal immune system. Mil Med Res 4, 14.
Shiraishi, K., Nakajima, T., Shichino, S., Deshimaru, S., Matsushima, K., and Ueha, S. (2019). In vitro expansion of endogenous human alveolar epithelial type II cells in fibroblast-free spheroid culture. Biochem Bioph Res Co 515, 579-585.
Sia, J.K., and Rengarajan, J. (2019). Immunology of Mycobacterium tuberculosis Infections. Microbiol Spectr 7.
Silbergeld, E.K. (2017). The Microbiome. Toxicol Pathol 45, 190-194.
Suliman, S., Murphy, M., Musvosvi, M., Gela, A., Meermeier, E.W., Geldenhuys, H., Hopley, C., Toefy, A., Bilek, N., Veldsman, A., et al. (2019). MR1-Independent Activation of Human Mucosal-Associated Invariant T Cells by Mycobacteria. Journal of Immunology 203, 2917-2927.
Thaiss, C.A., Zmora, N., Levy, M., and Elinav, E. (2016). The microbiome and innate immunity. Nature 535, 65-74.
Thomas, S., Izard, J., Walsh, E., Batich, K., Chongsathidkiet, P., Clarke, G., Sela, D. A., Muller, A. J., Mullin, J. M., Albert, K. (2017). The Host Microbiome Regulates and Maintains Human Health: A Primer and Perspective for Non-Microbiologists. Cancer Res.15, 1783–1812.
Thomas, S., Metzke, D., Schmitz, J., Dorffel, Y., and Baumgart, D.C. (2011). Anti-inflammatory effects of Saccharomyces boulardii mediated by myeloid dendritic cells from patients with Crohn's disease and ulcerative colitis. Am J Physiol Gastrointest Liver Physiol 301, G1083-1092.
Tran, V., Liu, J., and Behr, M.A. (2014). BCG Vaccines. Microbiol Spectr 2, MGM2-0028-2013.
Wang, J., Li, B.X., Ge, P.P., Li, J., Wang, Q., Gao, G.F., Qiu, X.B., and Liu, C.H. (2015). Mycobacterium tuberculosis suppresses innate immunity by coopting the host ubiquitin system. Nat Immunol 16, 237-245.
Weiss, G., and Schaible, U.E. (2015). Macrophage defense mechanisms against intracellular bacteria. Immunol Rev 264, 182-203.
Wong, E.B., Gold, M.C., Meermeier, E.W., Xulu, B.Z., Khuzwayo, S., Sullivan, Z.A., Mahyari, E., Rogers, Z., Kloverpris, H., Sharma, P.K., et al. (2019). TRAV1-2(+) CD8(+) T-cells including oligoconal expansions of MAIT cells are enriched in the airways in human tuberculosis. Commun Biol 2.
Wu, B.G., and Segal, L.N. (2018). The Lung Microbiome and Its Role in Pneumonia. Clin Chest Med 39, 677-689.

Zhang, J., Guo, M., Rao, Y., Wang, Y., Xiang, Q.Y., Yu, Q., Huang, Z.X., Wang, X., Bao, R., Yue, J.Q., et al. (2018). Mycobacterium tuberculosis Erdman infection of cynomolgus macaques of Chinese origin. J Thorac Dis 10, 3609-3621.

Zhang, Z., Li, F., Tian, Y., Cao, L., Gao, Q., Zhang, C., Zhang, K., Shen, C., Ping, Y., Maimela, N. R., et al. (2020). Metformin Enhances the Antitumor Activity of CD8 + T Lymphocytes via the AMPK-miR-107-Eomes-PD-1 Pathway. J Immunol 204, 2575-2588.

Zhang, M.X., Wang, Z., Graner, M.W., Yang, L., Liao, M.F., Yang, Q.T., Gou, J.Z., Zhu, Y.Z., Wu, C., Liu, H.Y., et al. (2011). B cell infiltration is associated with the increased IL-17 and IL-22 expression in the lungs of patients with tuberculosis. Cell Immunol 270, 217-223.

Zimmermann, P., and Curtis, N. (2018). The influence of the intestinal microbiome on vaccine responses. Vaccine 36, 4433-4439.

Zink, A.R., Sola, C., Reischl, U., Grabner, W., Rastogi, N., Wolf, H., and Nerlich, A.G. (2003). Characterization of Mycobacterium tuberculosis complex DNAs from Egyptian mummies by spoligotyping. J Clin Microbiol 41, 359-367.

Chapter II

Alternative routes for BCG vaccination in a murine model

Introduction

Since its introduction in the 1920s, BCG has been the most widely administered vaccine, and it remains the only licensed vaccine against TB (Ritz et al., 2008; Abebe, 2012, Shah et al., 2019; White et al., 2020). The BCG vaccine originated by continuous *in vitro* passages and was initially administered orally; however, since the 1970s, it has been intradermally administered worldwide (Abebe, 2012; Horvath and Xing, 2013; Aguilo et al., 2016; Darrah et al., 2020). In humans, intradermal BCG induces protection against extrapulmonary, and meningeal tuberculosis associated with pediatric cases; however, it is not effective against the adult pulmonary form (Hawkridge, 2009). Other reports have estimated that BCG is at best effective in 80% of the vaccinated, and in most of the cases, the protection lasts only 10 to 15 years (Brandt et al., 2002; Aronson et al., 2004; Pan et al., 2011; Abebe, 2012; Mangtani et al., 2014; Moliva et al., 2015). The reasons behind the poor and highly variable protection of BCG in adults are not entirely understood. However, it has been suggested that the genetic variability of a population caused by Single nucleotide polymorphisms (SNPs), the pre-exposition to non-tuberculous mycobacteria (NTM) and the use of different BCG substrains may explain some variability (Shah et al., 2019).

SNPs may cause variability in the effectiveness of the BCG vaccine by affecting cell signaling in the innate and adaptive immune responses (Messina et al., 2020). For instance, IFN-γ (Anuradha et al., 2008; Conceição et al., 2016), Natural resistance-associated macrophage protein 1 (NRAMP1) (Badawy et al., 2013) and Toll-interacting protein (TOLLIP) (Shah et al., 2017) SNPs directly impact the efficacy of the BCG vaccine. Exposure to NTM is one of the most accepted hypotheses to explain the BCG vaccination variability. In places such as Africa and India, where the exposure to NTM is higher,

vaccination confers low or non-detectable protection (Brandt et al., 2002). Besides, further studies have indicated that the absence of mycobacterial exposure before vaccination is associated with higher BCG efficacy (Poyntz et al., 2014; Cha et al., 2015). Some explanations behind the poor immunity observed in NTM preexposure individuals is that if BCG cannot multiplicate (because of the pre-existing immune response to NTM), it will not induce protective immunity (Dockrell and Smith, 2017; Fatima et al., 2020).

It has been estimated that more than 20 genetically distinct BCG vaccines have been used worldwide (Ritz et al., 2012). Several laboratories have generated such genetic diversity by subsequent passages of the BCG vaccine. The predominant BCG substrains produced, distributed, and administered are Denmark/Copenhagen strain 1331, Japanese/Tokyo strain 172, and Russian/Moscow, with similar protective results. The four substrains generated in China have considerable differences in the recovery of CFU of *M. tuberculosis*: from similar results with Danish 1331 strain (BCG Beijing) to complete lack of protection (BCG Chanchun) (Moliva et al., 2015). The whole-genome sequencing of BCG-China, BCG-Denmark 1331, BCG Russia, and BCG-Tice has shown that these strains differ in more than ten SNPs (Pan et al., 2011). Similarly, another study comparing 13 different BCG strains (BCG Frappier, BCG Glaxo, BCG Moreau, BCG Phipps, BCG Prague, BCG Sweden, BCG China, BCG Tice, BCG Russia, BCG Danish, BCG Mexico, BCG Tokyo, and BCG Pasteur) identified more than 2,000 SNPs and 25 Regions of deletion (RD) (Zhang et al., 2013).

In the last decades, many efforts have been made to develop an effective vaccine against *M. tuberculosis*, and even though BCG confers variable protection, the World health organization (WHO) continues advising neonatal BCG vaccination in countries with a high incidence of TB (WHO., 2018). An additional reason to continue using the BCG vaccine includes its proven protection and decrease of mortality rates in infants and adults against other infectious diseases such as influenza A (H1N1), acute lower and upper respiratory infections, and COVID-19 (Yitbarek et al., 2020).

Some studies have suggested that BCG vaccination may confer better protection depending on the administration route. Vaccination through the natural route of infection and the combination of routes (e.g., intranasal, intravenous, subcutaneous, intramuscular, and intratracheal) have been studied in animal models with variable results (Lyadova et al., 2001; White et al., 2015, Perdomo et al., 2016, Sharpe et al., 2016, White et al., 2020, Darrah et al., 2020). Intradermal and intramuscular vaccination are the most common parenteral routes of vaccination; however, they confer a variable immune response (Sharpe et al., 2016). Currently, the analysis of vaccination through the natural infection site is an attractive approach to priming natural host immunity. Previous studies with aerosolized γ-irradiated BCG have shown a robust expansion of antigen-specific CD4+ T cells producing TNF-α, IL-2, and IFN-γ, correlated with reducing *M. tuberculosis* HN878. Besides, vaccine boosting has shown more robust protection (Cha et al., 2015).

Studies about the higher protection that mucosal vaccination may confer have been done in mice and NHP animal models (Stary et al., 2015; Aguilo et al., 2020; Logerot et al., 2021). Most of the pathogens access the body through mucosal membranes. Therefore, the advantage of a mucosal vaccine is that the local memory immune response can neutralize or eliminate virus and bacteria at the infection site (Neutra and Kozlowski, 2006; Mato, 2019; Li et al., 2020). The rationale behind this is that mucosal vaccination induces humoral and cell mediates immune protection systemically and locally (Neutra and Kozlowski, 2006; Manjaly Thomas and McShane, 2015; Lycke, 2012; Li et al., 2019). For instance, nasal immunization can be protective in the upper and lower respiratory tract and gastric mucosa (Mato, 2019). In addition, the mucosal vaccination route has substantial advantages compared with parenteral vaccination. Mucosal vaccination does not require much training personnel and avoids the use of syringes and needles and the associated potential risk of spreading blood-borne infections. Also, it is practical, non-invasive, and suitable for mass vaccination (De Magistris, 2006; Srivastava et al., 2015). The mucosal immune system can be divided into inductive and effector sites. The inductive sites are lymphoid structures in the respiratory tract, including nasopharyngeal-associated lymphoid tissue (NALT) and bronchus-associated lymphoid tissue (BALT) (Cesta, 2006). Immune responses initiate by nasal and aerosol mucosal vaccination

starts in these sites. These specialized structures harbor the T cell zone and B cell follicle. When the antigen is taking up by immature DCs, this cell undergoes maturation and may leave the mucosal tissue for the draining lymph nodes. However, if DCs are already in the inductive site, they will prime naïve CD4+ and CD8+ T at the T zone. After activation of Naïve CD4+ T, this cell can be differentiating into various subsets such as Th1, Th2, Th17, Treg, or Tfh. Tfh cells are recruited to the B cell follicle to expand and differentiate activated B cells in the germinal center. Thus, Tfh is critical for developing long-lived plasma cells (having specific IgA antibodies in the site of infection) and memory B cells in the germinal center. In addition, mucosal vaccination can also induce systemic IgG responses. The effector sites are tissues where specific antibodies and CD8+ and CD4+ T cells effector and memory T cells reside (Macpherson et al., 2008; Brandtzaeg, 2009; Bernasconi et al., 2016; Hellfritzsch and Scherlie, 2019).

Intravenous vaccination (a parenteral delivery) has also been studied in the NHP and the mice model with promising results (Barclay et al., 1970; Darrah et al., 2020). Some studies have indicated that intravenous BCG vaccination induces more antigen-responsive CD4+ and CD8+ T cells in blood, spleen, BAL, and mediastinal lymph nodes (Darrah et al., 2020). Unlike intradermal and intramuscular delivery, intravenous delivery induces a high frequency of resident memory T cells in the lung, observed as non-signal of infection in 6 out of 10 vaccinated NHP (Darrah et al., 2020; Scriba and Mizrah, 2020).

CX3CR1 is a chemokine receptor expressed by monocytes, macrophages, NK cells, DCs, CD8+, and CD4+ T cells (Soos et al., 2006; Bottcher et al., 2015; Hertwig et al., 2016; Batista et al., 2020; Li et al., 2021). Its ligand, CX3CL1, is upregulated under inflammation and is expressed in airways smooth muscle, and lung endothelium (Mionnet et al., 2010; Batista et al., 2020). On the other hand, CXCL9 and CXCL10 are ligands of the CXCR3 chemokine receptor. These ligands induce effector Th1/Th17 cells to promote inflammation (Karin and Wildbaum, 2015; Karin et al., 2016). A robust immune response against *M. tuberculosis* needs CD4+ T cells with the release of antigen-specific IFN-γ and TNF-α. The induction of IL-2 is also crucial for central memory T cell responses and CD8+ T cells immune response (Manjaly Thomas and McShane, 2015). Also, *M. tuberculosis*

growth suppression requires direct interaction of CD4+ T cells with infected macrophages in the lung. Therefore, the ability of CD4+ T cells to migrate into the lung parenchyma is crucial. Previous studies with C57Bl/6 mice have determined that CX3CR1 and CXCR3, specific chemokine receptors expressed in CD4+ Th1 T cells, induce failure or protection against *M. tuberculosis*, respectively. The CD4+CXCR3+ T cells enter the lung parenchyma and can suppress the growth of *M. tuberculosis*, but in contrast, CD4+CX3CR1+ T cells are non-protective and they accumulate in the lung vasculature (Sakai et al., 2014, Sallin et al., 2017, Hoft et al., 2019).

Therefore, identifying these two populations is critical to analyze and compare alternative routes of BCG vaccination. It is essential to consider that a vaccine is effective if it can reduce the colony forming units (CFU) in the lung by more than one log10 CFU. One Log_{10} CFU reduction represents approximately 90% reduction in the mycobacterial burden (Henao-Tamayo et al., 2014; MacDonald and Izzo, 2015).

The present study examines the immune responses of different routes of BCG vaccinated mice to *M. tuberculosis*, and it is divided into two experiments, the first experiment (part I) analyzed BCG aerosol vaccination route focused on CD4+ T cells only (Appendix I, supplementary table S1), and the second experiment (part II) analyzed four routes of BCG vaccination, the aerosol, the subcutaneous, the intravenous and the intranasal, and it was focused on both CD4+ and CD8+ T cells (Appendix I, supplementary table S2).

Materials and Methods

Mice. Female C57BL/6J mice (6-8 weeks old) were purchased from Jackson Laboratories (Bar Harbor, ME) and maintained at Colorado State University for two weeks before experimentation. The use of these animals and protocols were reviewed and approved by the Institutional Animal Care and Use Committee at Colorado State University (Protocol ID: 16-6369A).

BCG vaccination. Mice were vaccinated at day 0 with BCG Pasteur TMC #1011. Vaccines were stored at -80^{o}C until needed. The BCG vaccine was thawed at room temperature and then diluted in physiological saline. In part I of the experiment, mice were vaccinated via aerosol with the same doses of part II. For part II of the experiment, subcutaneous vaccination was administered in the left flank in a $1x10^6$ CFU/mL dose. Intravenous vaccination was administered in the tail vein with a $1x10^6$ CFU/mL dose, and aerosol and intranasal groups were vaccinated with $1x10^7$CFU/mL.

***M. tuberculosis* infection.** *M. tuberculosis* H37Rv was diluted to $2x10^6$ CFU/mL and sonicated for 15 minutes to separate aggregates. Five mLs were loaded into a nebulizer to deliver 50-100 CFU to each mouse using the Inhalation Exposure System (Glas-Col, Terre Haute, IN). The inoculum was plated on 7H11 agar, and five mice were euthanized on the day of infection to assess the number of CFU implanted into the lung. The same inoculum dose was used for both experiments.

Experiment part I timeline

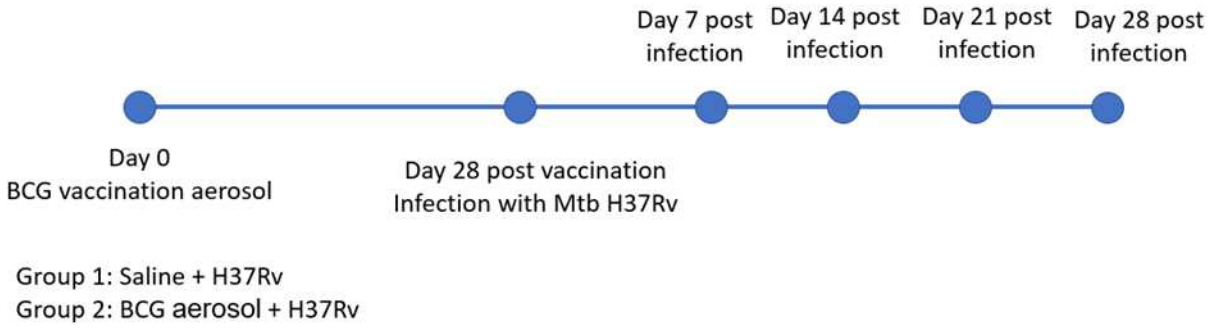

Figure 2.1. Timeline for part I. Flow cytometry and viable count of lung, spleen, and lymph nodes were performed at 7-, 14-, 21- and 28-days post-infection. Five mice were euthanized on days 0 and 28 post-vaccination (*M. tuberculosis* infection day), and ten mice (5 per group) were euthanized on days 7, 14, 21, and 28 post-infection.

Experiment part II timeline

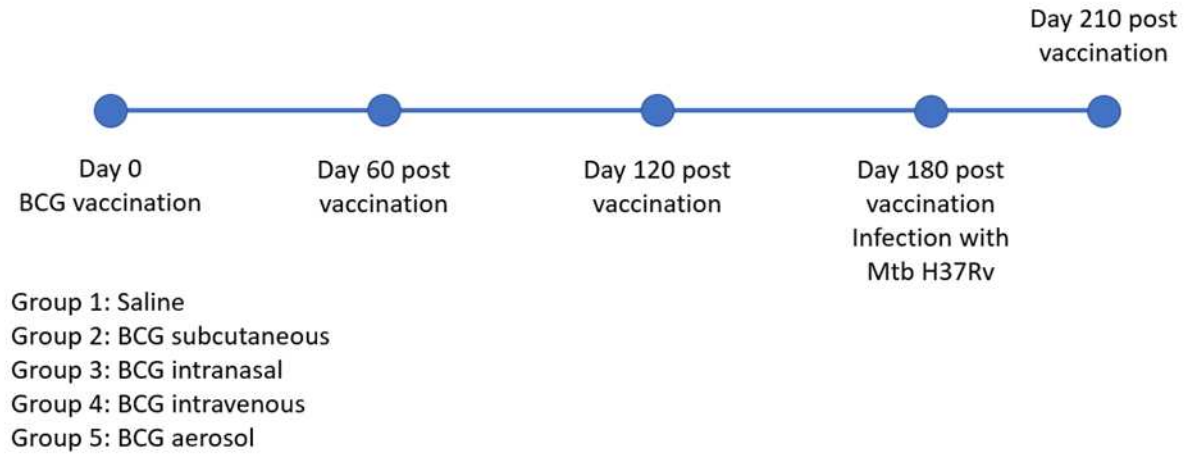

Figure 2.2. Timeline for part II. Flow cytometry analysis, viable count, and cytometric bead array were performed for this experiment. Viable count and cytometric bead array were performed at day 30 post *M. tuberculosis* infection (day 210 post-vaccination), and flow cytometry was performed at 60-, 120-, 180- and 210-days post-vaccination. Groups were divided as described, and five to six mice were euthanized at days 60, 120, 180, and 210 post-vaccination.

Flow cytometry. For part I, flow cytometry analysis was performed for lung, spleen, and lymph nodes at 7-, 14-, 21-, and 28-days post *M. tuberculosis* infection, and for experiment part II, flow cytometry analysis was performed for the same organs at 60-, 120-, 180-, and 210-days post-BCG vaccination. After mice necropsies, the lungs were

minced with a razor blade and incubated at 37°C in 0.5% liberase (Sigma Aldrich, St. Louis, MO) and incomplete RPMI media (Life Technologies, Carlsbad, CA). After 45 minutes, the lung pieces, spleens, and lymph nodes were passed through a 70 µm nylon cell strainer (Falcon, Corning, Durham, NC), and the single-cell suspension was collected after centrifugation. The pellet cells were resuspended in 2mL ACK red blood cell lysis buffer (Life Technologies, Carlsbad, CA) and incubated at room temperature for 5 minutes. The reaction was stopped with complete RPMI (RPMI-1640 with penicillin, streptomycin, HEPES (Sigma Aldrich, St. Louis, MO), sodium pyruvate (Sigma Aldrich, St. Louis, MO), L-glutamate (Sigma Aldrich, St. Louis, MO), and 10% fetal bovine serum (Atlas Biologicals, Fort Collins, CO). Cell suspensions were centrifugated and maintained in complete RPMI on ice. Cells were counted, and the concentration adjusted to $2x10^6$/mL in complete RPMI, pelleted, and then incubated for 20 minutes at 4°C in 2.4G2 hybridoma supernatant (Fcγ blocking antibody, ATCC® HB-197) diluted in PBS containing 5% of Fetal Bovine Serum (FBS) and 0.01% NaN3 (FACS buffer). After incubation, cells were centrifugated and resuspended in FACS buffer before being pelleted and stained with fluorochrome-conjugated antibodies (Supplemental Table S1 and S2). Cells were washed with FACS buffer, analyzed on a BD FACSCantoTM II flow cytometer. Data were analyzed using FlowJo software (FlowJo, LLC, Ashland, OR).

Cytokine analysis. Cytokine analysis was performed for experiment part II. On day 210 after vaccination (30 days after infection), lung homogenates from all groups were pelleted, and the cell-free supernatant was taken to quantify cytokine concentrations with a Cytometric Bead Array (CBA) assay using CBA mouse inflammation kit (BD Biosciences, San Jose, CA). Data were collected on a FACSCantoTM II cytometer (BD Biosciences, San Jose, CA) and analyzed using FCAP ArrayTM software (BD Biosciences).

Assessment of bacterial burden. In part I, viable *M. tuberculosis* counts in lungs, lymph nodes, and spleens were determined at days 7, 14, 21, and 28 post-infection. In part II, viable *M. tuberculosis* counts in lungs and spleens were determined 30 days post-infection that correspond to day 210 post-vaccination. Necropsy was performed to

remove organs that were then homogenized in sterile saline before being diluted and plated on 7H11 agar (Difco, BD Biosciences, San Jose, CA). Plates were incubated at 37ºC for 14-18 days. CFU was converted into Log_{10} for analysis, and All CFU analysis was performed with five to six mice per group unless specified otherwise.

Statistical analysis. All the statistical procedures were performed in Graph Pad Prism 7 (GraphPad Software, La Jolla, CA) as indicated. Data from some experiments were Log-10 transformed before analysis, and graphs were prepared using Graph Pad Prism 7. A significant effect was considered at p-value <0.05.

Results

Part I. Analysis of aerosol BCG vaccination

Mouse bacterial burden after infection with *M. tuberculosis*

Control and aerosol BCG vaccinated mice were exposed to a low-dose aerosol challenge with virulent *M. tuberculosis* H37Rv. At 7-, 14-, 21-, and 28-days post-infection, lungs, spleens, and lymph nodes were harvested, and the CFUs numbers were determined.

CD4+ T cells are a leading cellular player against *M. tuberculosis,* and according to Sakai et al., 2014; Sallin et al., 2017; and Hoft et al., 2019, two main subsets of Th1 CD4+ T cells are capable (CXCR3) or not (CX3CR1) to control *M. tuberculosis* growth according to the chemokine receptor expressed on the cell surface. Also, we included IFN-γ, TNF-α, and IL-2 cytokines to determine further the *M. tuberculosis* growth controlling capacity (Appendix I, supplementary table S1).

To assesses differences between the control and vaccination groups, ANOVA was performed in Graph Pad Prism 7. The statistical model considered the fixed effects of vaccine effect, time effect, and their interaction.

In the lung, the overall effect of vaccination was not significant (p-value=0.4669). We did not observe a significant effect of vaccine administration or the vaccinated and control groups' time points (Figure 2.3A).

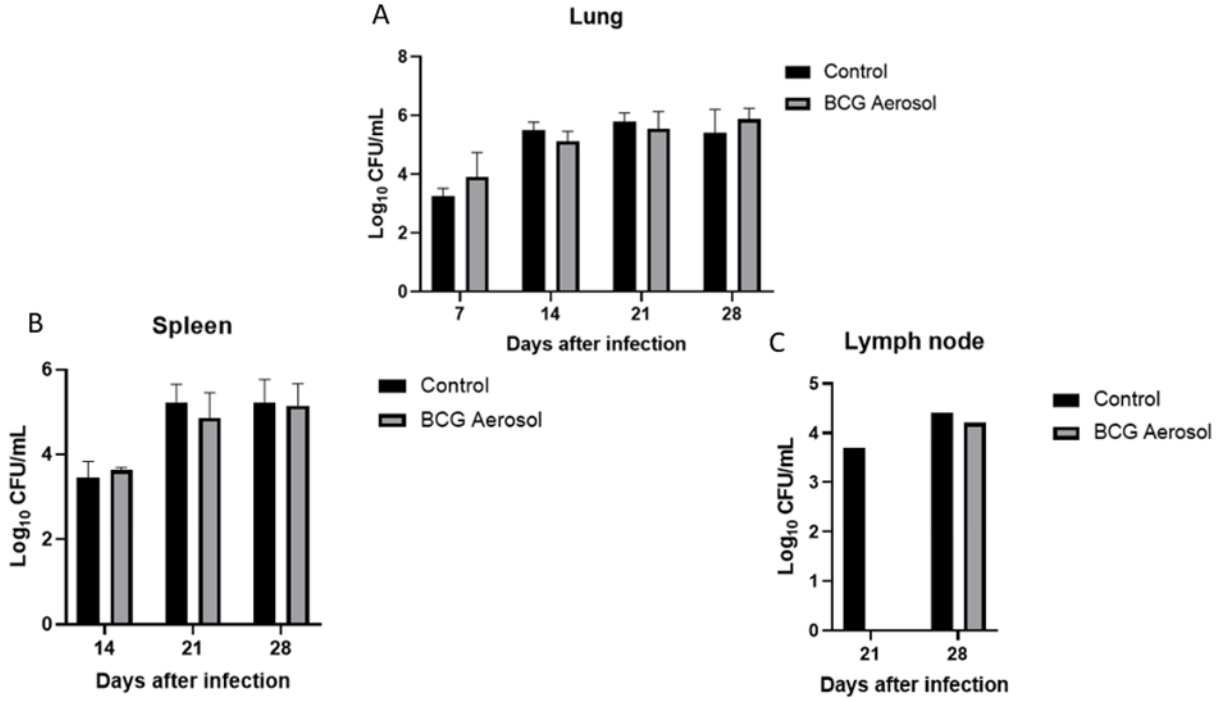

Figure 2.3. Colony-forming units obtained from lung, spleen, and lymph nodes of C57Bl/6J BCG vaccinated mice. Mice were vaccinated via an aerosol route with $1x10^7$ CFU/mL, rested for 28 days, and then infected with a low dose aerosol of *M. tuberculosis* H37Rv. Homogenates organs were incubated for 14 to 21 days at 37ºC on 7H11 agar. (A) lung (B) spleen (C) lymph node.

Besides, no colonies were obtained in control and vaccinated groups at day seven post-infection for the spleen (Figure 2.3B). In the lymph node, no colonies were obtained for both groups at days 7 and 14 post-infection. On day 21, no colonies were obtained from the aerosol group, and only one mouse from the control group had colonies (see Figure 2.3C). On day 28 after infection, colonies from lymph nodes were obtained only from two mice in the saline and one mouse in the vaccinated group. No statistical differences were observed for the spleen or lymph nodes.

Flow cytometry analysis

To determine differences in the number of the two phenotypes of CD4+ T cells being recruited at lung, spleen, and lymph nodes, a two-way ANOVA was performed in Graph Pad Prism 7. In this analysis, five mice per group and per time point were included. The gating strategy was performed identifying singlet cells using FSC-H and FSC-A, and lymphocytes were gated based on size and granularity (Figure 2.4).

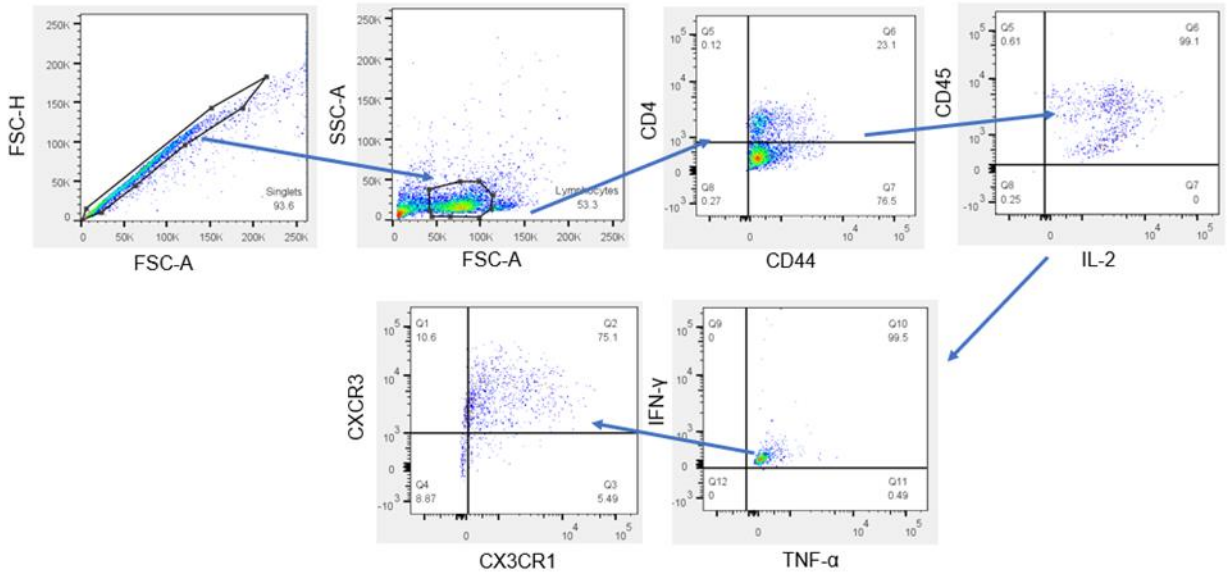

Figure 2.4. Flow cytometry gating strategy. Singlets were identify using FSC-H and FSC-A, and lymphocytes were gated based on size and granularity. Chemokine's markers CXCR3 and CX3CR1 were used to identify subpopulations of CD4+ T lymphocytes.

We did not observe significant differences in the number of CX3CR1+ cells in lungs at 7-, 14-, 21-, and 28-days post-infection (Figure 2.5.1A). In CXCR3+ cells, significant differences were only observed at day 28 post-infection (p-value= 0.0407) (Figure 2.5.1B).

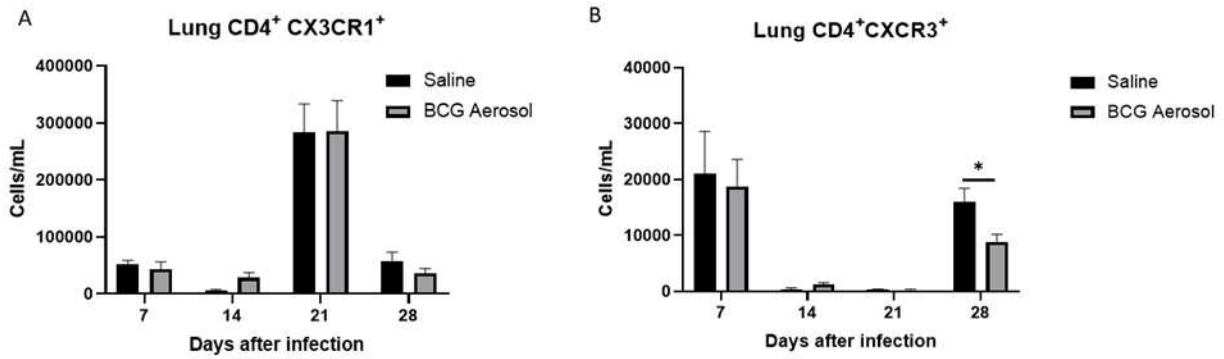

Figure 2.5.1. Number of CD4+CX3CR1+ (A) and CD4+CXCR3+ (B) cells obtained from the lung of C57Bl/6J mice at 7-, 14-, 21-, and 28-days post-infection with low dose aerosol of *M. tuberculosis* H37Rv. *p≤ 0.05.

In the lymph nodes, the CD4+ T lymphocytes expressing CX3CR1 chemokine receptor were significantly higher (p-value=0.086) at day 14 after infection in the saline group compared with vaccinated mice. However, no significant differences were found at days 7, 21, or 28 post-infection (Figure 2.5.2A). In the CXCR3 phenotype, no significant differences were found between groups at any time point (Figure 2.5.2B). Also, almost 100% of these two cell phenotypes (CX3CR1 and CXCR3) expressed IL-2 and INFN-γ.

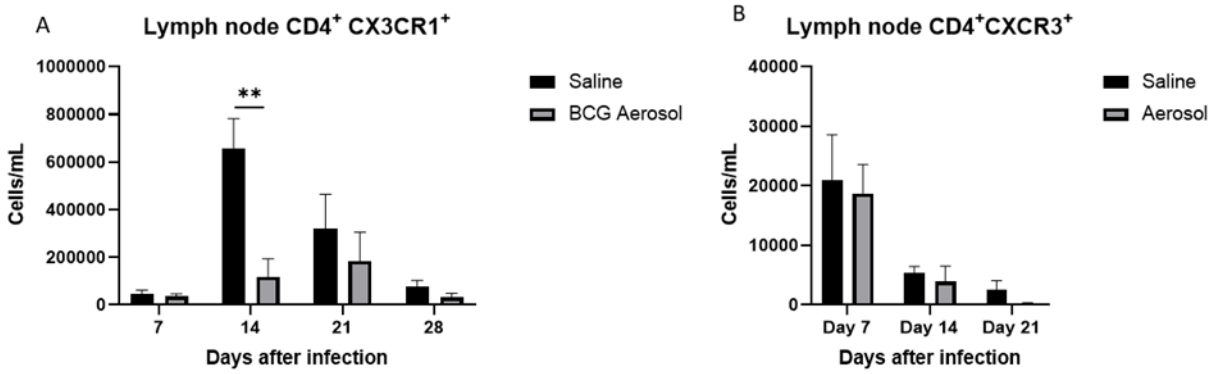

Figure 2.5.2. Number of CD4+CX3CR1+ (A) and CD4+CXCR3+ (B) cells obtained from lymph nodes of C57Bl/6J mice at 7-, 14-, 21-, and 28-days post-infection with low dose aerosol of *M. tuberculosis* H37Rv. **≤0.01.

The CD4+ T lymphocytes expressing CX3CR1 were significantly higher at day 21 in the spleen of BCG aerosol vaccinated mice (p-value=0.0176). However, no significant differences in the number of cells were found at 7-, 14-, and 28-days post-infection (Figure 2.5.3A). In CXCR3 expressing cells, no significant differences were found when

comparing saline and BCG vaccinated mice among all time points (Figure 2.5.3B). Also, both populations expressed high levels of IL-2 and INFN-γ.

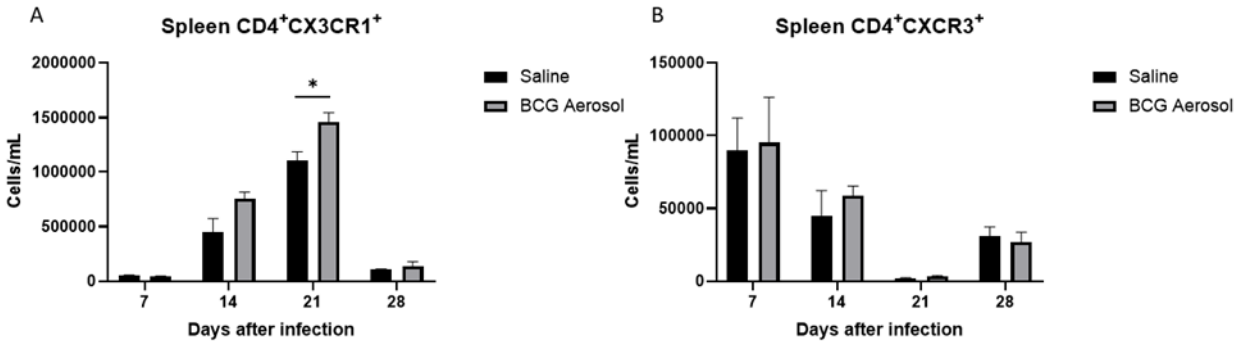

Figure 2.5.3. Number of CD4+CX3CR1+ (A) and CD4+CXCR3+ (B) cells obtained from the spleen of C57Bl/6J mice at 7-, 14-, 21-, and 28-days post-infection with low dose aerosol of *M. tuberculosis* H37Rv. *p≤ 0.05.

Part II. Analysis of aerosol, subcutaneous, intranasal, and intravenous routes of BCG Vaccination

Bacterial burden after infection with *M. tuberculosis*

A one-way ANOVA was used to determine differences at day 210 post-vaccination (day 30 post-infection with a low dose *M. tuberculosis* H37Rv) in the bacterial burden among subcutaneous, intranasal, intravenous, and vaccination routes of lung and spleen. In the lung, significant differences were found when the saline group was compared with the subcutaneous route (p-value=0.0269), intranasal route (p-value=0.0018), intravenous route (p-value=0.0377), and aerosol route (p-value=0.0139). No differences were obtained comparing among vaccinated groups (Figure 2.6A). In the spleen (Figure 2.6B), significant differences were found in saline and intranasal groups (p-value=0.0011), saline and intravenous groups (p-value=0.0241), saline and aerosol groups (p-value=0.082), and subcutaneous and intranasal groups (p-value=0.0259).

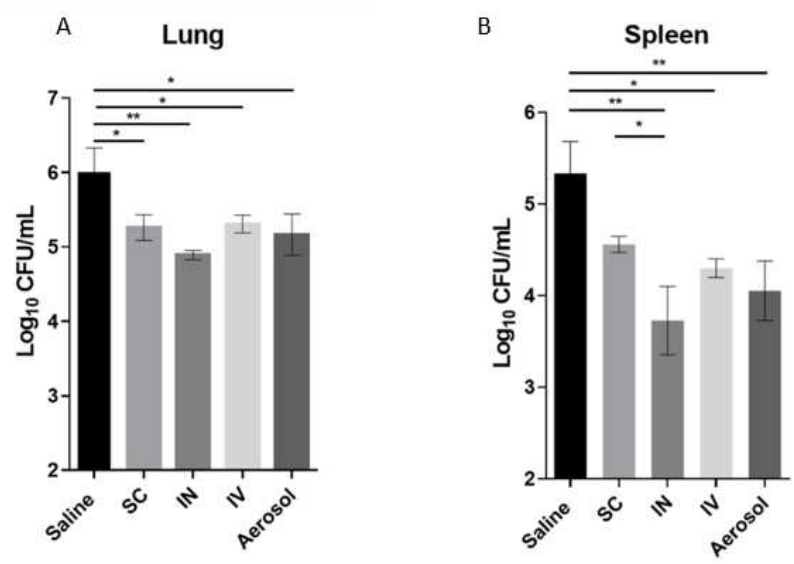

Figure 2.6. Colony-forming units were obtained from the lung and spleen of BCG vaccinated mice. Samples were obtained 210 days post-vaccination and 30 days after infection with *M. tuberculosis* H37Rv. Organ homogenates were incubated for 14 to 21 days at 37°C on 7H11 agar. (A) lung (B) spleen. *p ≤0.05, **p ≤0.01.

Flow cytometry analysis

To determine if the control of *M. tuberculosis* growth is associated with the route of vaccination and to a higher frequency of protective phenotype (CXCR3), and CD8+ T cells, we included CD4+, CD8+ T cell flow cytometry panels. For the CD4+ T cells panel, we also included cytokines important to control *M. tuberculosis* grow such as IFN-γ, and TNF-α, and the CD62L marker to determine migration patterns. controlling *M. tuberculosis* growth according to the chemokine receptor expressed on the cell surface. Also, we included IFN-γ, TNF-α, and IL-2 cytokines to further determine the *M. tuberculosis* growth controlling capacity. For CD8+ T cells we were focused on migration patterns based on expression of CD62L and CCR7, cytokines and PD-1 marker of T cell exhaustion (Appendix I, supplementary table S2 Panel 1 and Panel 2).

A two-way ANOVA and mixed-effect analysis were performed to determine statistical significance among vaccination groups and the control group. At day 210, statistical analyses were adjusted due to fewer mice in the saline group (n=3) than subcutaneous, intranasal, intravenous, and aerosol groups (n=6). Flow cytometry gating strategy was

performed to determine specific CD4+ (Figure 2.7) and CD8+ (Figure 2.8) T cell populations.

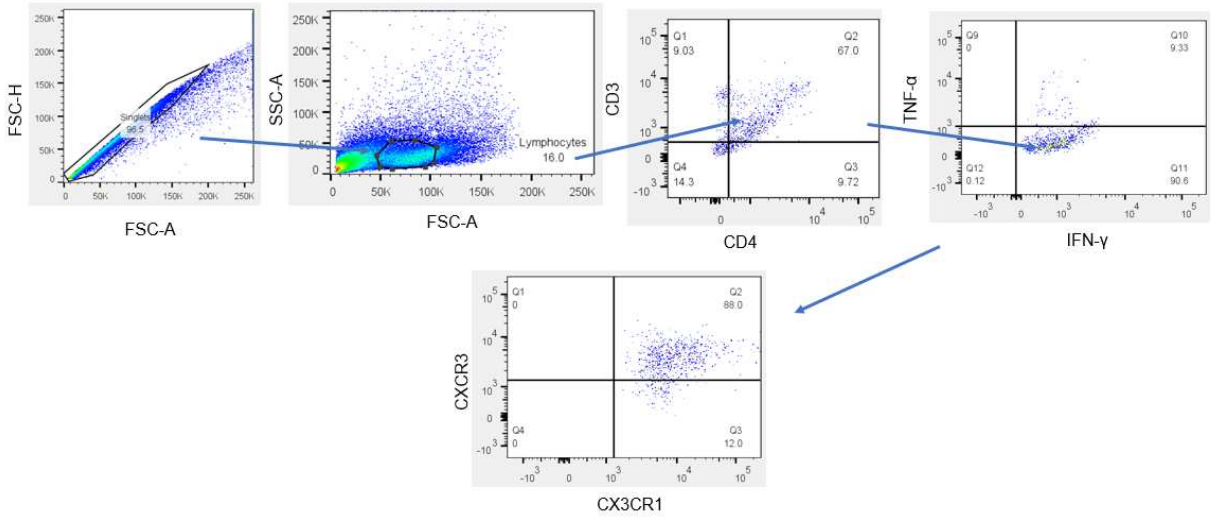

Figure 2.7. Flow cytometry gating strategy for CD4 panel. Singlets were identify using FSC-H and FSC-A, and lymphocytes were gated based on size and granularity. Chemokine markers CXCR3 and CXCR1 were used to identify subpopulations of CD4+ T lymphocytes after gating IFN-γ + cells.

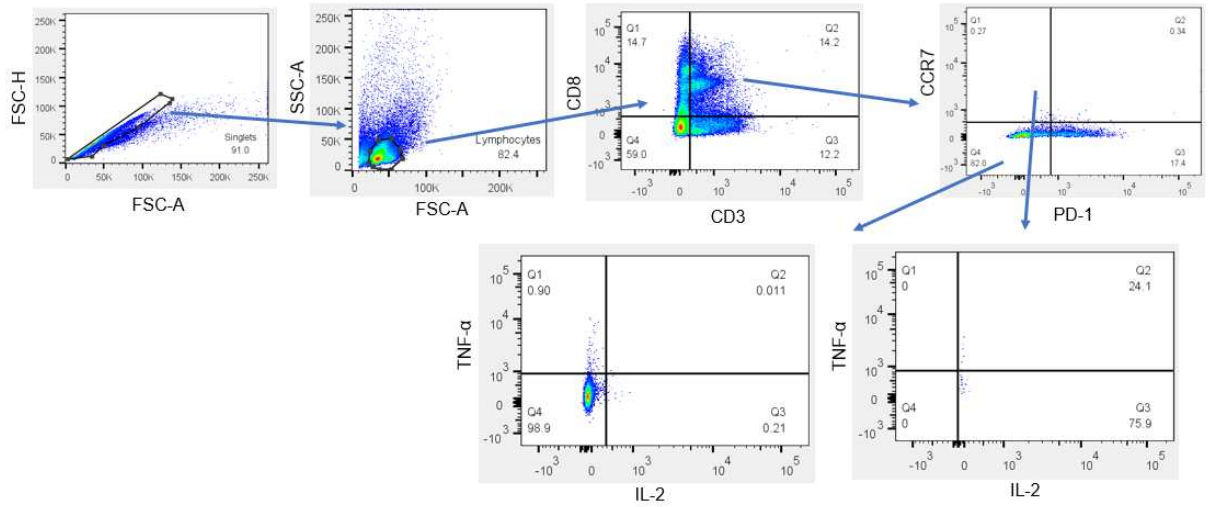

Figure 2.8. Flow cytometry gating strategy for CD8 panel. Singlets were identify using FSC-H and FSC-A, and lymphocytes were gated based on size and granularity. CCR7, PD-1, TNF- markers were used to identify subpopulations of effector and memory CD8+ T cells.

The CD4+ T lymphocytes expressing CX3CR1 chemokine receptor in the lung were significantly higher at day 120 post-vaccination when comparing saline with subcutaneous (p-value=0.0211) and intranasal groups (p-value=0.0196), and at day 180

post-vaccination when subcutaneous and intravenous groups were compared (p-value=0.0190) (Figure 2.7A). In the case of the CD4+CXCR3+ T cells recruitment, there were significant differences at days 120 and 180 post-vaccination. At day 120, the saline group recruited less CXCR3+ cells compared with intranasal (p-value=0.0706) and aerosol (p-value=0.025) groups. And intravenous recruited less cells at day 180 compared with aerosol group (p-value=0.0322) (Figure 2.7B).

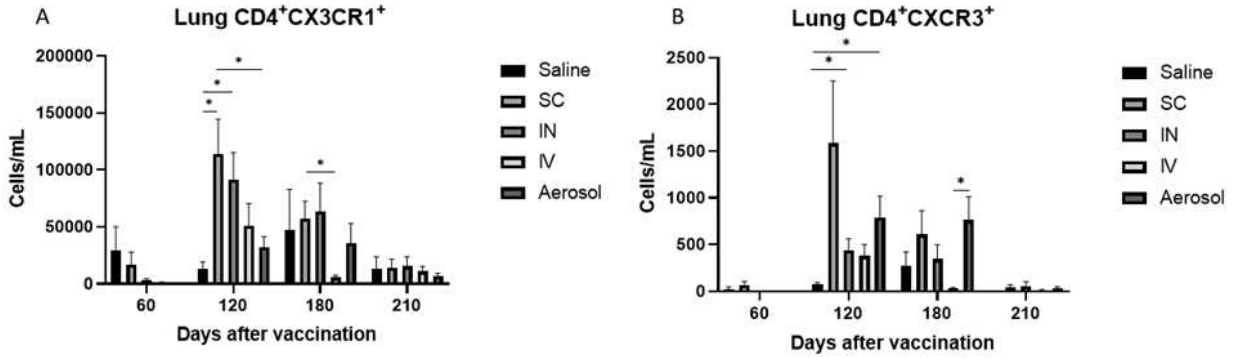

Figure 2.9.1 Number of CD4+CX3CR1+ (A) and CD4+CXCR3+ (B) cells obtained from the lung of C57Bl/6J mice at 60-, 120-, 180-, and 210-days post-BCG vaccination. Mice were infected with low dose aerosol of *M. tuberculosis* H37Rv at day 180 post-BCG vaccination. *p≤ 0.05.

In the case of lymph node, significant differences in the recruitment of CX3CR1 cells was observed only at day 210 post-vaccination (Figure 2.9.2A) in subcutaneous with intranasal vaccinated groups (p-value=0.0328) and subcutaneous and aerosol groups (p-value=0.0147). Significant differences were only observed in the recruitment of CXCR3 cells at day 120 post-vaccination (Figure 2.9.2B) in saline and subcutaneous (p-value=0.0059), intravenous (p-value=0.0296), and aerosol groups (p-value=0.0063).

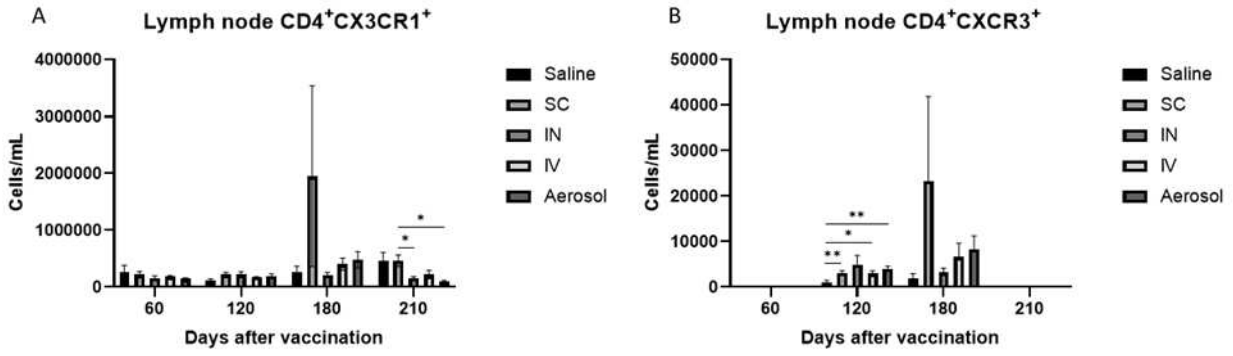

Figure 2.9.2. Number of CD4+CX3CR1+ (A) and CD4+CXCR3+ (B) cells obtained from the lymph node of C57Bl/6J mice at 60-, 120-, 180-, and 210-days post-BCG vaccination. Mice were

infected with low dose aerosol of *M. tuberculosis* H37Rv at day 180 post-BCG vaccination. *p≤ 0.05, **p≤ 0.01.

Significant differences were observed in the recruitment of CD8+ T cells in lung, spleen, and lymph node samples. Additionally, the higher recruitment of CD8+ T cells was mainly observed at day 120 post-vaccination for lung, spleen, and lymph nodes. In the case of CD8+ T cells in the lung (Figure 2.9.3A), significant differences were observed at day 60 post-vaccination comparing subcutaneous and intranasal routes (p-value=0.0026), intranasal and intravenous routes (p-value=0.0088), and intranasal and aerosol routes (p-value=0.002).

The CD8+ T cells expressing CCR7 receptors in the lung were statistically significant at day 120 post-vaccination, comparing saline and aerosol routes (p-value=0.0367), subcutaneous and aerosol routes (p-value=0.0444), and intranasal and aerosol routes (p-value=0.0401). This population's statistical difference was also observed at day 210 between saline and intranasal routes (p-value=0.0045) and intranasal and aerosol routes (p-value=0.0031).

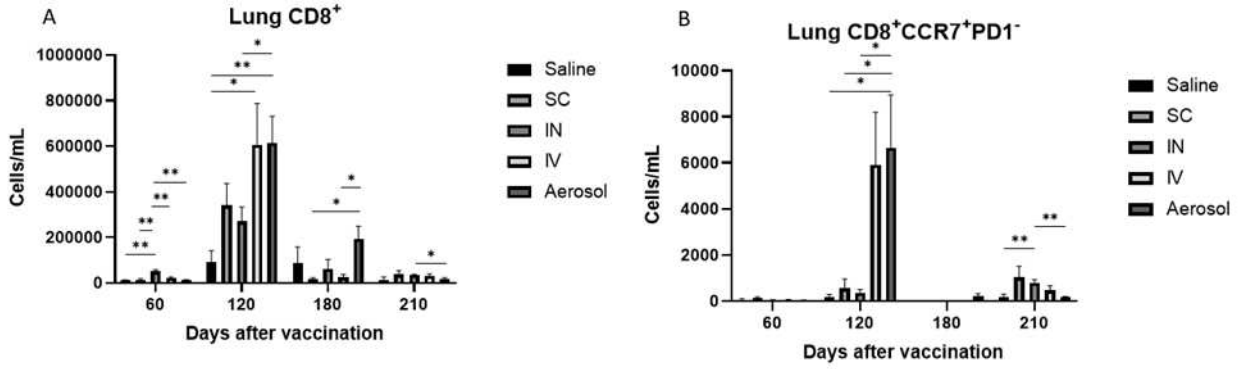

Figure 2.9.3. Number of CD8+ (A) and CD8+CCR7+PD- (B) cells obtained from the lung of C57Bl/6J mice at 60-, 120-, 180-, and 210-days post-BCG vaccination. Mice were infected with low dose aerosol of *M. tuberculosis* H37Rv at day 180 post-BCG vaccination. *p≤ 0.05, **p≤ 0.01.

The main difference in the recruitment of CD8+ T cells in the lymph node (Figure 2.9.4A) was observed at day 120 post-vaccination. The main statistical differences were observed comparing the subcutaneous and aerosol groups (p-value=0.0150), intranasal and aerosol groups (p-value=0.0439), and intravenous and aerosol groups (p-value=0.0014). Minimal recruitment of CD8+CCR7+ cells was observed in lymph nodes at days 60, 120, and 180 post-vaccination with statistical significance at day 120 post-vaccination between

subcutaneous and intravenous routes (p-value=0.0462) and intravenous and aerosol routes (p-value=0.0027). Statistical differences were also observed at day 210 post-vaccination between intravenous and aerosol routes (p-value=0.0367).

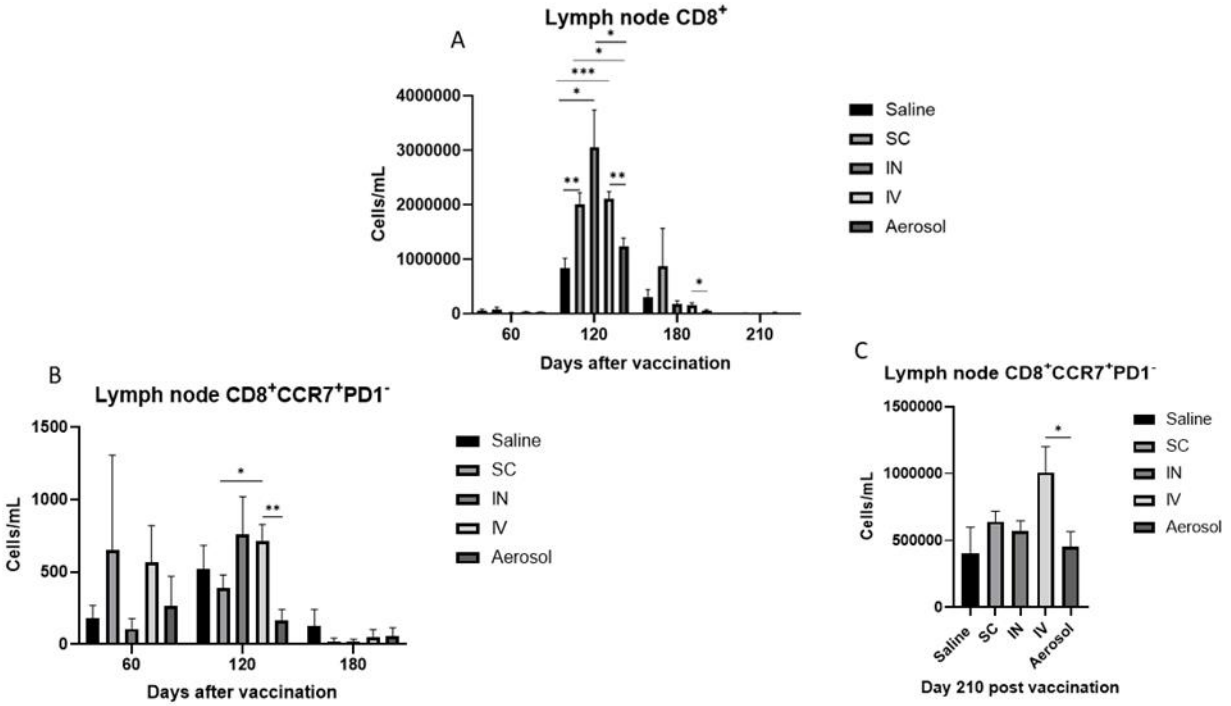

Figure 2.9.4. Number of CD8+ (A) and CD8+CCR7+PD- (B) (C) cells obtained from the lymph node of C57Bl/6J mice at 60-, 120-, 180-, and 210-days post-BCG vaccination. Mice were infected with low dose aerosol of *M. tuberculosis* H37Rv at day 180 post-BCG vaccination. *p ≤0.05, **p ≤0.01, ***p ≤0.001.

The highest recruitment of CD8+ T cells was observed in the spleen at day 120 post-vaccination; however, statistical significance was observed at 60-, 180-, and 120-days post-vaccination (Figure 2.9.5A). On day 60 post-vaccination, CD8+ T cells recruitment was significantly different comparing saline and intravenous routes (p≤0.0001), subcutaneous and intravenous routes (p-value=0.0034), subcutaneous and intravenous routes (p-value=0.0034), intranasal and intravenous routes (p-value=0.0002), and intravenous and aerosol routes (p-value=0.0002). Significant differences were also observed in the recruitment of CD8+ T cells expressing CCR7 receptor in saline and aerosol routes (p-value=0.0397), subcutaneous and aerosol routes (p-value=0.0283), and intranasal and aerosol routes (p-value=0.0272).

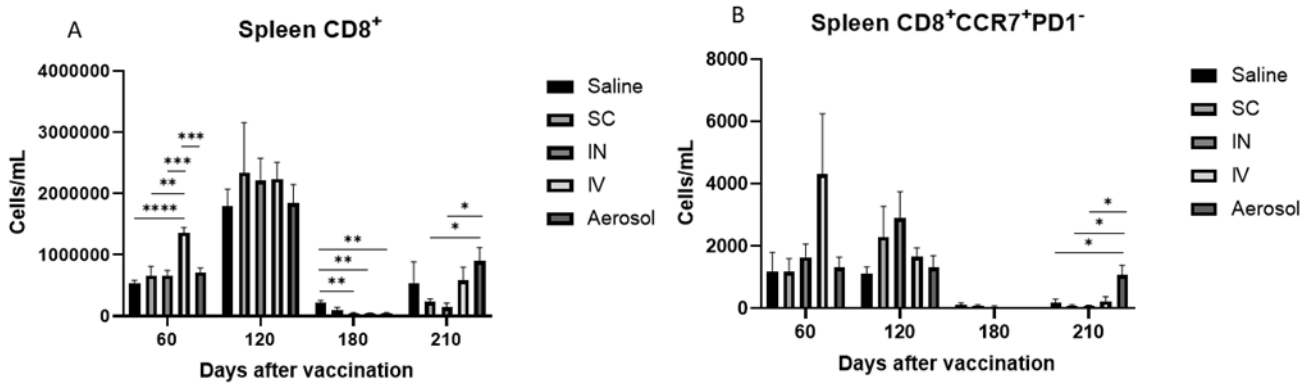

Figure 2.9.5. Number of CD8+ (A) and CD8+CCR7+PD- (B) cells obtained from the spleen of C57Bl/6J mice at 60-, 120-, 180-, and 210-days post-BCG vaccination. Mice were infected with low dose aerosol of *M. tuberculosis* H37Rv at day 180 post-BCG vaccination. *p ≤0.05, **p ≤0.01, ***p ≤0.001, ****p ≤0.0001.

Cytokine analysis

To evaluate the inflammatory response and cytokine profile of mice BCG vaccinated mice, a cytometric bead array of the lung was performed at day 210 post-vaccination and day 30 post-infection with a low dose *M. tuberculosis* H37Rv. A one-way ANOVA was performed to determine statistical significance among groups. More robust production of pro-inflammatory cytokines TNF-α, IFN-γ, and IL-6, was observed in the saline group compared with subcutaneous, intranasal, intravenous, and aerosol vaccinated mice. There was no statistical significance among groups in IL-10, IL-17A, and IL-2 cytokines. However, significant differences were found in TNF-α (Figure 2.9.6C) when comparing saline and subcutaneous groups (p-value=0.0056), saline and intranasal groups (p-value=0.0025), saline and intravenous groups (p-value=0.0005), and saline and aerosol groups (p-value=0.0016). IFN-γ (Figure 2.9.6D) statistical analysis also showed significant differences comparing the saline group with subcutaneous (p<0.0001), intranasal (p<0.0001), intravenous (p<0.0001), and aerosol (p<0.0001) groups.

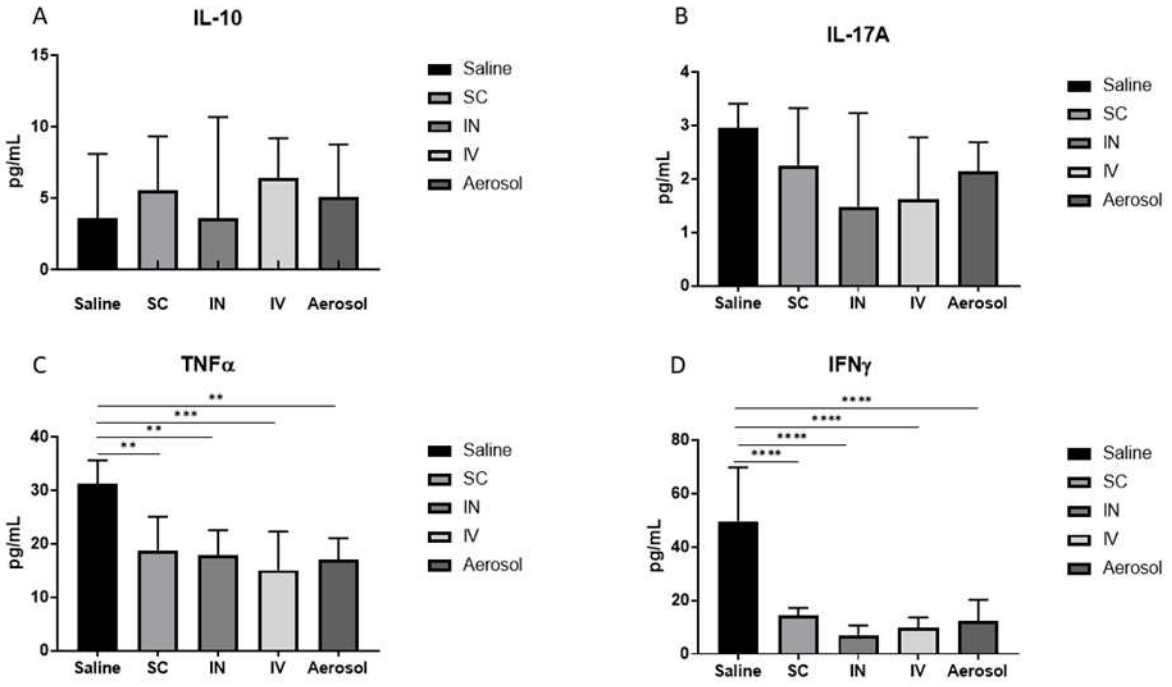

Figure 2.9.6. Cytometric bead array analysis from lung homogenates at day 30 post-infection. **p ≤0.01, ***p ≤0.001, ****p ≤0.0001.

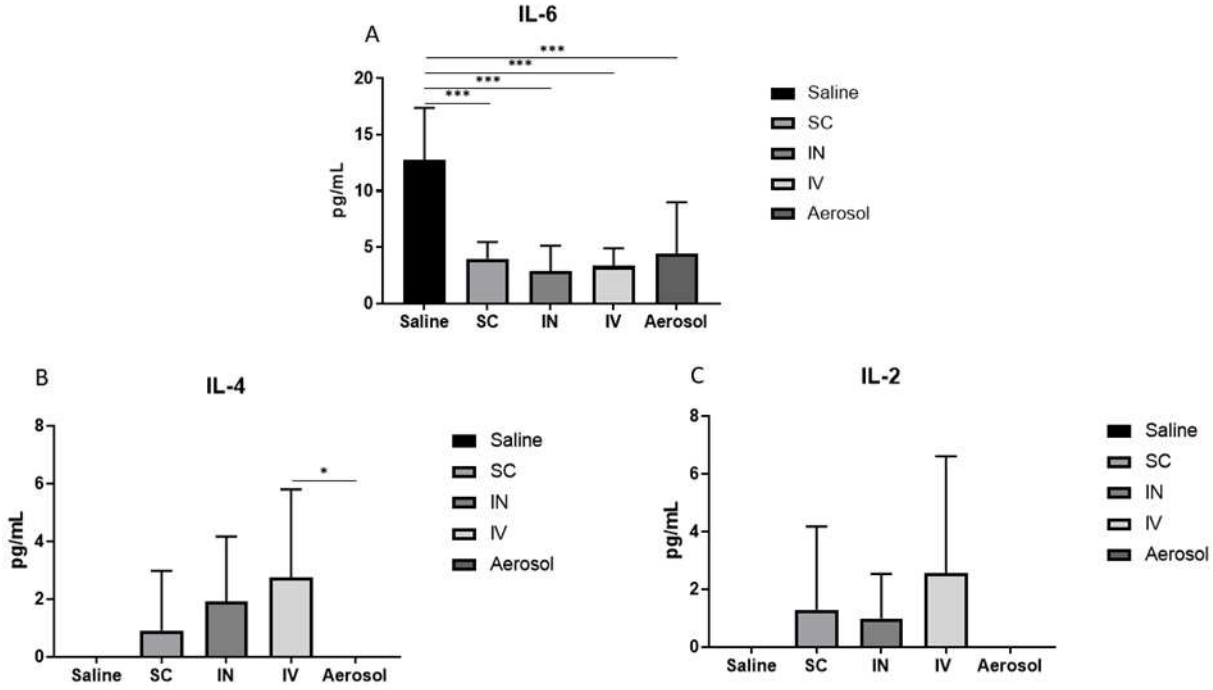

Figure 2.9.7 Cytometric bead array analysis from lung homogenates at day 210 post-BCG vaccination. **p ≤0.01, ***p ≤0.001.

In IL-6 (Figure 2.9.7A), no significant differences were found when vaccination routes were analyzed. However, significant differences were observed comparing control (saline) with subcutaneous (p-value=0.0008), intranasal (p-value=0.0002), intravenous (p-value=0.0003) and aerosol (p-value=0.0009) groups. The analysis of IL-4 cytokine (Figure 2.9.7B) showed a difference when intravenous and aerosol groups were compared (p-value=0.0308).

Discussion

Two experiments (part I and part II) were performed to characterize the immune response among different BCG delivery routes. Part I evaluated the protection of BCG aerosol vaccination at 7-, 14-, 21-, and 28-days post *M. tuberculosis* infection (Figure 2.1). Part II evaluated the protection of different routes of BCG vaccination (subcutaneous, intranasal, intravenous, and aerosol) at 60-, 120-, 180-, and 210-days post-vaccination day, and infected with *M. tuberculosis* at day 180 post-BCG vaccination (Figure 2.2). The effect of BCG routes, dose, and boosting on protective TB outcomes has not been thoroughly studied; however, it is acknowledged that T cell immunity is required to control infection and prevent clinical signs of TB. This study focused mainly on two key chemokine receptors expressed by CD4+Th1 cells to migrate into the lungs. The localization and migration of specific lymphocyte populations are critical in the immune response to infectious diseases and are regulated by chemokines and adhesion molecules (Karin and Wildbaum, 2015). It is currently suggested that subsets of lymphocytes may have different tissue tropism depending on the cell developmental stage and the chemokine profile expressed in the environment. This study was focused on the analysis of CXCR1 and CX3CR1 chemokine receptors expressed by CD4+ Th1 lymphocytes and the effect that the BCG delivery routes have on these populations' profiles. Previous studies have shown that CD4+CXCR3+ T cells can migrate into the lungs after *M. tuberculosis* infection and suppress *M. tuberculosis* growth. However, terminally differentiated CD4+ T cells expressing CX3CR1 in the lung do not migrate out of the blood vessels and do not affect *M. tuberculosis* (Sakai et al., 2014; Hoft et al., 2019).

M. tuberculosis H37Rv grew exponentially during the first four weeks (timepoint addressed in part I) in female C57BL/6 mice (Saini et al., 2012). With the dose used for the BCG aerosol vaccination, mice did not show the expected statistical reduction in the lung CFUs (Figure 2.3A). Additionally, *M. tuberculosis* dissemination was observed in the spleen starting at day 14 post-infection, and it remained similar between the control and BCG aerosol route until the end of the study at day 28 post-infection (Figure 2.3B). Interestingly, the tracheobronchial lymph nodes did no shown *M. tuberculosis* growth until day 28 post-infection (Figure 2.3C). This lack of growth could indicate that extrapulmonary *M. tuberculosis* dissemination in BCG aerosolized C57BL/6 mice occurs primarily via spleen and possibly liver followed by tracheobronchial lymph node presumably via bloodstream instead of lymphatic drainage. This trafficking is an essential point since antigens must be delivered to draining lymph nodes before a T cell immune response. Previous studies have indicated that at 9 to 11 days post-infection, *M. tuberculosis* disseminates to pulmonary lymph nodes via lymphatic drainage, and *M. tuberculosis*-specific T cells can be detected on day 14 after infection (Chackerian et al., 2002).

Interestingly, in our long-term study (part II), all BCG vaccination deliveries induced CFU statistical differences (day 210 post vaccination, day 30 post infection) when compared with controls (non-vaccinated). In the lung, intranasal BCG delivery showed the highest difference (Figure 2.8A). Thus, intranasal delivery could offer not only practical delivery advantages but also better efficacy. The effectiveness of intranasal BCG delivery has been previously associated with more rapid production of IFN-γ by T cells (Chen et al., 2004), and this could also be reflected by the low CFUs observed in the spleen (Figure 2.8B). However, it is essential to address that both intranasal and pulmonary delivery of a live vaccine could promote granulomatous lesions compared with subcutaneous vaccination.

The protection against *M. tuberculosis* with subcutaneous BCG vaccination depends on Th1 CD4+ T cell responses in mice. This T cell population is weak eliciting memory lymphocyte generation and a lack of mucosal-homing chemokine receptors that allow their arrival to the lung (Sakai et al., 2014; Perdomo et al., 2016, Ernst 2018). Thus, Th1,

CD4+CXCR3+ T cells are recruited to infection sites and may be required for protective immunity. In addition, experiment part II included CD8+ T cell analysis due to MHC-I restricted CD8+ T cell response also plays a role in *M. tuberculosis* immune response and granuloma formation.

In part I, similar results were found in CD4+CXCR3+ and CD4+CX3CR1+ populations at all time points. However, on day 120 in experiment part II, we observed that subcutaneous BCG administration elicits the highest CXCR3 expression in lung. Interestingly, the lowest number of this cell phenotype was observed in the group receiving intravenous BCG vaccination (Figure 2.7B), this concentration was even lower at day 30 after *M. tuberculosis* infection (day 210 after vaccination). Remarkably, one of the highest numbers of protective CXCR3+ was observed in the group that received the BCG aerosol vaccine (Figure 2.7A). These results suggest that BCG delivery routes strongly affect the induction of terminally differentiated CX3CR1+-non protective cells and less-differentiated CXCR3+ -protective cells.

Traditionally, the CD8+ T cells' role in the adaptive immune response to tuberculosis has been underexplored. However, studies performed in animal models propose a role of *M. tuberculosis*-specific CD8+ T cells in the *M. tuberculosis* infection control (Rozot et al., 2013). In this study, we included the evaluation of C-C chemokine receptor 7 (CCR7) that mediates homing to lymph nodes (Mahnke et al., 2013) and the PD-1 exhaustion marker in CD8+ T cells. The highest number of CD8+ and CD8+CCR7+PD1- cells were observed at day 120 post-vaccination, however at the end of the study (day 210 after vaccination and day 30 after infection), both cells' populations were low in lung, spleen, and lymph nodes.

In the cytokine profile obtained at day 30 post-infection (day 210 after vaccination), the production of IL-10 did not show significant differences among different routes of vaccine delivery. These results are interesting because this cytokine limits Th1 immune responses affecting the efficacy in controlling *M. tuberculosis* growth. Furthermore, the levels of IL-17A (produced by Th17 cells) did not have a statistical difference among BCG delivery

routes, and it was relatively low compared with other cytokines included in this study. In a contrasting context, an overproduction of IL-17A would not have protective effects and instead can affect the lung healing and homeostasis.

Overall, these data suggest a different pattern in the adaptive immune response based on the route of vaccination. The immune response is mainly elicited by CD4+ T cell immune response, being the intranasal delivery the most effective in decrease the growth of *M. tuberculosis* in lungs.

References

Abebe, F. (2012). Is interferon-gamma the right marker for bacille Calmette-Guerin-induced immune protection? The missing link in our understanding of tuberculosis immunology. Clin Exp Immunol 169, 213-219.

Aguilo, N., Alvarez-Arguedas, S., Uranga, S., Marinova, D., Monzon, M., Badiola, J., et al. (2016). Pulmonary but Not Subcutaneous Delivery of BCG Vaccine Confers Protection to Tuberculosis-Susceptible Mice by an Interleukin 17-Dependent Mechanism. Journal of Infectious Diseases 213(5), 831-839. doi: 10.1093/infdis/jiv503.

Aguilo, N., Uranga, S., Mata, E., Tarancon, R., Gomez, A.B., Marinova, D., et al. (2020). Respiratory Immunization With a Whole Cell Inactivated Vaccine Induces Functional Mucosal Immunoglobulins Against Tuberculosis in Mice and Non-human Primates. *Frontiers in Microbiology* 11. doi: ARTN 1339 10.3389/fmicb.2020.01339.

Anuradha, B., Rakh, S.S., Ishaq, M., Murthy, K.J.R., and Valluri, V.L. (2008). Interferon-gamma low producer genotype +874 overrepresented in bacillus Calmette-Guerin nonresponding children. *Pediatric Infectious Disease Journal* 27(4)**,** 325-329. doi: 10.1097/INF.0b013e31816099e6.

Aronson, N.E., Santosham, M., Comstock, G.W., Howard, R.S., Moulton, L.H., Rhoades, E.R., et al. (2004). Long-term efficacy of BCG vaccine in American Indians and Alaska Natives: A 60-year follow-up study. *JAMA* 291(17)**,** 2086-2091. doi: 10.1001/jama.291.17.2086.

Badawy, A.A., Yahya, R.S., Awad, S.I., Al-Sawah, G.A., and Kizilbash, N.A. (2013). Relationship between NRAMP1 gene polymorphism and efficacy of BCG vaccine in a helminth-infected population. *Genet Mol Res* 12(3)**,** 3048-3056. doi: 10.4238/2013.January.30.4.

Barclay, W.R., Anacker R.L., Brehmer W., Leif W., and Ribi E. (1970). Aerosol-Induced Tuberculosis in Subhuman Primates and the Course of the Disease After Intravenous BCG Vaccination. Infection and Immunity 2 (5), 574-582.

Batista, N.V., Chang, Y.H., Chu, K.L., Wang, K.C., Girard, M., and Watts, T.H. (2020). T Cell-Intrinsic CX3CR1 Marks the Most Differentiated Effector CD4(+) T Cells, but Is Largely Dispensable for CD4(+) T Cell Responses during Chronic Viral Infection. *Immunohorizons* 4(11)**,** 701-712. doi: 10.4049/immunohorizons.2000059.

Bernasconi, V., Norling, K., Bally, M., Hook, F., and Lycke, N.Y. (2016). Mucosal Vaccine Development Based on Liposome Technology. *J Immunol Res* 2016**,** 5482087. doi: 10.1155/2016/5482087.

Bottcher, J.P., Beyer, M., Meissner, F., Abdullah, Z., Sander, J., Hochst, B., et al. (2015). Functional classification of memory CD8(+) T cells by CX3CR1 expression. *Nat Commun* 6**,** 8306. doi: 10.1038/ncomms9306.

Brandt, L., Feino Cunha, J., Weinreich Olsen, A., Chilima, B., Hirsch, P., Appelberg, R., and Andersen, P. (2002). Failure of the Mycobacterium bovis BCG vaccine: some species of environmental mycobacteria block multiplication of BCG and induction of protective immunity to tuberculosis. Infect Immun 70, 672-678.

Brandtzaeg, P. (2009). Mucosal immunity: induction, dissemination, and effector functions. *Scand J Immunol* 70(6), 505-515. doi: 10.1111/j.1365-3083.2009.02319.x.

Cesta, M.F. (2006). Normal structure, function, and histology of mucosa-associated lymphoid tissue. *Toxicol Pathol* 34(5), 599-608. doi: 10.1080/01926230600865531.

Cha, S.B., Kim, W.S., Kim, J.S., Kim, H., Kwon, K.W., Han, S.J., Eum, S.Y., Cho, S.N., and Shin, S.J. (2015). Repeated Aerosolized-Boosting with Gamma-Irradiated Mycobacterium bovis BCG Confers Improved Pulmonary Protection against the Hypervirulent Mycobacterium tuberculosis Strain HN878 in Mice. PLoS One 10, e0141577.

Chackerian, A.A., Alt, J.M., Perera, T.V., Dascher, C.C., and Behar, S.M. (2002). Dissemination of Mycobacterium tuberculosis is influenced by host factors and precedes the initiation of T-cell immunity. Infect Immun 70, 4501-4509.

Chen, L., Wang, J., Zganiacz, A., and Xing, Z. (2004). Single intranasal mucosal Mycobacterium bovis BCG vaccination confers improved protection compared to subcutaneous vaccination against pulmonary tuberculosis. Infect Immun 72, 238-246.

Conceicao, E.L., Nascimento-Sampaio, F.S., Schwingel, P.A., Oliveira, E.S., Rocha, M.S., Vieira, I., et al. (2016). Revisiting the Heterogeneous IFN-gamma Response of Bacille of Calmette-Guerin (BCG)-Revaccinated Healthy Volunteers in a Randomized Controlled Trial: Effect of the Body Mass Index and of the IFNG+874 A/T Polymorphism. *PLoS One* 11(7), e0160149. doi: 10.1371/journal.pone.0160149.

Darrah, P.A., Zeppa, J.J., Maiello, P., Hackney, J.A., Ii, M.H.W., Hughes, T.K., et al. (2020). Prevention of tuberculosis in macaques after intravenous BCG immunization. *Nature* 577(7788), 95-+. doi: 10.1038/s41586-019-1817-8.

De Magistris, M.T. (2006). Mucosal delivery of vaccine antigens and its advantages in pediatrics. Advanced drug delivery reviews 58, 52-67.

Dockrell, H.M., and Smith, S.G. (2017). What Have We Learnt about BCG Vaccination in the Last 20 Years? *Frontiers in Immunology* 8. doi: ARTN 1134 10.3389/fimmu.2017.01134.

Ernst, J.D. (2018). Mechanisms of M. tuberculosis Immune Evasion as Challenges to TB Vaccine Design. Cell Host & Microbe 24, 34-42.

Fatima, S., Kumari, A., Das, G., and Dwivedi, V.P. (2020). Tuberculosis vaccine: A journey from BCG to present. *Life Sciences* 252. doi: ARTN 117594 10.1016/j.lfs.2020.117594.

Hawkridge, A. (2009). Clinical studies of TB vaccines. Hum Vaccines 5, 773-776.

Hellfritzsch, M. and Scherlie, R. (2019). Mucosal Vaccination Via Respiratory Tract. Pharmaceutics 11 (375), 1-24.

Henao-Tamayo, M., Ordway, D.J., and Orme, I.M. (2014). Memory T cell subsets in tuberculosis: What should we be targeting? *Tuberculosis* 94(5), 455-461. doi: 10.1016/j.tube.2014.05.001.

Hertwig, L., Hamann, I., Romero-Suarez, S., Millward, J.M., Pietrek, R., Chanvillard, C., et al. (2016). CX3CR1-dependent recruitment of mature NK cells into the central

nervous system contributes to control autoimmune neuroinflammation. *Eur J Immunol* 46(8), 1984-1996. doi: 10.1002/eji.201546194.
Hoft, S.G., Sallin, M.A., Kauffman, K.D., Sakai, S., Ganusov, V.V., and Barber, D.L. (2019). The Rate of CD4 T Cell Entry into the Lungs during Mycobacterium tuberculosis Infection Is Determined by Partial and Opposing Effects of Multiple Chemokine Receptors. Infect Immun 87.
Horvath, C.N., and Xing, Z. (2013). Immunization Strategies Against Pulmonary Tuberculosis: Considerations of T Cell Geography. Adv Exp Med Biol 783, 267-278.
Karin, N., and Wildbaum, G. (2015). The Role of Chemokines in Shaping the Balance Between CD4(+) T Cell Subsets and Its Therapeutic Implications in Autoimmune and Cancer Diseases. *Front Immunol* 6, 609. doi: 10.3389/fimmu.2015.00609.
Karin, N., Wildbaum, G., and Thelen, M. (2016). Biased signaling pathways via CXCR3 control the development and function of CD4+ T cell subsets. *J Leukoc Biol* 99(6), 857-862. doi: 10.1189/jlb.2MR0915-441R.
Li, J., Haifeng, Z., Fu, X., Zhang, M., Sun, F., and Fan, H. (2021). Dynamic role of macrophage CXCR1 expression in inflammatory bowel disease. Immunology Letters 232, 39-44.
Li, M., Wang, Y., Sun, Y., Cui, H., Zhu, S.J., and Qiu, H. (2020). Mucosal vaccines: Strategies and challenges. Immunology Letters 217, 116-125.
Logerot, S., Figueiredo-Morgado, S., Charmeteau-de-Muylder, B., Sandouk, A., Drillet-Dangeard, A.S., Bomsel, M., et al. (2021). IL-7-Adjuvanted Vaginal Vaccine Elicits Strong Mucosal Immune Responses in Non-Human Primates. *Frontiers in Immunology* 12. doi: ARTN 614115 10.3389/fimmu.2021.614115.
Lyadova, I.V., Vordermeier, H.M., Eruslanov, E.B., Khaidukov, S.V., Apt, A.S., and Hewinson, R.G. (2001). Intranasal BCG vaccination protects BALB/c mice against virulent Mycobacterium bovis and accelerates production of IFN-gamma in their lungs. *Clinical and Experimental Immunology* 126(2), 274-279. doi: DOI 10.1046/j.1365-2249.2001.01667.x.
Lycke, N. (2012). Recent progress in mucosal vaccine development: potential and limitations. *Nature Reviews Immunology* 12(8), 592-605. doi: 10.1038/nri3251.
Macpherson, A.J., McCoy, K.D., Johansen, F.E., and Brandtzaeg, P. (2008). The immune geography of IgA induction and function. *Mucosal Immunol* 1(1), 11-22. doi: 10.1038/mi.2007.6.
Mahnke, Y.D., Brodie, T.M., Sallusto, F., Roederer, M., and Lugli, E. (2013). The who's who of T-cell differentiation: Human memory T-cell subsets. European Journal of Immunology 43, 2797-2809.
Mangtani, P., Abubakar, I., Ariti, C., Beynon, R., Pimpin, L., Fine, P.E., et al. (2014). Protection by BCG vaccine against tuberculosis: a systematic review of randomized controlled trials. *Clin Infect Dis* 58(4), 470-480. doi: 10.1093/cid/cit790.
Manjaly Thomas, Z.R., and McShane, H. (2015). Aerosol immunisation for TB: matching route of vaccination to route of infection. Trans R Soc Trop Med Hyg 109, 175-181.
Mato, Y.L. (2019). Nasal route for vaccine and drug delivery: Features and current opportunities. *International Journal of Pharmaceutics* 572. doi: ARTN 118813 10.1016/j.ijpharm.2019.118813.

Messina, N.L., Netea, M.G., and Curtis, N. (2020). The impact of human single nucleotide polymorphisms on Bacillus Calmette-Guerin responses. *Vaccine* 38(40), 6224-6235. doi: 10.1016/j.vaccine.2020.07.032.

Mionnet, C., Buatois, V., Kanda, A., Milcent, V., Fleury, S., Lair, D., et al. (2010). CX3CR1 is required for airway inflammation by promoting T helper cell survival and maintenance in inflamed lung. *Nat Med* 16(11), 1305-1312. doi: 10.1038/nm.2253.

Moliva, J.I., Turner, J., and Torrelles, J.B. (2015). Prospects in Mycobacterium bovis Bacille Calmette et Guerin (BCG) vaccine diversity and delivery: why does BCG fail to protect against tuberculosis? Vaccine 33, 5035-5041.

Neutra, M.R., and Kozlowski, P.A. (2006). Mucosal vaccines: the promise and the challenge. *Nat Rev Immunol* 6(2), 148-158. doi: 10.1038/nri1777.

Pan, Y., Yang, X., Duan, J., Lu, N., Leung, A.S., Tran, V., et al. (2011). Whole-genome sequences of four Mycobacterium bovis BCG vaccine strains. *J Bacteriol* 193(12), 3152-3153. doi: 10.1128/JB.00405-11.

Perdomo, C., Zedler, U., Kuhl, A.A., Lozza, L., Saikali, P., Sander, L.E., Vogelzang, A., Kaufmann, S.H., and Kupz, A. (2016). Mucosal BCG Vaccination Induces Protective Lung-Resident Memory T Cell Populations against Tuberculosis. mBio 7.

Ritz, N., Hanekom, W.A., Robins-Browne, R., Britton, W.J., and Curtis, N. (2008). Influence of BCG vaccine strain on the immune response and protection against tuberculosis. Fems Microbiology Reviews 32(5), 821-841. doi: 10.1111/j.1574-6976.2008.00118.x.

Ritz, N., Tebruegge, M., Camacho-Badilla, K., Haeusler, G.M., Connell, T.G., and Curtis, N. (2012). To TST or not to TST: is tuberculin skin testing necessary before BCG immunisation in children? *Vaccine* 30(8), 1434-1436. doi: 10.1016/j.vaccine.2011.11.099.

Saini, D., Hopkins, G.W., Seay, S.A., Chen, C.J., Perley, C.C., Click, E.M., and Frothingham, R. (2012). Ultra-low dose of Mycobacterium tuberculosis aerosol creates partial infection in mice. Tuberculosis (Edinb) 92, 160-165.

Sakai, S., Kauffman, K.D., Schenkel, J.M., McBerry, C.C., Mayer-Barber, K.D., Masopust, D., et al. (2014). Cutting edge: control of Mycobacterium tuberculosis infection by a subset of lung parenchyma-homing CD4 T cells. *J Immunol* 192(7), 2965-2969. doi: 10.4049/jimmunol.1400019.

Shah, J.A., Lindestam Arlehamn, C.S., Horne, D.J., Sette, A., and Hawn, T.R. (2019). Nontuberculous Mycobacteria and Heterologous Immunity to Tuberculosis. J Infect Dis 220(7), 1091-1098. doi: 10.1093/infdis/jiz285.

Shah, J.A., Musvosvi, M., Shey, M., Horne, D.J., Wells, R.D., Peterson, G.J., et al. (2017). A Functional Toll-Interacting Protein Variant Is Associated with Bacillus Calmette-Guerin-Specific Immune Responses and Tuberculosis. *Am J Respir Crit Care Med* 196(4), 502-511. doi: 10.1164/rccm.201611-2346OC.

Sallin, M.A., Sakai, S., Kauffman, K.D., Young, H.A., Zhu, J., and Barber, D.L. (2017). Th1 Differentiation Drives the Accumulation of Intravascular, Non-protective CD4 T Cells during Tuberculosis. Cell Rep 18, 3091-3104.

Sharpe, S., White, A., Sarfas, C., Sibley, L., Gleeson, F., McIntyre, A., Basaraba, R., Clark, S., Hall, G., Rayner, E., et al. (2016). Alternative BCG delivery strategies improve protection against Mycobacterium tuberculosis in non-human primates:

Protection associated with mycobacterial antigen-specific CD4 effector memory T-cell populations. Tuberculosis (Edinb) 101, 174-190.
Soos, T.J., Sims, T.N., Barisoni, L., Lin, K., Littman, D.R., Dustin, M.L., et al. (2006). CX3CR1+ interstitial dendritic cells form a contiguous network throughout the entire kidney. *Kidney Int* 70(3)**,** 591-596. doi: 10.1038/sj.ki.5001567.
Srivastava, A., Gowda, D.V., Madhunapantula, S.V., Shinde, C.G., and Iyer, M. (2015). Mucosal vaccines: a paradigm shift in the development of mucosal adjuvants and delivery vehicles. *APMIS* 123(4)**,** 275-288. doi: 10.1111/apm.12351.
Stary, G., Olive, A., Radovic-Moreno, A.F., Gondek, D., Alvarez, D., Basto, P.A., et al. (2015). VACCINES. A mucosal vaccine against Chlamydia trachomatis generates two waves of protective memory T cells. *Science* 348(6241)**,** aaa8205. doi: 10.1126/science.aaa8205.
White, A.D., Sarfas, C., Sibley, L.S., Gullick, J., Clark, S., Rayner, E., Gleeson, F., Catala, M., Nogueira, I., Cardona, P.J., et al. (2020). Protective Efficacy of Inhaled BCG Vaccination Against Ultra-Low Dose Aerosol M. tuberculosis Challenge in Rhesus Macaques. Pharmaceutics 12.
White, A.D., Sarfas, C., West, K., Sibley, L.S., Wareham, A.S., Clark, S., Dennis, M.J., Williams, A., Marsh, P.D., and Sharpe, S.A. (2015). Evaluation of the Immunogenicity of Mycobacterium bovis BCG Delivered by Aerosol to the Lungs of Macaques. Clin Vaccine Immunol 22, 992-1003.
World Health Organization. (2018). BCG vaccine: WHO position paper, February 2018 - Recommendations. Vaccine 36, 3408-3410.
Yitbarek, K., Abraham, G., Girma, T., Tilahun, T., Woldie, M. (2020). The effect of Bacillus Calmette-Guerin (BCG) vaccination in preventing severe infectious respiratory diseases other than TB: implications for the COVID-19 pandemic. Vaccine 38, 6374–6380. doi: 10.1016/j.vaccine.2020.08.018

Chapter III

Mouse parenteral BCG vaccination and *Mycobacterium tuberculosis* infection alter the lung and gut microbiota and mycobiota

Introduction

Tuberculosis (TB) is a world-leading infectious disease caused by *M. tuberculosis*. According to the World Health Organization (WHO) Global Tuberculosis Report 2019, about 10 million people developed TB, and 1.4 million died (WHO, 2020). In humans, TB mainly affects the lower respiratory tract. When infection occurs, in most cases, the bacterium is contained by the host immune response as latent TB infection (Salgame et al., 2015, Chee et al., 2018). However, if coinfection or immune suppression occurs, the individual develops the active and infectious phase of the disease (Fatima et al., 2020). The only vaccine available against TB is the *M. bovis* Bacillus Calmette-Guérin (BCG), but this vaccine has a variable degree of protection (Cernuschi et al., 2018, Tanner et al., 2019, Fatima et al., 2020). The high variability of protection has been attributed to BCG strain variants, previous exposure to environmental mycobacteria, genetic variability on immune responses, and nutritional status (Dockrell and Smith, 2017; Zhu et al., 2018). To date, the development of a new and effective vaccine has been unsuccessful. This can be explained, to some extent, by the lack of knowledge in several key aspects of the immunopathogenesis of the disease. Additionally, the contribution of the local microbiota to the disease progression has not been elucidated, and the mycobiota remaining poorly studied (Wu et al., 2021).

The gut microbiota and its impact on infectious and non-infectious diseases are currently an intense research area (Li et al., 2016; Hakim et al., 2018; Ducarmon et al., 2019; Temraz et al., 2019). For instance, in the gut alone, microbial genes are hundreds of times more abundant than human genes, and they form a complex network within eukaryotic cells (Thomas et al., 2017). The gut microbiota is critical for the development and

homeostasis of the immune system, immune tolerance, catabolism of dietary fibers, and biosynthesis of amino acids and neuroactive amines (Radwan et al., 2020). Thus, the innate immune system and gut microbiota affect one another through complex interactions and pathways, and this crosstalk has been determined to be crucial for human health (Thaiss et al., 2016). The gut microbiota directly impacts the lung immune response, a communication known as the gut-lung axis (Marsland et al., 2015; Budden et al., 2017; Enaud et al., 2020). For instance, lung infection severity has been correlated with gut dysbiosis (Namasivayam et al., 2018). This interaction has implications in the lung capacity to control allergies and infectious diseases (Hufnagl et al., 2020). Short Chain Fatty Acids (SCFAs) produced by gut bacterial metabolism can travel through the bloodstream, induce immune cell development in the bone marrow, and influence lung immune responses (Cait et al., 2018; Hu et al., 2019; Radwan et al., 2020). Similarly, cells can migrate from the gut (Innate lymphoid cells and T helper 17 cells) to the lung and impact the local immunity (Wypych et al., 2019). Additionally, along with antibiotics, metabolic and infectious diseases trigger gut dysbiosis, which is linked with an impaired immune response in the lung (Carney et al., 2020). Regarding the fungal component, growing evidence of a significant influence of gut mycobiota on host's health has stimulated further recent research on gut mycobiota, especially in the context of IBD (Sokol et al., 2017; Tiew et al., 2020).

In the past decade, the lung was considered a sterile organ (Dickson and Huffnagle, 2015). Consequently, the US National Institute of Health initially neglected this organ in the Human Microbiome Project (Moffatt and Cookson, 2017; Salisbury et al., 2017; Wu and Segal, 2018). However, later it was revealed that the lung has a unique and complex microbiota worthy of analysis, whose composition and its particular and unique physiology govern biomass. Moreover, this organ is constantly exposed to microorganisms, and its composition and biomass are influenced by microbial inhalation, salivary micro-aspiration, cough, local immunity, and mucociliary clearance (Mathieu et al., 2018). Other considerations include that the lung microenvironment has unique characteristics such as an increased CO_2 and low O_2 partial pressure, elevated surface area, and higher temperature than the upper respiratory tract (Mathieu et al., 2018; Prisk and West, 2019).

Once again, the fungal component is less documented than the bacterial community. At the same time, lung mycobiota has been observed differing in patients with chronic inflammatory respiratory disease such as asthma, chronic obstructive pulmonary disease (COPD), cystic fibrosis (CF), and bronchiectasis compared with healthy lung mycobiome (Nguyen et al., 2015; Tipton et al., 2018; Vandenborght et al., 2021) Lung mycobiota can maintain microbial inter-kingdom crosstalk (Tipton et al., 2018; Soret et al., 2020) shaping local or long-reached host responses within the gut-lung-axis (Enaud et al., 2020).

Some diseases, such as asthma, COPD, and CF, have been associated with an imbalance of specific phyla and genera within the lung (Hilty et al., 2010; Nguyen et al., 2015; Cuthbertson et al., 2020). On the other hand, little is known about the impact that *M. tuberculosis* infection and BCG vaccination may have on the lung and gut microbiota. Comparing these two ways of potential lung and gut microbiota shifts may open new aspects of *M. tuberculosis* disease dynamics and explore how a parenteral vaccination may impact these two organs and the gut-lung axis. Exploring these questions would be essential to addressing the potential microbiota/mycobiota changes that BCG vaccination and *M. tuberculosis* infection cause in the host. Therefore, the lung and gut microbiota/mycobiota characterization can be helpful to detect disease markers, associate lung and gut dysbiosis with common infectious and non-infectious *M. tuberculosis* diseases, and contribute to the development of new therapeutics. The objective of this study was to establish gut and lung microbiota features in C57BL/6 mice after *M. tuberculosis* infection and BCG vaccination and to analyze the gut and lung microbiota/mycobiota to determine if specific microbial genus were implicated in the immunopathogenesis of TB.

Materials and methods

Study design and sample collection. Twenty-nine 6-8 weeks old female C57BL/6 mice (Jackson Laboratories, Bar Harbor, ME) were included in this study. Mice were divided into four groups: 1. Control (**Control**, n=6), 2. BCG vaccinated (**BCG**, n=6), 3. BCG vaccinated and *M. tuberculosis*-infected (**BCG+*M. tuberculosis***, n=6), and 4. *M.*

tuberculosis-infected (***M. tuberculosis***, n=6). Mice from groups 2 and 3 were vaccinated with BCG Pasteur via subcutaneous administration in the left flank in a $5x10^5$ CFU/mL dose. Thirty days after vaccination, mice from groups 3 and 4 were infected with *M. tuberculosis* H37Rv with $2x10^6$ CFU/mL to deliver 50-100 CFUs to each mouse using the Inhalation Exposure System (Glas-Col, Terre Haute, IN). The inoculum was plated on 7H11 agar to check inoculum purity, and five mice were euthanized on the day of infection to check the number of CFUs implanted into the lung. At 7- and 21-day post-infection, three mice per group were euthanized. The left lung lobe and a portion of the small intestine were aseptically removed from each mouse for DNA extractions.

DNA extraction and library preparation. According to the manufacturer's instructions, DNA was extracted from approximately 25mg of lung and intestine samples using the DNeasy Blood & Tissue kit (Qiagen, Hilden, Germany). Initial DNA concentration and quality were assessed using Nanodrop (Invitrogen, California USA) and stored at -80°C. DNA samples were used to sequence the variable 3–variable 4 (V3-V4) region of the 16S rRNA gene and the internal transcribed spacer 2 (ITS2) region of the fungal rRNA.

Two successive PCR tests were performed to amplify each target regions and attach adapters and indexes. For the PCR1, the DNA was standardized to 20ng/µL and checked in agarose gel to verify the amplicon size and the absence of unspecific bands. The microbial diversity and taxonomic composition of samples were assessed by using the V3-V4 region of the bacterial 16S rRNA gene and the ITS region of the fungal rRNA. The primers used to amplify the V3-V4 and ITS2 loci were 16S-Forward (TACGGRAGGCAGCAG) and 16S-Reverse (CTACCNGGGTATCTAAT) as well as ITS2-Forward (GTGARTCATCGAATCTTT) and ITS2-Reverse (GATATGCTTAAGTTCAGCGGGT) respectively, as previously described (Vandenborght et al., 2021). Controls included were the ZymoBIOMICSTM Microbial DNA Community Standard (mock community) and a no-template negative control, which were both processed alongside the mice samples, to validate the experimental procedures. Briefly, PCR amplification was performed by using barcoded primers (at a final concentration of 0.2 µM) with an annealing temperature of 50°C for 30 cycles and mixed in equimolar

amounts to be sequenced. PCR1 amplicons were purified to eliminate primers and primer dimers. Briefly, an adjusted volume of magnetic beads was added to each plaque well, mixed, and centrifuged 2min at 1800 rpm. The plaque was incubated for 5 min at room temperature and placed in DynaMagTM -96 Side Skirted Magnet (Invitrogen) for 2 min. After incubation, the supernatant was eliminated, and two consecutive washes with 70% EtOH were performed while keeping the plaque in the magnet. After EtOH washes, the plaque was let dry for 5 min and removed from the magnet. 25µL of 10mM Tris pH 8.5 was added to each well, mixed, centrifuged for 2 min at 1800 rpm, and incubated at room temperature for 2 min. The plaque was then placed in the magnet for 2 min, and 20µL of the clear supernatant was transferred to a new PCR plaque. After purification, master mix preparation was performed for PCR2 to add indexes and adapters. PCR1 products were diluted 1:10, and indexes were added at 5µM. PCR2 products were quantified to pool the samples in equimolar. The library's size was verified with Tapestation, normalized, and pooled before sequencing.

Sequencing and Bioinformatic analysis. Next-generation sequencing (NGS) was performed by using 250-bp paired-end technology on the MiSeq platform (Illumina, San Diego, CA) with V3 chemistry at the PGTB platform of Bordeaux University. The bacterial reads were demultiplexed, then 16S and ITS2 primers were removed using CutAdapt, with no mismatch allowed within the primer sequences. All samples were processed through the DADA2 pipeline in R (version 4.0.3) for quality filtering and trimming, dereplication, and merging of paired-ends reads (Callahan et al., 2016a, 2016b, 2017). According to a recent evaluation (Pauvert et al., 2019), only forward (R1) sequences were analyzed with DADA2 and no filter other than the removal of low-quality and chimeric sequences were applied for characterizing the fungal community. Two Amplicon Sequence Variant (ASV) tables were constructed, and taxonomy was assigned from Silva database (release 138). Mock community was used to avoid a non-efficient sequencing experiment, and negative controls to identify and remove potential reagent contaminants with microDecon R package (McKnight et al., 2019). ASVs present in less than 3 samples were removed (Holmes et al., 2020). The final read counts were 285256 (Mean of 11 886 ±SD) at the intestine site and 35 179 (Mean of 1466 ±SD) at the lung site.

Statistical analysis. A nonparametric Wilcoxon-Mann-Whitney test was used to compare quantitative variables between groups. Statistical analyses were performed with the RStudio program (Version 4.0 for WindowsTM). A p-value < 0.05 was considered indicative of statistical significance.

Alpha- and beta-diversity indexes were assessed using ASV occurrence counts and a multidimensional Scaling (MDS) ordination method with Bray-Curtis distance metric implemented by R package 'Phyloseq' for each microbial component (bacterial and fungal) and each organ (gut and lung). To compute beta-diversity, the ASVs table was first rarefied (using phyloseq's rarefy_even_depth function) at a minimum sequence depth. Between sample beta-diversity differences (measured using Bray Curtis dissimilarity) were tested using a permutational multivariate ANOVA (PERMANOVA) from vegan R package with 10,000 permutations, while accounting for individual identity as a covariate.

DESeq2 (Love et al., 2014) was used to perform two-class testing for differential relative abundance. Paired tests (by subject) were used when comparing gut and lung microbiota diversities of groups of mice, as follow: (i) Vaccination effect was assessed by comparing uninfected mice only (non-vaccinated mice vs vaccinated mice whatever the day (7 or 21) of sacrifice), and (ii) *M. tuberculosis* infection effect was assessed by comparing infected mice without vaccination on one side (control vs *M. tuberculosis* groups whatever the day (7 or 21) of sacrifice), and infected and vaccinated mice on the other side (*M. tuberculosis* vs BCG+*M. tuberculosis* whatever the day (7 or 21) of sacrifice).

To associate microbial composition to either BCG vaccination or *M. tuberculosis* infection effect on mice, we used Bayesian multinomial logistic-normal linear regression, implemented in the R package stray as the function pebble (Holmes at al., 2020; Silverman et al., 2018). As previously described (Holmes at al., 2020; Silverman et al., 2018), we chose this method because it considers uncertainty due to counting and compositional data usually known in targeted metagenomics. In addition, Holmes et al

(Holmes et al., 2020) proposed to transform results into centered log-ratio coordinates for interpretation, based on theory from compositional data analysis and credible intervals and figures.

Results

BCG vaccination and *M. tuberculosis* infection change the alpha-diversity in both the lung and gut; however, BCG vaccination has a more pronounced effect on lung diversity

To analyze the vaccination effect, uninfected mice were divided into two groups (n=6 per group) independently of the day (7 or 21) of sacrifice. Observed ASVs, Shannon, and Simpson indexes were used to determine differences within alpha-diversity of lung and gut microbiota between groups. While in the intestine, no statistical significance was observed (Figure 3.1A), not-vaccinated mice were statistically less diverse in the lung than the vaccinated group (Figure 3.1B, p-value= 0.0131 of Shannon index).

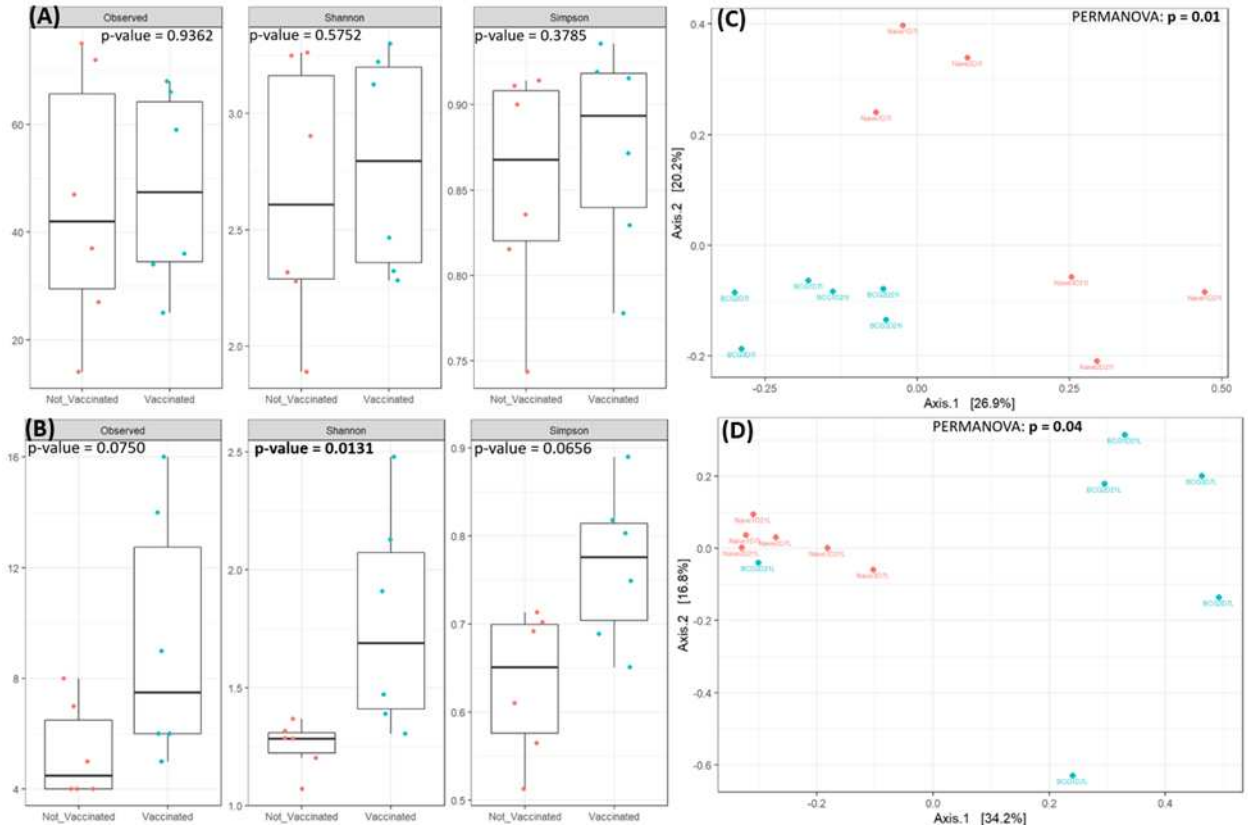

Figure 3.1. Vaccination effect on gut (A, C) and lung (B, D) microbiota alpha- (A, B) and beta-diversities (C, D) (based on uninfected mice analysis (non-vaccinated mice (●) *vs* vaccinated mice (●)).

To analyze the effect of *M. tuberculosis* infection in the lung and gut microbiota, infected and non- infected mice were divided into two groups (n=6 per group), independent of the time of euthanizes (7- or 21-days post-infection) and accordingly if they were or not vaccinated (Figures 3.2 and 3.3, respectively). Comparing infected and vaccinated mice to vaccinated but non-infected mice confirmed that statistical significance was not observed in the alpha-diversity measures at the gut level (Figure 3.2A). However, *M. tuberculosis* infected and unvaccinated mice showed a higher alpha-diversity in the lungs than uninfected unvaccinated mice (Figure 3.3B, p-values at 0.0131 and 0.0202 Shannon and Simpson indexes).

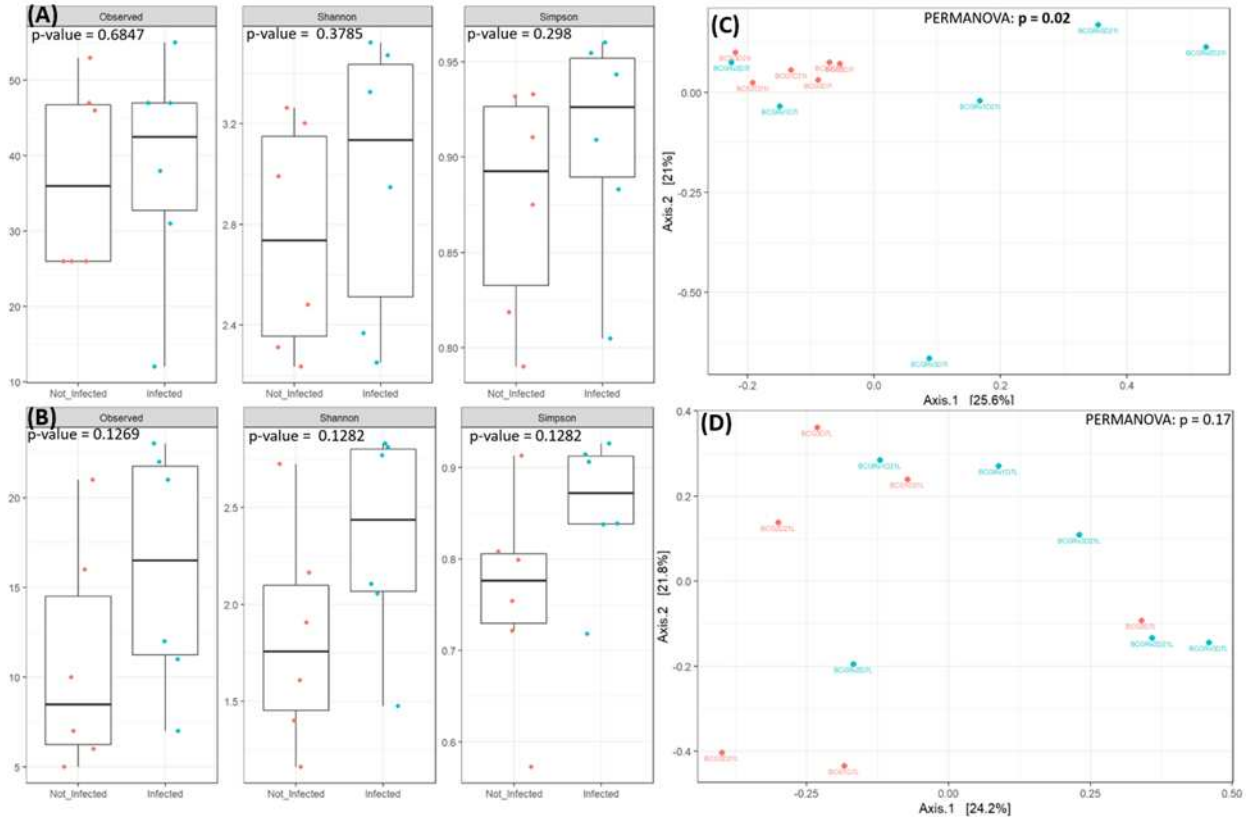

Figure 3.2. *M. tuberculosis* infection effect on gut (A, C) and lung (B, D) microbiota alpha- (A, B) and beta-diversities (C, D) based on infected plus vaccinated mice analysis (vaccinated but non-infected mice (●) *vs M. tuberculosis* infected and vaccinated mice (●))

Lung and gut beta-diversity confirms separation in groups according to BCG vaccination and *M. tuberculosis* infection

At the beta-diversity level, vaccinated uninfected mice were in closer proximity in both organs' lungs and intestines, which indicated similar gut and lung microbial community composition (Figures 3.1C, 3.1D, PERMANOVA p=0.01 and 0.04 respectively). This clustering according to BCG vaccination was confirmed when analyzing vaccinated and infected mice at the intestine level (Figure 3.2C; PERMANOVA p=0.02).

At the lung level, we confirmed the effect of *M. tuberculosis* infection on alpha-diversity. We observed that samples obtained from the infected and non-vaccinated mice group (*M. tuberculosis*) from day 7 and day 21 post-infection were in very nearness indicated a highly similar lung microbial community composition among these mice (Figure 3.3D, PERMANOVA p=0.01).

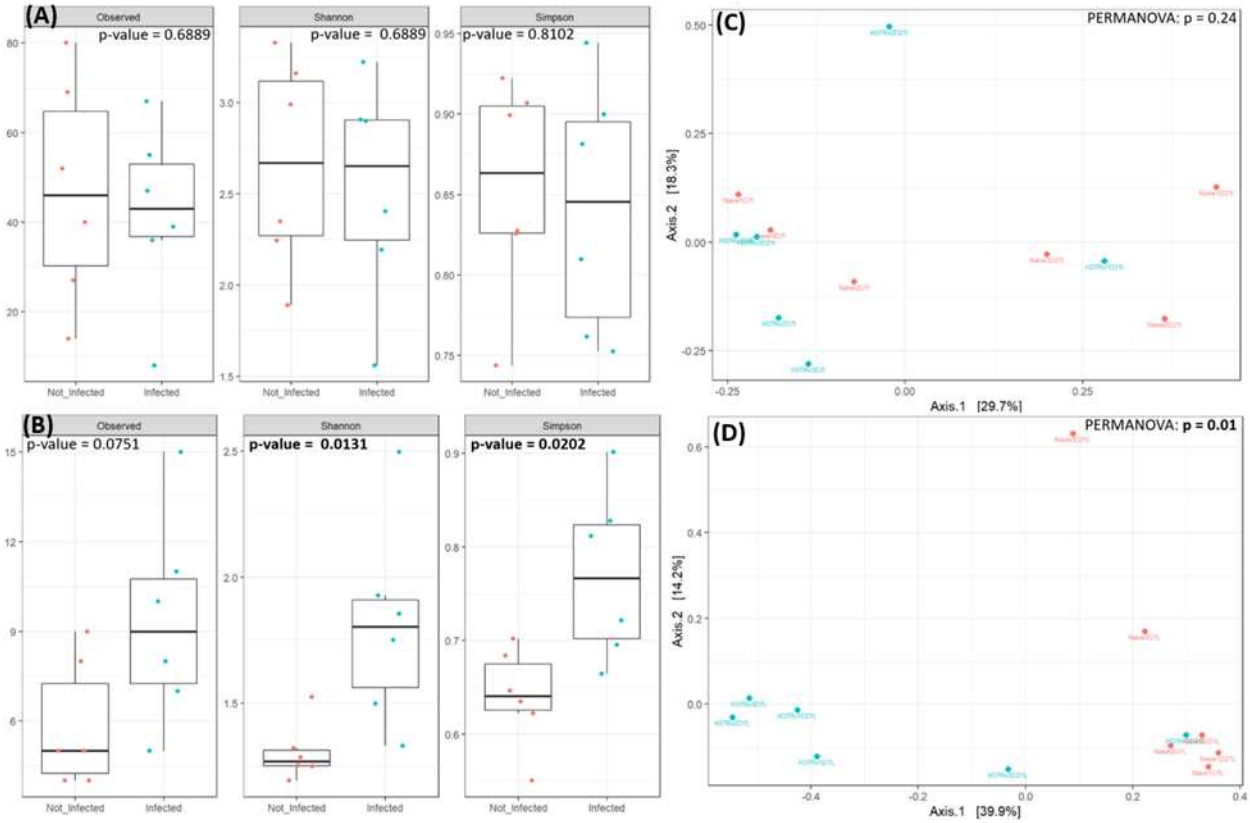

Figure 3.3. *M. tuberculosis* infection effect on gut (A, C) and lung (B, D) microbiota alpha- (A, B) and beta-diversities (C, D) based on infected unvaccinated mice analysis (non-vaccinated non-infected mice (●) *vs M. tuberculosis* infected but non-vaccinated mice (●))

Firmicutes, Bacteroidetes, and Proteobacteria abundances were the most affected phyla after BCG vaccination and *M. tuberculosis* infection

Interestingly, in the vaccinated mice, both whatever the *M. tuberculosis* infection status (uninfected (BCG group) Figures 3.4A and 3.4D, and infected group (BCG+*M. tuberculosis*) figures 3.4B and 3.4E), there was a significant increase in the relative abundance of Firmicutes and Bacteroidetes at the lung level (Figures 3.4D and 3.4E); the same trend is observed at the intestine level (Figures 3.4A and 3.4B). Remarkably, Proteobacteria phylum appeared in a higher proportion in the control group (Figure 3.4D) and was significantly decreased when vaccinated mice were infected (Figure 3.4E). Tenericutes phylum was significantly decreased in vaccinated and infected groups (BCG + *M. tuberculosis* mice) at the intestine level (Figure 3.4B).

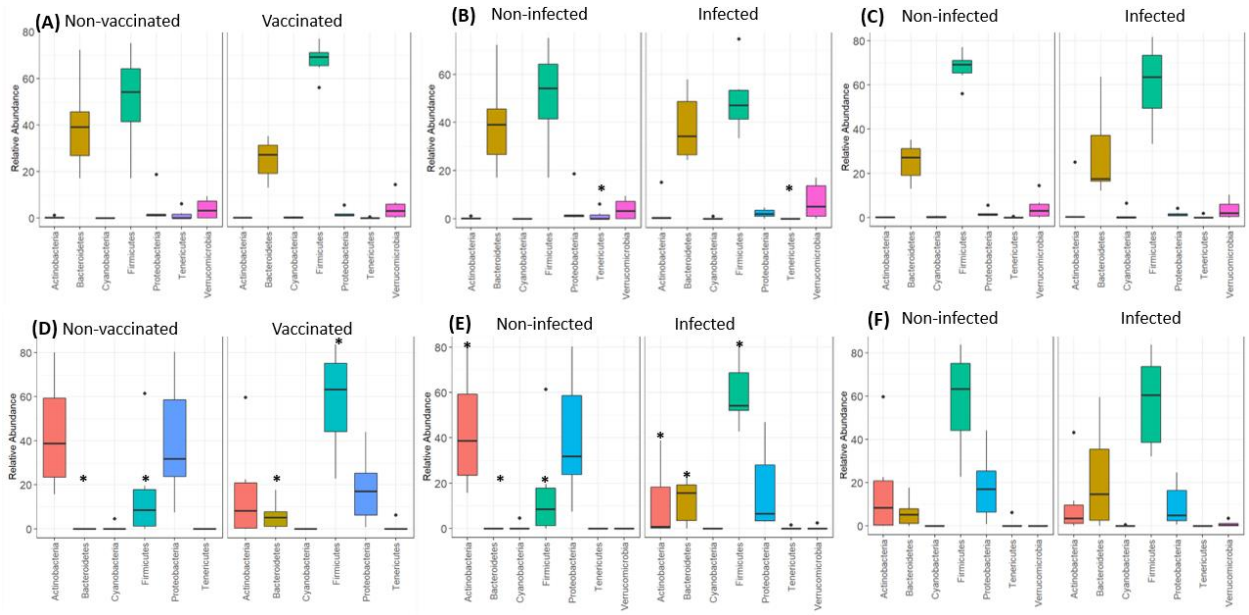

Figure 3.4. Phylum relative abundance distribution when comparing vaccination and *M. tuberculosis* infection effects on gut (A-C) and lung (D-F) microbiota composition of non-vaccinated *vs* vaccinated mice (A, D), non-infected *vs* infected mice among unvaccinated mice (B, E), and non-infected *vs* infected mice among BCG vaccinated mice (C, F). Only significant p (*p<0.05 using Wilcoxon rank sum test with continuity correction) are notified among Actinobacteria ■, Bacteroidetes ■, Cyanobacteria ■, Firmicutes ■, Proteobacteria ■, Tenericutes ■, and Verrucomicrobia ■.

These results were confirmed using a multivariate regression model previously applied to microbiota analysis (Holmes et al., 2020). Firmicutes relative abundance was positively correlated with BCG vaccination and *M. tuberculosis* infection in the gut at day 7 (Figure 3.5A) and with BCG vaccination gut at day 21 in lungs (Figure 3.5B), when the adaptive immune response against *M. tuberculosis* was established (from day 7 post-infection to day 21 post-infection). A similar positive correlation was observed in the lung at both times (Figures 3.5C and 3.5D). These results could have some association with the protective immune response induced by BCG in *M. tuberculosis* infected mice. No statistical difference was observed comparing groups or days in the abundance of Bacteroidetes or Proteobacteria, excepted in the lung at day 21. An increase in the relative abundance of Bacteroidetes and a decreased relative abundance of Proteobacteria were observed (Figure 3.5D). Surprisingly, quantitative differences in the relative abundances of Cyanobacteria were associated with BCG vaccination at the gut level. An increase in Cyanobacteria relative abundance at day 7 was first associated with BCG vaccination

(Figure 3.5A), while a decrease in Cyanobacteria relative abundance was then associated with BCG vaccination and *M. tuberculosis* infection at day 21. This Cyanobacteria abundance decrease was also found at the lung level associated with both BCG vaccination and *M. tuberculosis* infection (Figures 3.5C, 3.5D).

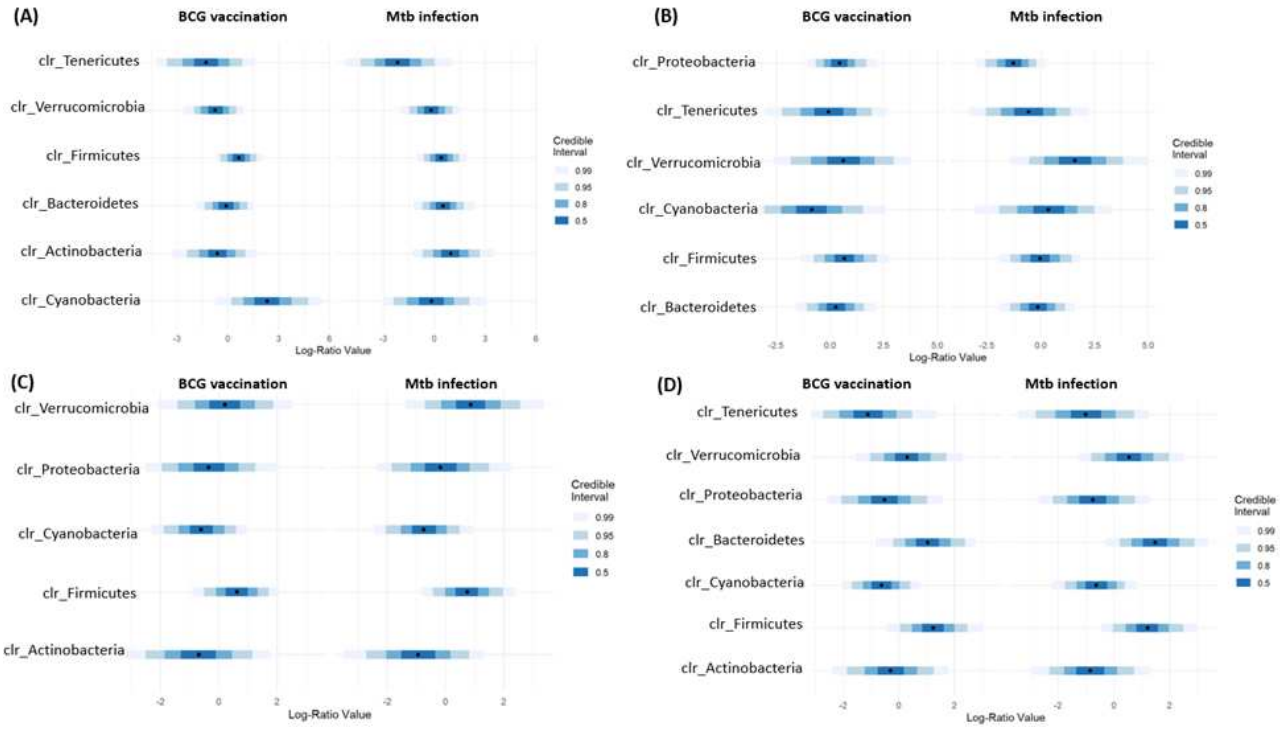

Figure 3.5. Phyla found to be credibly associated with BCG vaccination and *M. tuberculosis* infection status on gut (A, B) and lung (C, D) in at least one of our two conditions at day 7 (A, C) and day 21 (B, D) using a multivariate regression model.

Genus credibly associated with BCG vaccination and *M. tuberculosis* infection status and the gut-lung axis evolution

Based on the same multivariate regression model applied to microbiota analysis at the genus level, numerous genera were correlated with either BCG vaccination or *M. tuberculosis* infection (Figures 3.6 and 3.7), with an increased genus number at day 21 compared with day 7 at lung level (Figure 3.7). Among them, several genera were selected as associated with a non-zero effect.

At the intestine level, BCG vaccination was associated with lower abundances of *Alistipes*, *Erysipelatoclostridium*, and a higher abundance of *Bacillus* at day 7 (Figure

3.6A). On day 21, genus changes were more numerous; vaccination was associated with lower abundances of *Bacillus* and *Rhizobium* and with higher abundances of *Intestinimonas*, *Bacteroides*, *Turicibacter*, *Romboutsia*, and *Clostridium* (Figure 3.6B).

M. tuberculosis infection was associated with lower abundances of Eggerthellaceae (DNF00809) and *Angelakisella* and a higher abundance of Ruminococcaceae_UCG-014 at day 7 (Figure 3.6A). On day 21, it was associated with lower abundances of *Escherichia/Shigella*, *Romboutsia*, *Clostridium*, and *Proteus*, and with higher abundances of *Intestinimonas* and *Erysipelatoclostridium* (Figure 3.6B).

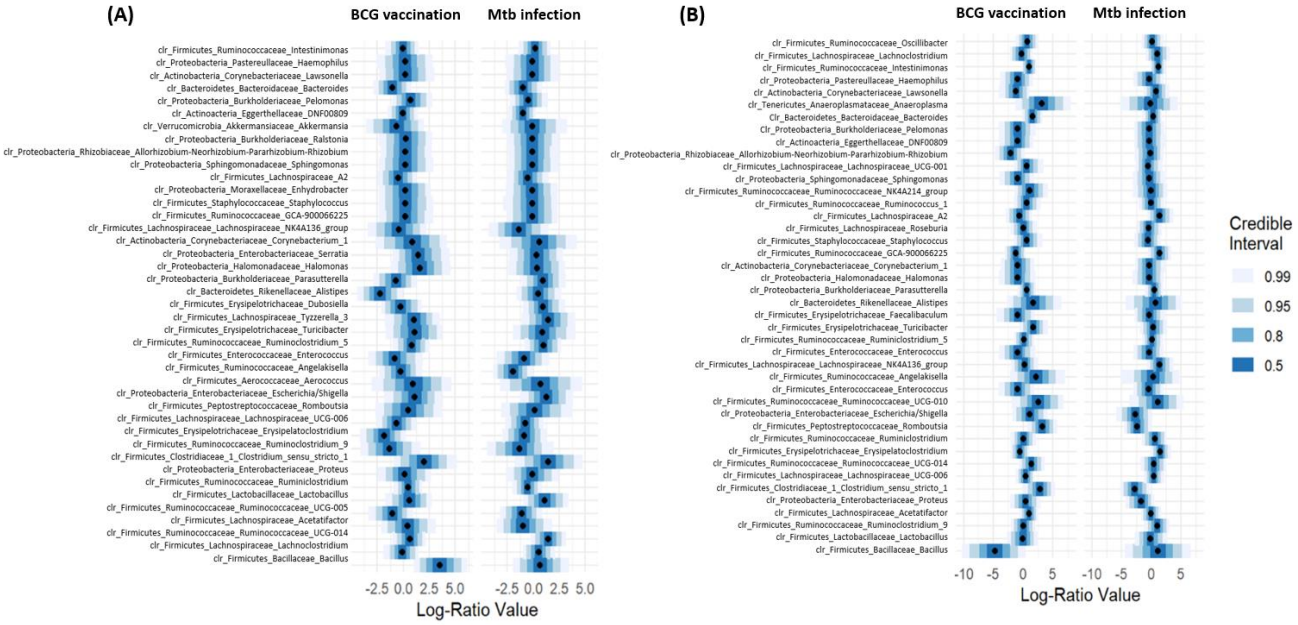

Figure 3.6. Genera found to be credibly associated with BCG vaccination and *M. tuberculosis* infection status on gut in at least one of our two conditions at day 7 (A) and day 21 (B) using a multivariate regression model.

At the lung level, few genera were associated with vaccination status: an only high abundance of Lachnospiraceae was associated with BCG vaccination at day 7, confirmed at day 21 (Figures 3.7A, 3.7B). On day 21, vaccination was also associated with higher abundances of *Lactobacillus* and *Ruminiclostridium* and a lower abundance of *Lawsonella* (Figure 3.7B).

On the other side, *M. tuberculosis* infection was associated with a more significant number of genera. On day 7, infection was associated with lower abundances of

Aerococcus, *Flavonifractor*, *Ralstonia*, and *Pseudomonas*, and with higher abundances of *Bifidobacterium*, *Alistipes*, *Clostridium*, *Dubosiella*, *Turicibacter*, Lachnospiraceae, *Lactobacillus*, *Romboutsia*, *Ruminiclostridium*, and *Akkermansia* (Figure 3.7A). These associations were confirmed on day 21, excepted abundance of *Flavonifractor*, *Ralstonia*, *Bifidobacterium*, *Alistipes*, *Dubosiella*, and *Lactobacillus*. In addition, infection was associated with lower abundances of *Corynebacterium*, *Lawsonella*, *Staphylococcus*, *Escherichia*/*Shigella*, *Proteus*, *Serratia*, *Halomonas*, and *Enhydrobacter*, and with higher abundances of *Roseburia*, *Oscillibacter*, and *Ruminococcus* (Figure 3.7B).

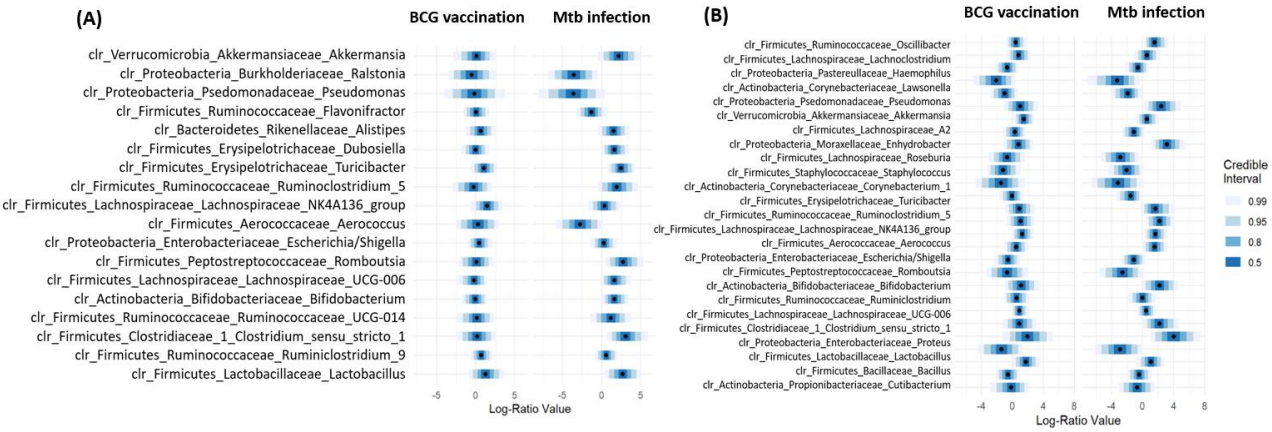

Figure 3.7. Genera found to be credibly associated with BCG vaccination and *M. tuberculosis* infection status on lung in at least one of our two conditions at day 7 (A) and day 21 (B) using a multivariate regression model.

Focusing on the gut-lung axis, our multivariate regression approaches allowed us to compare the profile evolution of microbiota of both intestine and lungs at days 7 and 21. More genera have modified relative abundances (not centered on log 0; Figure 3.6) associated with BCG vaccination status at a gut level compared with lungs, especially at day 21 (Figure 3.6B). Conversely, at the lung level, genera that have modified relative abundances associated with *M. tuberculosis* infection were numerous at both time points (Figure 3.7), indicated that the local host response against infection impacted the whole microbial flora while the immune response after vaccination modified mainly the gut microbiota.

Mycobiota genus credibly associated with BCG vaccination and *M. tuberculosis* infection status and the gut-lung axis evolution

We performed mycobiota analysis based on the same multivariate regression model applied to microbiota analysis. Only a few fungi genera were correlated with either BCG vaccination or *M. tuberculosis* infection (Figures 3.8 and 3.9). Among them, several genera were selected as associated with a non-zero effect.

Our multivariate regression approaches allowed us to compare the profile evolution of mycobiota of intestine and lungs at days 7 and 21. Some genera have modified relative abundances (not centered on log 0; Figures 3.8 and 3.9) associated with BCG vaccination status at lung level at day 7 (Figure 3.8) and associated with vaccination and infection at day 21 on the gut (Figure 3.9).

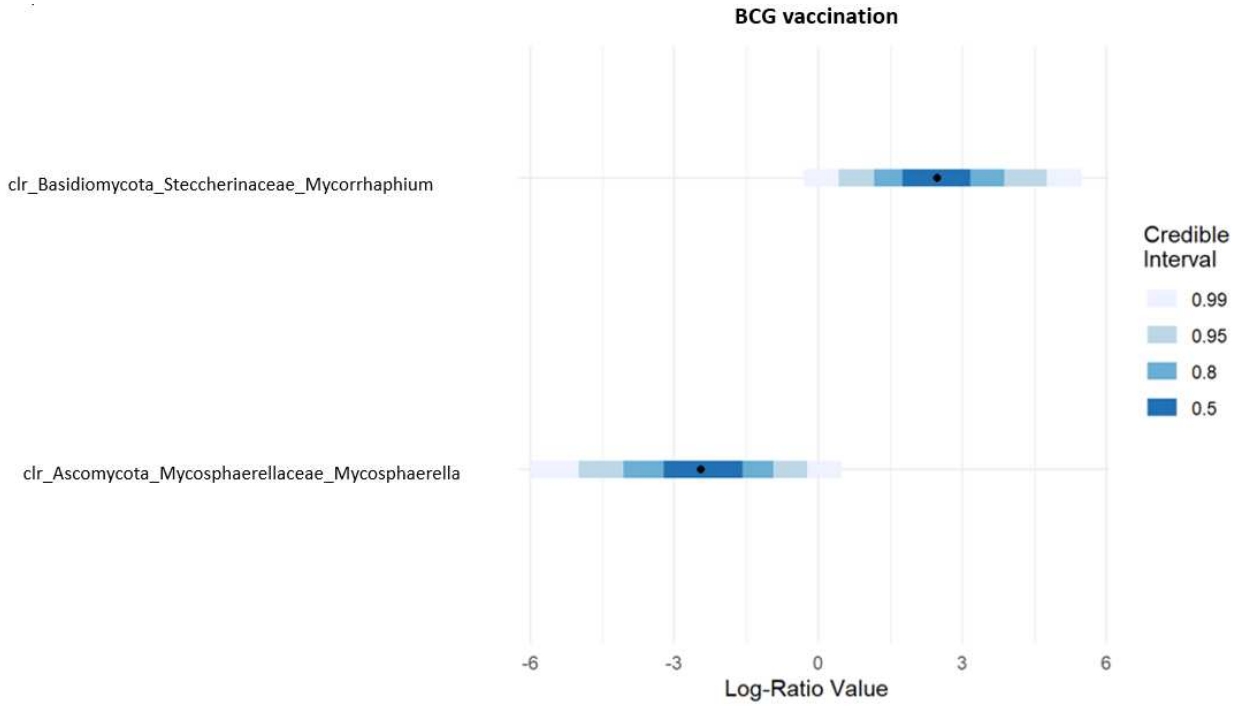

Figure 3.8. Genera found to be credibly associated with BCG vaccination on lung at day 7 using a multivariate regression model.

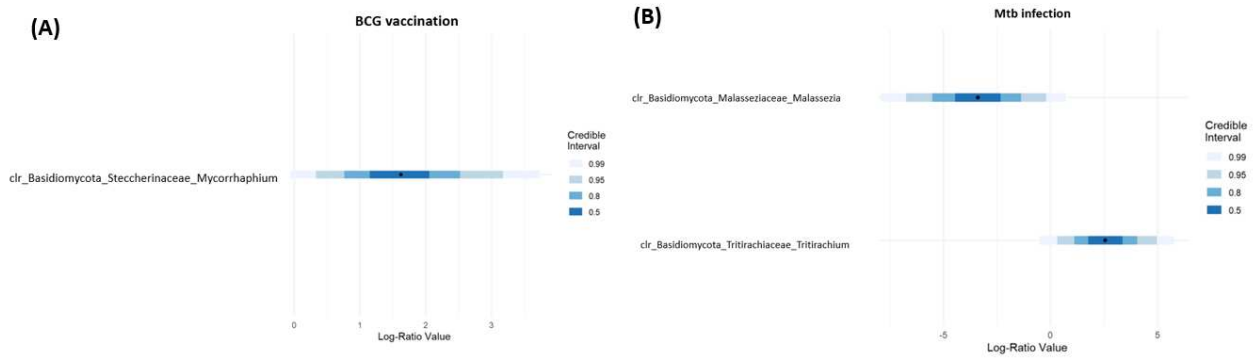

Figure 3.9. Genera found to be credibly associated with BCG vaccination (A) and *M. tuberculosis* infection (B) status on gut in at day 21 using a multivariate regression model.

At the lung level, only two genera were associated with vaccination status. *Mycorrhaphium* abundance was positively associated, and *Mycosphaerella* was negatively associated with BCG vaccination at day 7 (Figure 3.8). At the gut level day 21, only *Mycorrhaphium* and *Tritirachium* were positively correlated with vaccination with infection, respectively. Also, *Malassezia* was negatively associated with infection (Figure 3.9).

Discussion

The lung and the gut micro- and mycobiota were analyzed to determine critical bacterial changes associated with the effect of *M. tuberculosis* infection and BCG vaccination. Four groups of mice were included in this study: 1. Control (Control, n = 6), 2. BCG vaccinated (BCG, n=6), 3. BCG vaccinated and *M. tuberculosis*-infected (BCG+*M. tuberculosis*, n=6), and 4. *M. tuberculosis*-infected (*M. tuberculosis*, n=6). Thirty days after the BCG vaccination of groups 2 and 3, groups 3 and 4 received a low dose of *M. tuberculosis* infection via the aerosol route. Lung and gut tissue samples were then obtained for microbiota analysis from all groups on day 7 and 21 post- *M. tuberculosis* infection.

Like the human lung, the most prevalent phyla found in the mice lung were Firmicutes, Proteobacteria, and Bacteroidetes. The prevalence of these three phyla has been previously reported (Wang et al., 2017; Yang et al., 2019 (a), Barcik et al., 2020; Invernizzi et al., 2020). However, we observed high variability in the relative abundance at the

phylum and genus levels based on the treatment group (Figures 3.1-3.3). As previously reported, we observed higher abundances of *Escherichia*/*Shigella*, and *Alistipes* in the gut microbiota of mice vaccinated and infected (Guo et al., 2020). Nevertheless, comparing the two organs (Figures 3.4-3.6), the lung was the most affected organ after *M. tuberculosis* infection and BCG vaccination in our study.

To date, it has been established that a healthy lung has low biomass and high bacterial diversity (Liu et al., 2019; O'Dwyer et al., 2019; Liu et al., 2020). However, our data show that both *M. tuberculosis* infection and BCG vaccination increase bacterial alpha-diversity in the lungs. Some studies in mice have noted that an increased lung bacterial diversity may precede pathological outcomes in the lungs, as observed in our results. For instance, Yang et al., 2019 (b) showed that an increased alpha-diversity precedes lung fibrosis via IL17R signaling in C57BL/6 mice. Another study (Cui et al., 2012) showed that infected patients with symptomatic *M. tuberculosis* infection without being treated had higher bacterial diversity and more unique taxa than controls. Although infection and vaccination increase lung diversity, our results, including alpha- and beta-diversity data, show that infection and vaccination mainly differ in the dominance of specific bacterial genera such as *Pseudomonas*, *Corynebacterium*, *Clostridium*, *Roseburia*, *Akkermansia*, and *Ruminococcus*.

Interestingly, *Pseudomonas*, an opportunistic pathogen associated with chronic lower respiratory infections, was found in lower abundance in the infected group. These results are remarkable because *Pseudomonas* is usually present as a primary pathogen in patients with chronic lung diseases such as cystic fibrosis, chronic obstructive pulmonary disease, idiopathic pulmonary fibrosis, and bronchiectasis (Collie et al., 2015; Waters et al., 2017; Maurice et al., 2018; Invernizzi et al., 2020; Soret et al., 2020). This pathogen can form biofilms during lung infection (Waters et al., 2017; Maurice et al., 2018) and has been recognized as a critical bacterium associated with lung disease progression and severity, especially in CF (Davies et al., 2006; Vandeplassche et al., 2020). In addition, *Pseudomonas* was found more abundant in *M. tuberculosis* patients who were

unsuccessfully treated and had recurrent cases compared with other patient groups (Wu et al., 2013).

Corynebacterium was also observed in lower abundance in infected mice. This genus usually is present in the respiratory tract (Kanmani et al., 2017; Yang et al., 2018) but with contradictory effects on the host. In BALB/c mice, the presence of this genus has been associated with resistance to viral and bacterial infections (Kanmani et al., 2017); however, in humans, it has been associated with pneumonia (Yang et al., 2018; Baek et al., 2020). Future analysis is needed at this point as we can determine, with shotgun metagenomic, the specific species associated with this change.

Conversely, *Clostridium*, *Roseburia*, *Akkermansia*, and *Ruminococcus* were observed in higher abundances of infected mice lungs. While these genera have been associated with gut dysbiosis in human *M. tuberculosis* infection, only *Clostridium* was increased in the gut microbiota of *M. tuberculosis* patients compared with controls (Hu et al., 2019).

As previously reported in *M. tuberculosis* infection (Krishna et al., 2016), Firmicutes were significantly elevated in the lungs of infected mice compared with uninfected mice. Proteobacteria, which appears in a higher proportion in the control group, decreased the abundance after infection and vaccination. Remarkably, a decrease in the relative abundance of Proteobacteria has been previously observed in lung aging studies. Lee et al., 2019 observed that an increase of Firmicutes (also observed in our three treatment groups) and a decrease of Proteobacteria were associated with elderly lung and reduced lung function. Thus, our results seem to indicate that lung dysbiosis induced by vaccination and infection may induce physiological lung changes and local oxidative stress typically observed in elderly and tuberculosis patients (Teskey et al., 2018). Firmicutes-dominated dysbiosis in the lung, in agreement with our results, has been associated with the expression of pro-inflammatory genes in pulmonary leukocytes (Budden et al., 2017). These changes can also be correlated with local shifts observed by specific T and B cell immune responses previously reported in BCG vaccinated and infected mice (Hoft et al., 1998; Abebe 2012; Bull et al., 2018; Ogongo et al., 2019). The

published data and ours confirmed that lung Firmicutes' relative abundance changes are observed as signs of the typical innate and adaptive immune response to *M. tuberculosis*. A metanalysis study performed by Eshetie and Soolingen (Eshetie and Soolingen, 2019) compared the lung microbiota of healthy and TB patients, showing that Bacteroidetes are present in higher abundance in healthy controls (23.5% of abundance). Our results indicated that Bacteroidetes in the C57BL/6 model were present in very low abundance in lungs of mice and that BCG vaccination significantly increased the relative abundance of this phylum as observed in lungs of vaccinated mice compared with non-vaccinated mice (Figure 3.4D). However, these results need to be further documented since we also observed a significant increase of Bacteroidetes in the lungs of infected mice among unvaccinated mice (Figure 3.4E); the same trend is observed when infected mice among BCG vaccinated mice were analyzed (Figure 3.4F).

The Firmicutes/Bacteroidetes (F/B) ratio is essential to maintaining normal intestinal homeostasis. For instance, an increased or decreased ratio has been associated with obesity or inflammatory bowel disease, respectively (Mariat et al., 2009; Magne et al., 2020; Stojanov et al., 2020). Our study showed that infected mice previously vaccinated (BCG+*M. tuberculosis*) together with the control group and the BCG only vaccinated mice had a more similar intestine F/B ratio, compared with only infected mice (control: 2.13 ±0.77; BCG: 2.96±0.63; BCG+*M. tuberculosis*: 3.18±0.78; *M. tuberculosis*: 1.56±0.44).

Moreover, our study demonstrated that the intestine and the lung have direct bidirectional communication with microbiota changes as early as 7 days post-*M. tuberculosis* infection. Using a multivariate regression approach in the micro and mycobiota, we were able to show that microbiota profile evolution was more marked after BCG vaccination at the intestine site and after *M. tuberculosis* infection at the lung site (Figures 3.6, 3.7). This profile has indicated that the local host response against infection impacted the whole microbial flora while the immune response after vaccination modified mainly the gut microbiota. At the mycobiome level, only a few genera were associated with vaccination and infection (Figures 3.8, 3.9).

Several of the modified taxa we identified have been previously described as host immune modulators: For example, Bacteroides (a phylum increased in the gut microbiota of vaccinated mice at 21 days; Figure 3.6B) produced polysaccharides that mediate mucosal tolerance via upregulation of Treg cells (Shen et al., 2012). *Lactobacillus* can modulate adaptive but also innate immune responses via direct binding to pattern recognition receptors (Wells, 2011), which is congruent with the identification of this phylum as increased primary (at day 7 but not at day 21) and in both sites (lungs and intestine) (Figures 3.6, 3.7). As observed in previous experiments, possible bidirectional gut-lung communications may include (i) direct migration of innate lymphoid and Th17 cells (Gray et al., 2017; Huang et al., 2018), (ii) elicitation of lung Interferon through the microbial metabolite desamirotyrosine produced in the intestine (Steed et al., 2017), and (iii) development of immune cells in the bone marrow through the effect of unmetabolized short-chain fatty acids (SCFAs) derived from the metabolism of dietary fibers (Trompette et al., 2014; 2018).

Finally, we demonstrated for the first time that lung and gut dysbiosis are also induced via parenteral vaccination through the subcutaneous route. The specific microbiota interactions observed in the gut and lung after *M. tuberculosis* infection must be further studied, especially through shotgun metagenomics. Well-designed studies on the *M. tuberculosis* long-term effects could determine specific bacterial species involved in the disease progression and could also determine whether treatment with specific microbiota such as fecal transplantation shown to improve Th1 immunity and lesser Treg cell populations and to reduce severity to *M. tuberculosis* infection of animals (Khan et al., 2016) or their metabolites in the lung and the gut may favor immunopathogenesis of TB.

Shortly, microbial therapies could help treat patients suffering from TB or improve BCG vaccination response, but further studies focused on the gut-lung axis are warranted to confirm the interest of such a holistic approach.

References

Abebe, F. (2012). Is interferon-gamma the right marker for bacille Calmette-Guerin-induced immune protection? The missing link in our understanding of tuberculosis immunology. *Clinical and Experimental Immunology* 169(3), 213-219. doi: 10.1111/j.1365-2249.2012.04614.x.

Baek, M.G., Woo, S.J., Kim, N.E., Baek, C., Won, S., Kim, Y., et al. (2020). Respiratory microbiome profiles differ by recent hospitalization and nursing home residence in patients on mechanical ventilation. *J Transl Med* 18(1), 464. doi: 10.1186/s12967-020-02642-z.

Barcik, W., Boutin, R.C.T., Sokolowska, M., and Finlay, B.B. (2020). The Role of Lung and Gut Microbiota in the Pathology of Asthma. *Immunity* 52(2), 241-255. doi: 10.1016/j.immuni.2020.01.007.

Budden, K.F., Gellatly, S.L., Wood, D.L., Cooper, M.A., Morrison, M., Hugenholtz, P., et al. (2017). Emerging pathogenic links between microbiota and the gut-lung axis. *Nat Rev Microbiol* 15(1), 55-63. doi: 10.1038/nrmicro.2016.142.

Bull, N.C., Kaveh, D.A., Garcia-Pelayo, M.C., Stylianou, E., McShane, H., and Hogarth, P.J. (2018). Induction and maintenance of a phenotypically heterogeneous lung tissue-resident CD4(+) T cell population following BCG immunisation. *Vaccine* 36(37), 5625-5635. doi: 10.1016/j.vaccine.2018.07.035.

Cait, A., Hughes, M.R., Antignano, F., Cait, J., Dimitriu, P.A., Maas, K.R., et al. (2018). Microbiome-driven allergic lung inflammation is ameliorated by short-chain fatty acids. *Mucosal Immunology* 11(3), 785-795. doi: 10.1038/mi.2017.75.

Callahan, B.J., McMurdie, P.J., and Holmes, S.P. (2017). Exact sequence variants should replace operational taxonomic units in marker-gene data analysis. *ISME J* 11(12), 2639-2643. doi: 10.1038/ismej.2017.119.

Callahan, B.J., McMurdie, P.J., Rosen, M.J., Han, A.W., Johnson, A.J., and Holmes, S.P. (2016a). DADA2: High-resolution sample inference from Illumina amplicon data. *Nat Methods* 13(7), 581-583. doi: 10.1038/nmeth.3869.

Callahan, B.J., Sankaran, K., Fukuyama, J.A., McMurdie, P.J., and Holmes, S.P. (2016b). Bioconductor Workflow for Microbiome Data Analysis: from raw reads to community analyses. *F1000Res* 5, 1492. doi: 10.12688/f1000research.8986.2.

Carney, S.M., Clemente, J.C., Cox, M.J., Dickson, R.P., Huang, Y.J., Kitsios, G.D., et al. (2020). Methods in Lung Microbiome Research. *American Journal of Respiratory Cell and Molecular Biology* 62(3), 283-299. doi: 10.1165/rcmb.2019-0273TR.

Cernuschi, T., Malvolti, S., Nickels, E., and Friede, M. (2018). Bacillus Calmette-Guerin (BCG) vaccine: A global assessment of demand and supply balance. *Vaccine* 36(4), 498-506. doi: 10.1016/j.vaccine.2017.12.010.

Chee, C.B.E., Reves, R., Zhang, Y., and Belknap, R. (2018). Latent tuberculosis infection: Opportunities and challenges. *Respirology* 23(10), 893-900. doi: 10.1111/resp.13346.

Collie, D., Glendinning, L., Govan, J., Wright, S., Thornton, E., Tennant, P., et al. (2015). Lung Microbiota Changes Associated with Chronic Pseudomonas aeruginosa Lung Infection and the Impact of Intravenous Colistimethate Sodium. *Plos One* 10(11). doi: ARTN e0142097 10.1371/journal.pone.0142097.

Cui, Z.L., Zhou, Y.H., Li, H., Zhang, Y., Zhang, S.L., Tang, S.J., et al. (2012). Complex sputum microbial composition in patients with pulmonary tuberculosis. *Bmc Microbiology* 12. doi: Artn 276 10.1186/1471-2180-12-276.

Cuthbertson, L., Walker, A.W., Oliver, A.E., Rogers, G.B., Rivett, D.W., Hampton, T.H., et al. (2020). Lung function and microbiota diversity in cystic fibrosis. *Microbiome* 8(1)**,** 45. doi: 10.1186/s40168-020-00810-3.

Davies, G., Wells, A.U., Doffman, S., Watanabe, S., and Wilson, R. (2006). The effect of Pseudomonas aeruginosa on pulmonary function in patients with bronchiectasis. *European Respiratory Journal* 28(5)**,** 974-979. doi: 10.1183/09031936.06.00074605.

Dickson, R.P., and Huffnagle, G.B. (2015). The Lung Microbiome: New Principles for Respiratory Bacteriology in Health and Disease. *Plos Pathogens* 11(7). doi: ARTN e1004923 10.1371/journal.ppat.1004923.

Dockrell, H.M., and Smith, S.G. (2017). What Have We Learnt about BCG Vaccination in the Last 20 Years? *Frontiers in Immunology* 8. doi: ARTN 1134 10.3389/fimmu.2017.01134.

Ducarmon, Q.R., Zwittink, R.D., Hornung, B.V.H., van Schaik, W., Young, V.B., and Kuijper, E.J. (2019). Gut Microbiota and Colonization Resistance against Bacterial Enteric Infection. *Microbiol Mol Biol Rev* 83(3). doi: 10.1128/MMBR.00007-19.

Enaud, R., Prevel, R., Ciarlo, E., Beaufils, F., Wieers, G., Guery, B., et al. (2020). The Gut-Lung Axis in Health and Respiratory Diseases: A Place for Inter-Organ and Inter-Kingdom Crosstalks. *Front Cell Infect Microbiol* 10**,** 9. doi: 10.3389/fcimb.2020.00009.

Eshetie, S., and van Soolingen, D. (2019). The respiratory microbiota: new insights into pulmonary tuberculosis. *Bmc Infectious Diseases* 19. doi: ARTN 92 10.1186/s12879-019-3712-1.

Fatima, S., Kumari, A., Das, G., and Dwivedi, V.P. (2020). Tuberculosis vaccine: A journey from BCG to present. *Life Sciences* 252. doi: ARTN 117594 10.1016/j.lfs.2020.117594.

Gray, J., Oehrle, K., Worthen, G., Alenghat, T., Whitsett, J., and Deshmukh, H. (2017). Intestinal commensal bacteria mediate lung mucosal immunity and promote resistance of newborn mice to infection. *Science Translational Medicine* 9(376). doi: ARTN eaaf9412 10.1126/scitranslmed.aaf9412.

Guo, J.G., Tang, J., Kang, T.S., Xiong, Y., Xiang, Z.G., and Qin, C. (2020). Different immunization methods lead to altered gut flora and varied responses to Mycobacterium tuberculosis infection in mice. *Journal of Infection in Developing Countries* 14(10)**,** 1170-+. doi: 10.3855/jidc.12697.

Hakim, H., Dallas, R., Wolf, J., Tang, L., Schultz-Cherry, S., Darling, V., et al. (2018). Gut Microbiome Composition Predicts Infection Risk During Chemotherapy in Children With Acute Lymphoblastic Leukemia. *Clinical Infectious Diseases* 67(4)**,** 541-548. doi: 10.1093/cid/ciy153.

Hilty, M., Burke, C., Pedro, H., Cardenas, P., Bush, A., Bossley, C., et al. (2010). Disordered Microbial Communities in Asthmatic Airways. *Plos One* 5(1). doi: ARTN e8578 10.1371/journal.pone.0008578.

Hoft, D.F., Brown, R.M., and Roodman, S.T. (1998). Bacille Calmette-Guerin vaccination enhances human gamma delta T cell responsiveness to mycobacteria suggestive of a memory-like phenotype. *J Immunol* 161(2)**,** 1045-1054.

Holmes, Z.C., Silverman, J.D., Dressman, H.K., Wei, Z.Z., Dallow, E.P., Armstrong, S.C., et al. (2020). Short-Chain Fatty Acid Production by Gut Microbiota from Children with Obesity Differs According to Prebiotic Choice and Bacterial Community Composition. *Mbio* 11(4). doi: ARTN e00914-20 10.1128/mBio.00914-20.

Hu, Y.F., Feng, Y.Q., Wu, J.N., Liu, F., Zhang, Z.G., Hao, Y.N., et al. (2019). The Gut Microbiome Signatures Discriminate Healthy From Pulmonary Tuberculosis Patients. *Frontiers in Cellular and Infection Microbiology* 9. doi: ARTN 90 10.3389/fcimb.2019.00090.

Huang, Y.F., Mao, K., Chen, X., Sun, M.A., Kawabe, T., Li, W.Z., et al. (2018). S1P-dependent interorgan trafficking of group 2 innate lymphoid cells supports host defense. *Science* 359(6371)**,** 114-119. doi: 10.1126/science.aam5809.

Hufnagl, K., Pali-Scholl, I., Roth-Walter, F., and Jensen-Jarolim, E. (2020). Dysbiosis of the gut and lung microbiome has a role in asthma. *Semin Immunopathol* 42(1)**,** 75-93. doi: 10.1007/s00281-019-00775-y.

Invernizzi, R., Lloyd, C.M., and Molyneaux, P.L. (2020). Respiratory microbiome and epithelial interactions shape immunity in the lungs. *Immunology* 160(2)**,** 171-182. doi: 10.1111/imm.13195.

Kanmani, P., Clua, P., Vizoso-Pinto, M.G., Rodriguez, C., Alvarez, S., Melnikov, V., et al. (2017). Respiratory Commensal Bacteria Corynebacterium pseudodiphtheriticum Improves Resistance of Infant Mice to Respiratory Syncytial Virus and Streptococcus pneumoniae Superinfection. *Front Microbiol* 8**,** 1613. doi: 10.3389/fmicb.2017.01613.

Khan, N., Vidyarthi, A., Nadeem, S., Negi, S., Nair, G., and Agrewala, J.N. (2016). Alteration in the Gut Microbiota Provokes Susceptibility to Tuberculosis. *Frontiers in Immunology* 7. doi: ARTN 529 10.3389/fimmu.2016.00529.

Krishna, P., Jain, A., and Bisen, P.S. (2016). Microbiome diversity in the sputum of patients with pulmonary tuberculosis. *Eur J Clin Microbiol Infect Dis* 35(7)**,** 1205-1210. doi: 10.1007/s10096-016-2654-4.

Lee, S.Y., Mac Aogain, M., Fam, K.D., Chia, K.L., Binte Mohamed Ali, N.A., Yap, M.M.C., et al. (2019). Airway microbiome composition correlates with lung function and arterial stiffness in an age-dependent manner. *PLoS One* 14(11)**,** e0225636. doi: 10.1371/journal.pone.0225636.

Li, S.X., Armstrong, A.J.S., Neff, C.P., Shaffer, M., Lozupone, C.A., and Palmer, B.E. (2016). Complexities of Gut Microbiome Dysbiosis in the Context of HIV Infection and Antiretroviral Therapy. *Clinical Pharmacology & Therapeutics* 99(6)**,** 600-611. doi: 10.1002/cpt.363.

Liu, F., Li, J.J., Guan, Y.B., Lou, Y.F., Chen, H.Y., Xu, M.Y., et al. (2019). Dysbiosis of the Gut Microbiome is associated with Tumor Biomarkers in Lung Cancer. *International Journal of Biological Sciences* 15(11)**,** 2381-2392. doi: 10.7150/ijbs.35980.

Liu, N.N., Ma, Q., Ge, Y., Yi, C.X., Wei, L.Q., Tan, J.C., et al. (2020). Microbiome dysbiosis in lung cancer: from composition to therapy. *Npj Precision Oncology* 4(1). doi: ARTN 33 10.1038/s41698-020-00138-z.

Love, M.I., Huber, W., and Anders, S. (2014). Moderated estimation of fold change and dispersion for RNA-seq data with DESeq2. *Genome Biology* 15(12). doi: ARTN 550 10.1186/s13059-014-0550-8.

Magne, F., Gotteland, M., Gauthier, L., Zazueta, A., Pesoa, S., Navarrete, P., et al. (2020). The Firmicutes/Bacteroidetes Ratio: A Relevant Marker of Gut Dysbiosis in Obese Patients? *Nutrients* 12(5). doi: ARTN 1474 10.3390/nu12051474.

Mariat, D., Firmesse, O., Levenez, F., Guimaraes, V.D., Sokol, H., Dore, J., et al. (2009). The Firmicutes/Bacteroidetes ratio of the human microbiota changes with age. *Bmc Microbiology* 9. doi: Artn 123 10.1186/1471-2180-9-123.

Marsland, B.J., Trompette, A., and Gollwitzer, E.S. (2015). The Gut-Lung Axis in Respiratory Disease. *Ann Am Thorac Soc* 12 Suppl 2**,** S150-156. doi: 10.1513/AnnalsATS.201503-133AW.

Mathieu, E., Escribano-Vazquez, U., Descamps, D., Cherbuy, C., Langella, P., Riffault, S., et al. (2018). Paradigms of Lung Microbiota Functions in Health and Disease, Particularly, in Asthma. *Frontiers in Physiology* 9. doi: ARTN 1168 10.3389/fphys.2018.01168.

Maurice, N.M., Bedi, B., and Sadikot, R.T. (2018). Pseudomonas aeruginosa Biofilms: Host Response and Clinical Implications in Lung Infections. *American Journal of Respiratory Cell and Molecular Biology* 58(4)**,** 428-439. doi: 10.1165/rcmb.2017-0321TR.

McKnight, D.T., Huerlimann, R., Bower, D.S., Schwarzkopf, L., Alford, R.A., and Zenger K.R. (2019). microDecon: A highly accurate read-subtraction tool for the post-sequencing removal of contamination in metabarcoding studies. *Env. DNA* 1, 14-25. doi.org/10.1002/edn3.11

Moffatt, M.F., and Cookson, W.O.C.M. (2017). The lung microbiome in health and disease. *Clinical Medicine* 17(6)**,** 525-529.

Namasivayam, S., Sher, A., Glickman, M.S., and Wipperman, M.F. (2018). The Microbiome and Tuberculosis: Early Evidence for Cross Talk. *Mbio* 9(5). doi: ARTN e01420-18 10.1128/mBio.01420-18.

Nguyen, L.D.N., Viscogliosi, E., and Delhaes, L. (2015). The lung nnycobiome: an emerging field of the human respiratory microbiome. *Frontiers in Microbiology* 6. doi: ARTN 89 10.3389/fmicb.2015.00089.

O'Dwyer, D.N., Ashley, S.L., Gurczynski, S.J., Xia, M., Wilke, C., Falkowski, N.R., et al. (2019). Lung Microbiota Contribute to Pulmonary Inflammation and Disease Progression in Pulmonary Fibrosis. *American Journal of Respiratory and Critical Care Medicine* 199(9)**,** 1127-1138. doi: 10.1164/rccm.201809-1650OC.

Ogongo, P., Porterfield, J.Z., and Leslie, A. (2019). Lung Tissue Resident Memory T-Cells in the Immune Response to Mycobacterium tuberculosis. *Frontiers in Immunology* 10. doi: ARTN 992 10.3389/fimmu.2019.00992.

Prisk, G.K., and West, J.B. (2019). Deriving the arterial PO2 and oxygen deficit from expired gas and pulse oximetry. *Journal of Applied Physiology* 127(4)**,** 1067-1074. doi: 10.1152/japplphysiol.01100.2018.

Radwan, S., Gilfillan, D., Eklund, B., Radwan, H.M., El Menofy, N.G., Lee, J., et al. (2020). A comparative study of the gut microbiome in Egyptian patients with Type I and Type II diabetes. *PLoS One* 15(9)**,** e0238764. doi: 10.1371/journal.pone.0238764.

Salgame, P., Geadas, C., Collins, L., Jones-Lopez, E., and Ellner, J.J. (2015). Latent tuberculosis infection - Revisiting and revising concepts. *Tuberculosis* 95(4)**,** 373-384. doi: 10.1016/j.tube.2015.04.003.

Salisbury, M.L., Han, M.K., Dickson, R.P., and Molyneaux, P.L. (2017). Microbiome in interstitial lung disease: from pathogenesis to treatment target. *Current Opinion in Pulmonary Medicine* 23(5)**,** 404-410. doi: 10.1097/Mcp.0000000000000399.

Shen, Y., Torchia, M.L.G., Lawson, G.W., Karp, C.L., Ashwell, J.D., and Mazmanian, S.K. (2012). Outer Membrane Vesicles of a Human Commensal Mediate Immune Regulation and Disease Protection. *Cell Host & Microbe* 12(4)**,** 509-520. doi: 10.1016/j.chom.2012.08.004.

Silverman, J.D., Durand, H.K., Bloom, R.J., Mukherjee, S., and David, L.A. (2018). Dynamic linear models guide design and analysis of microbiota studies within artificial human guts. *Microbiome* 6. doi: ARTN 202 10.1186/s40168-018-0584-3.

Sokol, H., Leducq, V., Aschard, H., Pham, H.P., Jegou, S., Landman, C., et al. (2017). Fungal microbiota dysbiosis in IBD. Gut 66(6), 1039-1048. doi: 10.1136/gutjnl-2015-310746.

Soret, P., Vandenborght, L.E., Francis, F., Coron, N., Enaud, R., Avalos, M., et al. (2020). Respiratory mycobiome and suggestion of inter-kingdom network during acute pulmonary exacerbation in cystic fibrosis. *Scientific Reports* 10(1). doi: ARTN 3589 10.1038/s41598-020-60015-4.

Steed, A.L., Christophi, G.P., Kaiko, G.E., Sun, L.L., Goodwin, V.M., Jain, U., et al. (2017). The microbial metabolite desaminotyrosine protects from influenza through type I interferon. *Science* 357(6350)**,** 498-502. doi: 10.1126/science.aam5336.

Stojanov, S., Berlec, A., and Strukelj, B. (2020). The Influence of Probiotics on the Firmicutes/Bacteroidetes Ratio in the Treatment of Obesity and Inflammatory Bowel disease. *Microorganisms* 8(11). doi: ARTN 1715 10.3390/microorganisms8111715.

Tanner, R., Villarreal-Ramos, B., Vordermeier, H.M., and McShane, H. (2019). The Humoral Immune Response to BCG Vaccination. *Frontiers in Immunology* 10. doi: ARTN 1317 10.3389/fimmu.2019.01317.

Temraz, S., Nassar, F., Nasr, R., Charafeddine, M., Mukherji, D., and Shamseddine, A. (2019). Gut Microbiome: A Promising Biomarker for Immunotherapy in Colorectal Cancer. *Int J Mol Sci* 20(17). doi: 10.3390/ijms20174155.

Teskey, G., Abrahem, R., Cao, R., Gyurjian, K., Islamoglu, H., Lucero, M., et al. (2018). Glutathione as a Marker for Human Disease. *Adv Clin Chem* 87**,** 141-159. doi: 10.1016/bs.acc.2018.07.004.

Thaiss, C.A., Levy, M., Korem, T., Dohnalova, L., Shapiro, H., Jaitin, D.A., et al. (2016). Microbiota Diurnal Rhythmicity Programs Host Transcriptome Oscillations. *Cell* 167(6)**,** 1495-1510 e1412. doi: 10.1016/j.cell.2016.11.003.

Thomas, S., Izard, J., Walsh, E., Batich, K., Chongsathidkiet, P., Clarke, G., et al. (2017). The Host Microbiome Regulates and Maintains Human Health: A Primer and Perspective for Non-Microbiologists. *Cancer Res* 77(8)**,** 1783-1812. doi: 10.1158/0008-5472.CAN-16-2929.

Tiew, P.Y., Mac Aogain, M., Ali, N., Thng, K.X., Goh, K., Lau, K.J.X., et al. (2020). The Mycobiome in Health and Disease: Emerging Concepts, Methodologies and Challenges. Mycopathologia 185(2), 207-231. doi: 10.1007/s11046-019-00413-z.

Tipton, L., Muller, C.L., Kurtz, Z.D., Huang, L., Kleerup, E., Morris, A., et al. (2018). Fungi stabilize connectivity in the lung and skin microbial ecosystems. Microbiome 6(1), 12. doi: 10.1186/s40168-017-0393-0.

Trompette, A., Gollwitzer, E.S., Pattaroni, C., Lopez-Mejia, I.C., Riva, E., Pernot, J., et al. (2018). Dietary Fiber Confers Protection against Flu by Shaping Ly6c(-) Patrolling Monocyte Hematopoiesis and CD8(+) T Cell Metabolism. *Immunity* 48(5), 992-+. doi: 10.1016/j.immuni.2018.04.022.

Trompette, A., Gollwitzer, E.S., Yadava, K., Sichelstiel, A.K., Sprenger, N., Ngom-Bru, C., et al. (2014). Gut microbiota metabolism of dietary fiber influences allergic airway disease and hematopoiesis. *Nature Medicine* 20(2), 159-166. doi: 10.1038/nm.3444.

Vandenborght, L.E., Enaud, R., Urien, C., Coron, N., Girodet, P.O., Ferreira, S., et al. (2021). Type 2-high asthma is associated with a specific indoor mycobiome and microbiome. *J Allergy Clin Immunol* 147(4), 1296-1305 e1296. doi: 10.1016/j.jaci.2020.08.035.

Vandeplassche, E., Sass, A., Ostyn, L., Burmolle, M., Kragh, K.N., Bjarnsholt, T., et al. (2020). Antibiotic susceptibility of cystic fibrosis lung microbiome members in a multispecies biofilm. *Biofilm* 2, 100031. doi: 10.1016/j.bioflm.2020.100031.

Wang, J., Li, F.Q., and Tian, Z.G. (2017). Role of microbiota on lung homeostasis and diseases. *Science China-Life Sciences* 60(12), 1407-1415. doi: 10.1007/s11427-017-9151-1.

Waters, E.M., Neill, D.R., Kaman, B., Sahota, J.S., Clokie, M.R.J., Winstanley, C., et al. (2017). Phage therapy is highly effective against chronic lung infections with Pseudomonas aeruginosa. *Thorax* 72(7), 666-667. doi: 10.1136/thoraxjnl-2016-209265.

Wells, J.M. (2011). Immunomodulatory mechanisms of lactobacilli. *Microbial Cell Factories* 10. doi: Artn S17 10.1186/1475-2859-10-S1-S17.

World Health Organization. Global Tuberculosis Report (2020). https://www.who.int/publications/i/item/9789240013131 [Accessed May 10, 2021].

Wu, X., Xia, Y., He, F., Zhu, C., and Ren, W. (2021). Intestinal mycobiota in health and diseases: from a disrupted equilibrium to clinical opportunities. *Microbiome* 9(1), 60. doi: 10.1186/s40168-021-01024-x.

Wu, B.G., and Segal, L.N. (2018). The Lung Microbiome and Its Role in Pneumonia. *Clinics in Chest Medicine* 39(4), 677-+. doi: 10.1016/j.ccm.2018.07.003.

Wu, J., Liu, W., He, L., Huang, F., Chen, J., Cui, P., et al. (2013). Sputum microbiota associated with new, recurrent and treatment failure tuberculosis. *PLoS One* 8(12), e83445. doi: 10.1371/journal.pone.0083445.

Wypych, T.P., Wickramasinghe, L.C., and Marsland, B.J. (2019). The influence of the microbiome on respiratory health. *Nature Immunology* 20(10), 1279-1290. doi: 10.1038/s41590-019-0451-9.

Yang, D.P., Xing, Y.Y., Song, X.Y., and Qian, Y.C. (2019a). The impact of lung microbiota dysbiosis on inflammation. *Immunology* 159(2), 156-166. doi: 10.1111/imm.13139.

Yang, D.P., Chen, X., Wang, J.J., Lou, Q., Lou, Y.W., Li, L., et al. (2019b). Dysregulated Lung Commensal Bacteria Drive Interleukin-17B Production to Promote Pulmonary Fibrosis through Their Outer Membrane Vesicles. *Immunity* 50(3), 692-+. doi: 10.1016/j.immuni.2019.02.001.

Yang, K., Kruse, R.L., Lin, W.V., and Musher, D.M. (2018). Corynebacteria as a cause of pulmonary infection: a case series and literature review. *Pneumonia (Nathan)* 10**,** 10. doi: 10.1186/s41479-018-0054-5.

Zhu, B.D., Dockrell, H.M., Ottenhoff, T.H.M., Evans, T.G., and Zhang, Y. (2018). Tuberculosis vaccines: Opportunities and challenges. *Respirology* 23(4)**,** 359-368. doi: 10.1111/resp.13245.

APPENDIX

Supplementary Figures and Tables

Supplementary Table S1

Details of antibodies used for flow cytometry in the experiment part I.

Marker	Fluorophore	Isotype	Dilution
CD4	PerCP-Cy5.5	Rat IgG2a	1:20
CXCR3	PECy7	Arm. Ham IgG	1:20
CX3CR1	BV421	Mouse IgG2a k	1:20
CD44	FITC	Rat IgG2b	1:40
IFN-γ	APC	Rat IgG1	1:20
IL-2	PE	Rat IgG2b	1:20
TNF-α	BV510	Rat IgG1	1:20
CD45	AF700	Rat IgG2b	1:20

Supplementary Table S2

Details of antibodies used for flow cytometry in the experiment part II.

Panel 1.

Marker	Fluorophore	Isotype	Dilution
CD4	PerCP-Cy5.5	Rat IgG2a	1:20
PD-1	PeCy7	Arm. Ham IgG	1:20
CD3	V450	Rat IgG1	1:20
CD62L	FITC	Rat IgG2b	1:40
IFN-γ	APC	Rat IgG1	1:20
CXCR3	PE	Rat IgG2b	1:20
CX3CR1	BV510	Rat IgG1	1:20
TNF-α	AF700	Rat IgG2b	1:20

Panel 2.

Marker	Fluorophore	Isotype	Dilution
CD8	PerCP-Cy5.5	Rat IgG2a	1:20
PD-1	PeCy7	Arm. Ham IgG	1:20
CD127	APC	Rat IgG1	1:20
CD3	BV510	Rat IgG1	1:20
TNF-α	AF700	Rat IgG2b	1:20
CD62L	FITC	Rat IgG2b	1:40
IL-2	PE	Rat IgG2b	1:20
CCR7	BV421	Mouse IgG2ak	1:20